Distribution Agreement

In presenting this thesis or dissertation as partial fulfillment of the requirements for an advanced degree from Emory University, I hereby grant to Emory University and its agents the non-exclusive license to archive, make accessible, and display my thesis or dissertation in whole or in part in all forms of media, now or hereafter known, including display on the world wide web. I understand that I may select some access restrictions as part of the online submission of this thesis or dissertation. I retain all ownership rights to the copyright of the thesis or dissertation. I also retain the right to use in future works (such as articles or books) all or part of this thesis or dissertation.

Signature:

_____	_____
Jasmine C. Moody	Date

The PIX-1 Signaling Pathway that Includes the Rho GEF PIX-1 and the Rho GAP RRC-1 Direct Assembly or Stability of Integrin Adhesion Complexes in Striated Muscle

By
Jasmine Chantel Moody
Doctor of Philosophy
Graduate Division of Biological and Biomedical Science
Genetics and Molecular Biology

_____
Guy M. Benian
Advisor

_____
Anita Corbett
Committee Member

_____
Richard Kahn
Committee Member

_____
David Katz
Committee Member

_____
Dorothy Lerit
Committee Member

Accepted:

_____
Kimberly Jacob Arriola, Ph.D.
Dean of the James T. Laney School of Graduate Studies

_____
Date

The PIX-1 Signaling Pathway that Includes the Rho GEF PIX-1 and the Rho GAP RRC-1 Direct Assembly or Stability of Integrin Adhesion Complexes in Striated Muscle

By

Jasmine Chantel Moody
B.S., Spelman College, 2016

Advisor: Guy M. Benian, MD

An abstract of
A dissertation submitted to the Faculty of the
James T. Laney School of Graduate Studies of Emory University
in partial fulfillment of the requirements for the degree
of Doctor of Philosophy
in Graduate Division of Biological and Biomedical Science
Genetics and Molecular Biology
2022

Abstract

The PIX-1 Signaling Pathway that Includes the RhoGEF PIX-1 and the RhoGAP RRC-1 Direct Assembly or Stability of Integrin Adhesion Complexes in Striated Muscle

By Jasmine Chantel Moody

Integrin adhesion complexes (IACs) permit the attachment of cells to the extracellular matrix (ECM) and are essential for tissue and organ development and cell motility. Although much is known about the composition and initial assembly of IACs, what determines where and when an IAC will form remain unknown. In striated muscle, IACs attach the muscle cell to the ECM and transmit the force of muscle contraction. *C. elegans* is an excellent model to study muscle assembly, maintenance, and regulation and their striated muscle has IACs at the M-line, dense body, and attachment plaque at muscle cell boundaries (MCBs). I discovered that loss of function of the gene *pix-1* results in the absence of IAC components only at MCBs. PIX-1 deficiency or overexpression results in disrupted MCBs, decreased whole animal locomotion, and muscle-specific expression of wildtype PIX-1 rescues the MCB phenotype. PIX proteins are guanine nucleotide exchange factors (GEFs) that activate Rac and Cdc42 and have numerous functions in various cell types. Mutations in genes encoding proteins at known steps of the PIX signaling pathway, including the Rac, CED-10, the scaffold GIT-1, and the effector protein kinases, PAK-1, and PAK-2, show defects at MCBs. Either constitutively active or catalytically dead protein kinase *pak-1* mutants also show disrupted MCBs, indicating that increased or decreased output of the PIX pathway yields the same phenotype. Rho GTPases function as molecular switches between active and inactive states, via GEF and GAP (GTPase activating) proteins respectively. However, a GAP for the PIX pathway had not been identified for any organism or cell type. Upon screening mutants of 18 muscle-expressed genes that encode proteins with RhoGAP domains, I discovered that RRC-1 deficiency yields the MCB defect. *rrc-1* loss of function mutants lack IAC protein accumulation at MCBs and have reduced motility. RRC-1 and PIX-1 both localize to MCBs and show complex genetic interactions. Together this is the first evidence of a role for the PIX pathway in muscle and the discovery of a GAP for the pathway. An important goal for future research is to understand the molecular mechanisms by which the PIX pathway affects the assembly of IACs.

The PIX-1 Signaling Pathway that Includes the Rho GEF PIX-1 and the Rho GAP RRC-1 Direct Assembly or Stability of Integrin Adhesion Complexes in Striated Muscle

By

Jasmine Chantel Moody
B.S., Spelman College, 2016

Advisor: Guy M. Benian, MD

A dissertation submitted to the Faculty of the
James T. Laney School of Graduate Studies of Emory University
in partial fulfillment of the requirements for the degree of
Doctor of Philosophy
in Graduate Division of Biological and Biomedical Science
Genetics and Molecular Biology
2022

Acknowledgments

I would like to acknowledge the efforts of those that have provided me with tremendous assistance and support while writing this dissertation.

I would first like to thank my advisor Guy Benian, whose expertise and compassion significantly guided my work and training. It has truly been an honor to have the opportunity to work with someone as dedicated and talented as you. I would like to give special thanks to Hiroshi Qadota whose skills and experience were invaluable to my training. Thank you for your insightful feedback and for always challenging me to think critically. Yohei and Courtney thank you for sharing your experience, assistance, and contributions to my work over the years as well as the great energy you both brought to the lab. I also would like to thank Dr. April Reedy, a previous postdoctoral fellow in the Benian lab, for conducting the painstaking screen of nearly 600 MMP mutant strains that led to the identification of the single mutant strain with the MCB defect. Your work ultimately led to the identification of the *pix-1* gene which served as the basis of my thesis.

I would like to thank Dr. Tiffany Oliver, my mentor since I was an undergraduate student at Spelman who encouraged me to pursue research as a career. You have been in my corner since before I started graduate school and have truly been one of my biggest cheerleaders throughout this journey and I really appreciate you for that. I want to acknowledge Anita Corbett, whose training and mentorship have greatly influenced and helped me on this journey as well. Thank you for everything, from taking me under your wing when I was an undergrad to helping me navigate getting into and through graduate school.

I also want to acknowledge my whole family for always supporting my dreams and love of learning and science. To my Granny Sue, I love you so much, I would not be here without you! You knew very early on that I would accomplish great things, and you always cringed at my strange fascination with bugs. Thank you for all your support and love over the years. Mom, thank you for always challenging me to go beyond my comfort zone and planting those small seeds when I was younger that really helped me develop my love science, from all the science camps to science fairs thank you for always being supportive. Dad thank you for always teaching me to never give up, the importance of working hard and being dedicated to your goals. Your kind words and wisdom helped me see the brighter side of the tough days I've experienced over the years. To my siblings, thank you all for believing in me when I was struggling to believe I could do this and always uplifting and encouraging me.

Finally, I would like to dedicate this body of work to my greatest motivation in life, my son, Kingston. You are so incredible! You can do anything you put your mind to! Never stop reaching for your dreams, no matter how difficult the journey, because I will always be there to help you along the way! You have been on this journey with me since the very beginning, from the tiny kicks in my stomach as a first-year student to the very intelligent young man you've become as I prepare to graduate. You have made this journey worth every second, I love you and I'm so proud to be your mom! Thank you for your daily inspiration! XOXO

TABLE OF CONTENTS

LIST OF TABLES

LIST OF FIGURES

Chapter 1

Introduction

I. Purpose

Human skeletal and cardiac muscle cells are tightly packed full of bundles of myofibrils each surrounded by the sarcoplasmic reticulum and T-tubules. These myofibrils are connected to each other via intermediate filaments, and the myofibrils at the periphery of the cell are connected to the muscle cell membrane via costameres, which are muscle-specific focal adhesions. Myofibrils are long chains of sarcomeres. The sarcomere is the fundamental unit of muscle contraction consisting of a precisely ordered assemblage of several hundred types of proteins that are highly conserved throughout the animal kingdom. However, the molecular mechanism of assembly and maintenance of these sarcomeres, myofibrils, and their molecular connectors, is not well understood. This question is relevant to the pathogenesis of diseases that affect muscle cell structure and function including cardiomyopathies and muscular dystrophies.

The free-living nematode *C. elegans* is a great model to investigate new and conserved features of muscle cell assembly, maintenance, and regulation (Waterston, 1988; Moerman and Fire, 1997; Gieseler, Qadota and Benian, 2017). This model has several unique features that make it an exceptional genetic system to study striated muscle, including its optical transparency, allowing easy assessment of muscle structure by polarized light microscopy and localization of fluorescently tagged proteins; a rapid (3 day) lifecycle with ~300 progeny per adult; and because they usually reproduce as self-fertilizing hermaphrodites, mutants in muscle proteins that would render them severely paralyzed and unable to mate can still reproduce. Most of the muscle in *C. elegans* is located in the body wall, arranged in four quadrants just underlying the hypodermis and cuticle. This body wall muscle is required for locomotion of the worm, and mutations in various components of the sarcomere result in slow or uncoordinated ("Unc") movement. *C. elegans*

muscle form and function are very similar to that of vertebrate skeletal and cardiac muscle. Their facile genetic manipulation, including traditional mutagenesis screens, RNAi, transgenics, and now CRISPR-generated mutants, allow for the identification of new genes or gene pathways, and unexpected roles for genes that would otherwise be difficult to identify using purely biochemical or cell biological approaches. The conservation of muscle proteins and structures ensures results in *C. elegans* are relevant to humans. Notable discoveries about muscle have been made using *C. elegans*. For example, the cloning, sequencing, and analysis of the first complete myosin heavy chain led to a model for parallel assembly of myosin rods in the thick filament which also explains the conserved distance between adjacent pairs of myosin heads on the surface of thick filaments (Epstein et al., 1974; McLachlan and Karn, 1982). Other notable discoveries include: (1) that integrin and its associated proteins are critical for initial sarcomere assembly in the embryo (Williams and Waterston, 1994; Hresko et al., 1994); (2) discovery of the first myosin head chaperone, UNC-45, which is required for folding of the myosin head and also for assembly of myosin into thick filaments (Epstein and Thomson, 1974; Barral et al., 1998; Barral et al., 2002); (3) the first complete sequence of a giant titin-like protein, twitchin (Benian et al., 1989).

My studies have focused on understanding the molecular mechanisms that establish integrin-adhesion-complex (IAC) assembly in striated muscle. IACs, also commonly known as focal adhesions, are required for the attachment of cells to an extracellular matrix. While the composition of IACs is known, *what determines when and where these multi-protein complexes form is not understood.* Muscle-specific IACs are known as “costameres” and function to attach myofibrils of vertebrate muscle at the periphery of muscle cells to the cell membrane and surrounding extracellular matrix (ECM) (Ervasti, 2003; Henderson et al., 2017). In *C. elegans* body wall

muscle, IACs are found in three locations: the base of M-lines, the base of dense bodies (Z-disks), and at the adhesion plaques of muscle cell boundaries. Using the power of *C. elegans* genetics, my results provide the first evidence for the requirement of the PIX signaling pathway for assembly and/or stability of IACs in the muscle in any organism. PIX is a RacGEF, that is, a protein that activates the small GTPase Rac, by promoting the exchange of GDP for GTP. Screening for the same mutant phenotype as *pix-1* mutants, I was also able to identify the first RhoGAP for the PIX pathway in any organism, RRC-1, a protein that promotes the hydrolysis of GTP to GDP, thereby inactivating Rac.

II. Muscle

All activities that require body movement in most organisms are made possible by the presence of muscle. In mammals, there are three different muscle types including smooth muscle, skeletal muscle, and cardiac muscle, each of which has distinct functions facilitated by their specialized structures. Smooth muscle is non-striated and controlled involuntarily and it functions in pupil dilation and constriction, food digestion, tissue oxygenation, blood pressure regulation, and more (Hafen and Burns 2021). Skeletal muscle is essential for the voluntary muscle contraction involved in basic activities such as standing, walking, or exercising (Frontera and Ochala, 2015). Cardiac muscle makes up the atrial and ventricular walls of the heart and plays a vital role in pumping blood throughout the body. While skeletal and cardiac muscle has somewhat different structures, both are classified as striated muscle because each has "striations", or alternating dark and light bands, visible by low-powered light microscopy due to the lateral registration of chains of sarcomeres.

Striated muscle is structurally organized by the repetitive presence of the functional units of contraction, the sarcomeres, which link end to end in long chains forming "myofibrils". The sarcomere is the fundamental unit of contraction and consists of highly organized protein assemblages that are evolutionarily conserved. One sarcomere is defined as the distance between consecutive Z-disks. The Z-disks are the attachment points of thin filaments, primarily composed of F-actin, and on each side of the sarcomere, the F-actin has an opposite orientation, with the plus or barbed end of each filament anchored at the Z-disk. In the center of the sarcomere is the M-line, a structure that organizes a parallel array of thick filaments, each primarily composed of myosin. This parallel, in-register array of thick filaments is called the A-band. From either side

of the sarcomere, there is a variable overlap of thin and thick filaments. The portions of the sarcomere in which thin filaments do not overlap thick filaments are called the I-band. (Figure 1.1) (Mukund and Subramaniam, 2020).

In most vertebrate striated muscle, thick filaments are approximately 1.6 μm long, (also the length of the A-band), and the entire sarcomere spans 2.2 to 2.5 μm. In many invertebrates, including *C. elegans*, the thick filaments can be as large as 10 μm long, and the sarcomeres span approximately 12 μm. By conventional light microscopy and electron microscopy, the A-bands, the Z-disks, and the M-lines, appear dark and the I-bands appear light. A-bands are an abbreviation of "Anisotropic bands" and I-bands are an abbreviation for "Isotropic bands", explaining how these structures interact with polarized light. Under polarizing optics, A-bands and Z-disks appear light, and I-bands appear dark. Although sarcomeres primarily consist of myosin and actin, at least several hundred additional proteins are known to be required for the assembly, stability, and function of the sarcomere (Benian and Epstein, 2011).

Although mammalian skeletal and cardiac muscles are classified as striated muscles based on shared structural and functional characteristics, some important differences distinguish them. First, skeletal muscle cells are much longer than cardiac muscle cells; skeletal muscle cells are 10-100 μm in diameter and can be as long as 35 cm, whereas cardiac muscle cells are approximately 15 μm in diameter but only 80-100 μm long. Second, skeletal muscle cells have multiple nuclei resulting from the fusion of many myoblasts during development, and these nuclei are located near the periphery of the cell. In contrast, cardiac muscle cells have one or sometimes 2 nuclei and these are centrally placed. Third, skeletal muscle cells are long cylinders whereas cardiac muscle cells usually have two branches. Fourth, in cardiac muscle, the shorter cardiac muscle cells are attached

to adjacent cells by a special type of junctional complex called the intercalated disk. In addition, adjacent cardiac muscle cells are electrically linked by numerous gap junctions. Thus, the intercalated disks and gap junctions permit large numbers of heart cells to contract as single units. Finally, skeletal muscle contains resident stem cells known as “satellite cells”, and stem cells are lacking in cardiac muscle. Satellite cells become activated in response to muscle damage induced by exercise or injury. Upon activation, these satellite cells stimulate the proliferation of myogenic progenitors that will give rise to new muscle cells but also self-renew to replenish the satellite cell pool (Dumont et al., 2015). Because of the absence of stem cells in cardiac muscle, after myocardial infarction and death of cardiac muscle cells, new muscle is not regenerated, only fibrosis or scar tissue, resulting in a significant reduction in the contractile capability of the heart (Uygur and Lee 2016).

Sliding filament model of muscle contraction

Despite differences in structure, regulation, and physiological function, skeletal, cardiac, and smooth muscle all contract based on the same mechanism, a cyclical interaction of two proteins, myosin, and actin. The “sliding filament mechanism” (Huxley, 2004) was first proposed in 1954: as the sarcomere contracts, thin filaments primarily composed of F-actin and opposite polarity are pulled inwards, and thus the distance between consecutive Z-disks, and the sarcomere shortens. Neither the thick nor thin filaments change their lengths. This pulling occurs by the cyclical attachment, pulling, and detachment of “myosin heads” (the motor portion of myosin) on the surface of thick filaments, with thin filaments. The energy for this process is derived from the hydrolysis of ATP. Conversion of ATP to ADP and Pi and release of this Pi results in small

conformational changes in the myosin head, and these are magnified by pivoting of the 10 nm long myosin neck domain which acts as a "lever arm." Each interaction of a myosin head with a thin filament involves hydrolysis of a single ATP molecule and about 50% of the energy of the terminal phosphate bond is converted into mechanical work which is highly efficient. Also, each pulling involves 3-4 pN of force and a displacement of only 5-15 nm (or about 1-3 actin monomers along an F-actin filament) (Finer et al., 1994).

Cardiomyopathies

Cardiomyopathies are heart muscle diseases associated with mechanical and electrical dysfunction, heart failure, and a high risk of sudden cardiac arrest. There are three major types of human inherited cardiomyopathies, hypertrophic (HCM), dilated (DCM), and arrhythmogenic right ventricular (ARVCM) (Cahill, Ashrafian, Watkins, 2013; McNally, Barefield, Puckelwartz, 2015). These are mostly monogenic disorders with autosomal dominant inheritance with incomplete penetrance and variable expressivity (Reza, Musunuru, Owens, 2019). Prevalence is quite high; for DCM approximately 1 in 2500, and HCM, approximately, 1 in 500. For HCM and DCM nearly all known mutations are in genes encoding sarcomeric proteins. For example, 50% of the known HCM mutations are in genes encoding either β-myosin heavy chain (MYH7) or in the myosin binding protein 3 (MYBPC3); most of the known DCM mutations are in the genes encoding titin (TTN; 25% of the cases), lamin-A/C (LMNA), myosin-7 and -6 (MYH7 and MYH6), sodium channel protein type 5 subunit alpha (SCN5A), MYBPC3 and troponin T2 (TNNT2). ARVCM results from mutations in genes encoding desmosomal proteins which are components of intercalated disks. However, it should be noted that although the best clinical genetic labs screen suspected CM patients for mutations in about 50 genes, mutations can be found

in only half of the cases (Pugh et al., 2014; Li et al., 2017; Corrado, Link, & Calkins, 2017). One possibility is that more cardiomyopathy genes need to be identified. Based on my results with *pix-1* in worms (Moody et al., 2020), our lab collaborated with Jennifer Kwong's lab (Emory, Dept. of Pediatrics) to generate a heart-specific knockout of the mouse PIX-1 ortholog called β-PIX. These β-PIX heart KO mice develop a DCM at 8 months of age. Thus, I hypothesize that one new human cardiomyopathy gene encodes β-PIX (ARHGEF7). As I have shown the same muscle phenotype for deficiency of the nematode ortholog of ARHGEF7 (PIX-1) as for deficiency of other known members of the PIX pathway (RRC-1, GIT-1, PAK-1, and Rac), possible new cardiomyopathy genes in humans might be expanded by 5 more genes. Our *C. elegans* work also shows that the worm ortholog, PIX-1, is required for assembly or stability of costamere-like structures. This is consistent with previous studies in humans and mice showing that deficiency of costamere proteins results in cardiomyopathy. For human HCM or DCM, these include mutations in the genes for vinculin, α-actinin-2, four and a half LIM protein-2 (FHL2), and ILK (3). In mice, heart-specific knock out (KO) of ILK results in DCM and die of heart failure by 6 weeks and show separation between cardiomyocytes (White et al., 2006) ; mice doubly homozygous for PINCH1 and PINCH2 in the myocardium also develop DCM and die of heart failure within 4 weeks (Liang et al., 2009); KO of kindlin-2 at late gestation or in adult cardiomyocytes results in DCM and progressive heart failure beginning at ~13 months of age (Zhang et al., 2016).

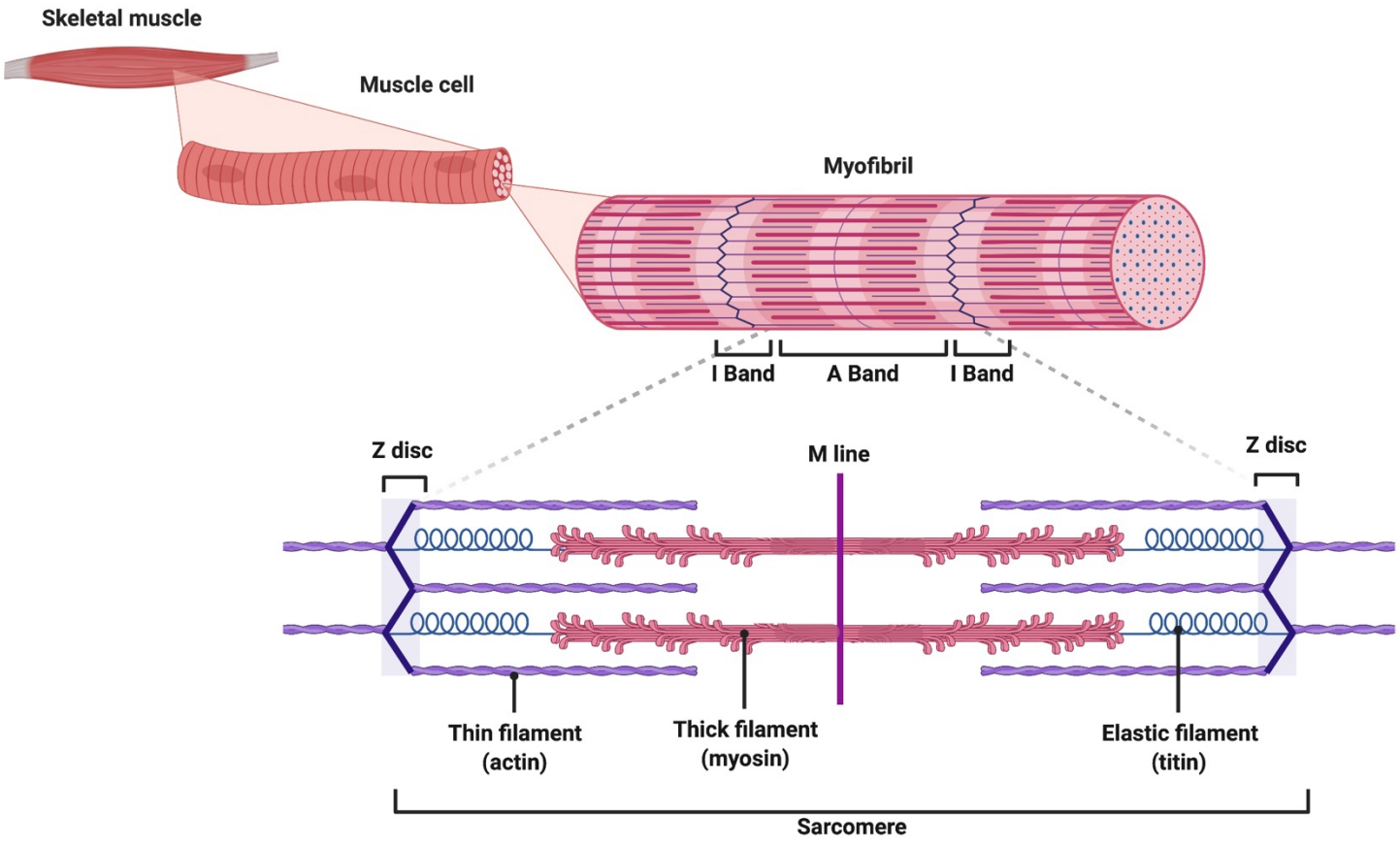
Skeletal muscle
Muscle cell
Myofibril
I Band
A Band
I Band
Z disc
M line
Z disc
Thin filament
(actin)
Thick filament
(myosin)
Elastic filament
(titin)
Sarcomere

Figure 1.1 Organization of the contractile apparatus in vertebrate skeletal muscle. Schematic diagram of vertebrate muscle structure from the level of a single muscle cell (often called a "muscle fiber") down to the level of the filaments within the sarcomere, each of which have been evolutionarily conserved. A single muscle cell contains bundles of myofibrils that are connected to each other via intermediate filaments and attached to the muscle cell membrane (often called the "sarcolemma") via costameres at the peripheral areas of the cell. Each myofibril consists of long chains of sarcomeres, the fundamental units of muscle contraction. The sarcomeres are made up of overlapping thick filaments and thin filaments that mainly consist of myosin and actin, respectively. The Z-disks are the attachment points of the thin filaments one on each side of the sarcomere, primarily composed of F-actin. The portions of the sarcomere in which thin filaments do not overlap thick filaments are called the I-band. The M-line is a structure that organizes a parallel array of thick filaments located at the center of the sarcomere. The A-band is arranged into a parallel array of thick filaments that are in register. Muscle contraction occurs by attachment and pulling of myosin heads on the thin filaments, such that thin filaments of opposite polarity are pulled inwards, thus reducing the width of the I-bands. Depicted also is the so-called "elastic filament" or "third filament"; this consists of the giant polypeptide titin, which can be as large as 4 MDa, and spans half a sarcomere (1.2 mm), from its N-terminus attached to the Z-disc to its C-terminus attached to the M-line. The portion of titin that lies in the A-band helps to organize the A-band and M-line, and the portion of titin in the I-band acts as a molecular spring and provides recoil to bring the sarcomere back to a set resting position during muscle relaxation. *Made using BioRender

III. *C. elegans* as a model for gaining new insights into muscle assembly, maintenance, and regulation

Caenorhabditis elegans is an excellent model system to study new aspects of sarcomere assembly, maintenance, and regulation as its muscle structure, function, and the proteins involved are mostly evolutionarily conserved. The major striated muscle of *C. elegans* is found in the body wall and is required for whole animal locomotion. *C. elegans* are cost-effective, require relatively low maintenance and easy cultivation requirements in a lab setting (Nigon and Felix, 2017). *C. elegans* are characterized by their microscopic size, an adult is typically 1.5 mm in length, which allows thousands of animals to live on a single agar petri dish. They have a simple diet consisting of *E. coli* bacteria (strain OP50) and thrive at the optimal growth temperature of 20°C. While *C. elegans'* small stature and simplistic lab maintenance make them an ideal model system they also have several advantageous developmental and reproductive characteristics.

Caenorhabditis elegans have several unique features that make them a great model system to uncover new and conserved principles of biology (Corsi et al., 2015). They have a rapid lifecycle of about 3 days (at 20°C growth temperature) from fertilized oocyte to young adult in most wildtype strains and produce massive brood sizes with an average of 280-315 progeny per individual worm. They are an easy to genetically manipulate diploid organism that naturally exists as two sexes, self-fertilizing hermaphrodites, and males. The frequency of males in the population is very low at about 0.1% resulting from a spontaneous non-disjunction of the X chromosome in the hermaphrodite germline. Subsequently, the population of males increases to around 50% upon successful mating with hermaphrodites. This dichotomy provides a useful tool for setting up genetic crosses that are used to outcross mutant strains to remove potential confounding

background mutations. Additionally, genetic crosses are implemented for moving mutations between strains and creating double and/or triple mutant lines. Its hermaphroditic self-fertilization allows the propagation of mutants that are uncoordinated or paralyzed, as well as the generation of genetically identical progeny (Altun and Hall, 2009). While the implications of these characteristics have made *C. elegans* a useful tool, they have been especially useful to employ studies on muscle structure and function.

C. elegans are optically transparent which enables the assessment of its muscle structure using various microscopy techniques. These methods include the use of polarized light to assess the organization of A- and I-bands, and localization of fluorescently tagged proteins in transgenic or CRISPR'd worms while still alive without fixation (Gieseler, Qadota and Benian, 2017). Since its introduction as a model system, technological advancements have made the system even more useful than previously considered. *C. elegans* was one of the first organisms to have its whole genome sequenced and made readily available, as well as having its entire cell lineage characterized (Corsi et al., 2015). There are also a multitude of databases that provide scientists with invaluable resources to exploit the advantages of the model system including the Million Mutation Project (Thompson, 2013) and the Caenorhabditis Genetics Center (CGC).

*C. elegan*s has become a powerful genetic tool for the study of new aspects of sarcomere assembly, maintenance, regulation, and aging. At least 200 proteins have been identified as being crucial for sarcomere assembly and organization from studies utilizing *C. elegans* as a model (Benian and Epstein, 2011). This species of nematodes has multiple types of muscle, including those in the pharyngeal, gastrointestinal, somatic gonadal, uterine, vulval, and body wall (Waterston, 1988). However, the body wall muscle is the most abundant and required for whole

animal locomotion. Its body wall striated muscle structure and function are analogous to both vertebrate skeletal and cardiac muscle.

In the adult, the body wall muscle is organized into four quadrants that extend the length of the organism, consisting of 95 spindle-shaped cells arranged as interlocking pairs (Moerman and Williams, 2006). Within each quadrant lies 24 diploid, mononucleated cells, except the left ventral quadrant which only has 23 cells (Sulston and Horvitz, 1977). Each cell has distinct components including the (1) cell body, containing the nucleus and the cytoplasmic organelles, (2) the arm, a connection that extends from the cell body to the dorsal or ventral nerve cord that is essential for the communication between the synaptic input of motor neurons, and (3) the spindle, the region of the contractile components that make up the myofilament lattice (Wood and Waterston, 1988).

In *C. elegans,* the myofibrils are arranged adjacent and parallel to the hypodermis and cuticle, restricted to an ~ 1.5μm deep layer that forms an obliquely striated pattern. The basic structure consists of thick filaments comprised of mostly myosin positioned in the center of two interdigitating layers of thin filaments containing mostly actin that extend from both ends of the structural unit. The thin filaments are attached to the dense bodies, Z-disk analogs in vertebrates, at one end and overlap with the bipolar end of thick filaments. The M-lines are aligned in the area around the thick filaments. These structures are remarkably analogous to the structures of vertebrate muscle, thus making them analogous and useful for the study of muscle (Wood and Waterston, 1988) During muscle contraction, the myosin heads on the thick filaments pull the actin-containing thin filaments inwards to generate force. Both dense bodies and M-lines are anchored to the cell membrane and the overlying extracellular matrix and are important for the

transduction of force to the outside of the muscle cell during muscle contraction thus resulting in whole animal movement. The anchoring of the dense bodies and M-lines is facilitated by muscle-specific adhesion complexes, called costameres, and are analogous to focal adhesions in non-muscle cells (Geisler, Qadota, and Benian, 2017). Each of the complexes begins with integrin, a transmembrane heterodimer that interacts with several hundreds of intercellular and extracellular components.

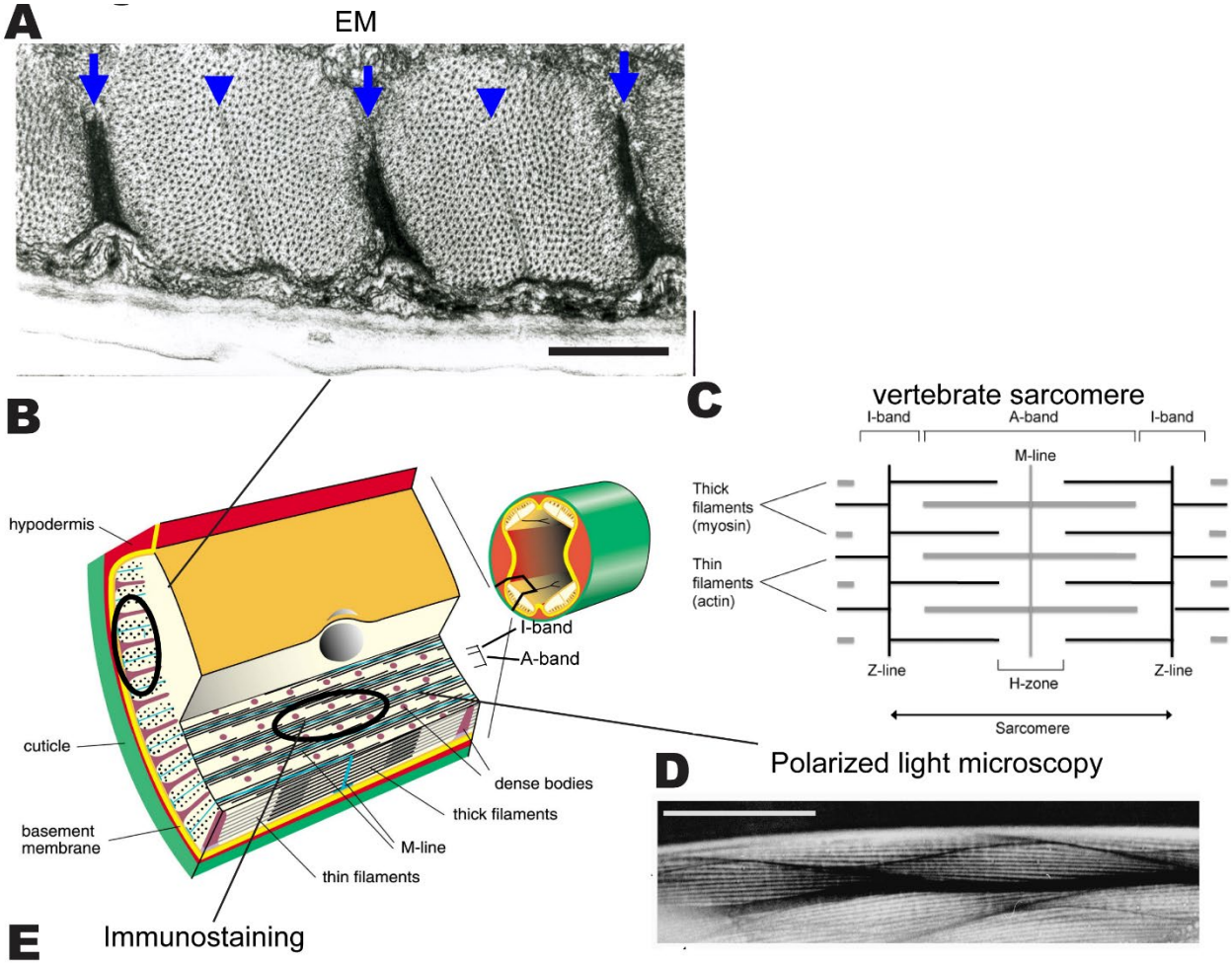
A
EM
B
hypodermis
cuticle
basement membrane
I-band
A-band
dense bodies
thick filaments
M-line
thin filaments
C
vertebrate sarcomere
I-band
A-band
I-band
M-line
Thick filaments (myosin)
Thin filaments (actin)
Z-line
H-zone
Z-line
Sarcomere
D
Polarized light microscopy
E
Immunostaining
MYO-3 (MHC A) - middle of A-band
ATN-1 (a-actinin) - dense bodies
PAT-6 (actopaxin) - M-lines & dense bodies
UNC-89 (obscurin) - M-lines

Figure 1.2 *C. elegans* is an excellent model to study striated muscle structure and function. A. Electron microscopy imaging of nematode body wall muscle cells. The blue arrows indicate the dense body structure which is an electron dense region of the cell that is attached to the muscle cell membrane. Dense bodies are analogs of Z-discs in vertebrate striated muscle. The blue triangles are indicative of the M-line structure. Both the dense bodies and M-lines are anchored to the sarcolemma and this attachment is crucial for the transmission of force generated by muscle contraction to the outside of the worm, and consequent whole animal locomotion. **B.** A schematic cross-sectional view of C. elegans body wall muscle highlighting the structure that consists of four quadrants. Each quadrant consists of interlocking pairs of mononuclear spindle-shaped cells (23 or 24 per quadrant). The myofilament lattice is limited to one side of the cell rather than filling the entire cross-sectional area as in a vertebrate striated muscle cell, as shown in the enlarged figure (left). Several planes of section are depicted, one of which emphasizes the muscle's striated organization with typical A-bands containing thick filaments organized around M-lines, and overlapping thin filaments probably attached to Z-disk-like structures called dense bodies. The sarcomere, which is defined as the repeating distance from one dense body to the next dense body is approximately 12µm in adult muscle. **C.** A simple diagram showing the basic structures of the sarcomere which is made up of overlapping parallel layers of the thick filaments of myosin and thin filaments of actin. The A-bands are the thick filaments organized into parallel rows at the center of the sarcomere. The thin filaments are anchored in opposite direction and are organized on the outer regions of each sarcomeres also known as the I bands. **D.** Polarized light microscopy imaging of a wildtype nematode muscle exhibiting the A-band and I -band organization in two muscle quadrants, with pairs of spindle-shaped cells in each quadrant. **E.** Confocal microscopy imaging of wildtype C. elegans immunostained with several different antibodies: MYO-3 (myosin heavy chain A, MHC A) localized to the middle of the A-bands; ATN-1 (α-actinin) localized to dense bodies; UNC-89 (obscurin) localized to M-lines; and PAT-6 (a-parvin) localized to both M-lines and dense bodies. Scale bar, 10µm.

Gieseler K, Qadota H, Benian GM. Development, structure, and maintenance of C. elegans body wall muscle. In: WormBook: The Online Review of C. elegans Biology [Internet]. Pasadena (CA): WormBook; 2005-2018. Figure 1, The body wall muscle of C. elegans. Available from: https://www.ncbi.nlm.nih.gov/books/NBK426064/figure/bodywallmuscle_figure1/

IV. Rho Family GTPases and Signaling Roles in Cytoskeleton Dynamics

Small GTPases, also known as small guanosine triphosphatases, or small G-proteins, are members of the Ras superfamily and act as molecular switches. They become activated upon binding to GTP and inactivated by hydrolysis of GTP to GDP. In humans, the superfamily is comprised of over 150 different low-molecular-weight proteins that are evolutionarily conserved with important roles in the regulation of a broad range of cellular processes. Some of these functions include cell differentiation, cell proliferation, cell migration, vesicle trafficking, cytoskeleton dynamics, in addition to nuclear import and/or export. This large group of small GTPases is divided into the five branches of subfamilies based on structure and function which consists of the Ras, Rho, Rab, Arf, and Ran-families (Wennerberg et al., 2005).

The Ras protein was the founding member of the superfamily and serves as the reference protein for small GTPases. Ras was identified in "**Ra**t **s**arcoma" and is implicated in most cancers due to its oncogenic nature when misregulated. The Ras-family GTPases regulate cell growth, proliferation, and differentiation (Hancock 2003). "**Ra**s in **b**rain", also known as Rab GTPases are among the largest group of small GTPases that control intracellular membrane trafficking consisting of about 60 members that have diverse functions in humans (Stenmark, 2009). The "**A**denosine diphosphate-**R**ibosylation **F**actor" or Arf-family is involved in various cell behaviors including cell proliferation, motility, differentiation, as well as regulation of membrane trafficking and cytoskeleton function (Kahn et al., 2005). The "**Ra**s-related **n**uclear protein" or Ran is a single protein that makes up its own subfamily due to its major structural difference in that it lacks a highly conserved membrane anchoring motif at the C terminus found in many other small GTPases. Additionally, it is found in both the nuclear and cytoplasmic portions of the cell which

facilitates its role in transporting molecules through the nuclear pore complex as well as microtubule polymerization and formation of mitotic spindles during cell cycle progression (Boudhraa et al., 2020). "**R**as-**ho**mology" or Rho-family GTPases or RhoG proteins have important roles in cytoskeletal organization, cell polarity, cell migration, and cell membrane protrusion (Reiner and Lundquist, 2018) and will be the focus of this chapter.

Rho GTPases are monomeric proteins that are typically ~20 kDa and comprised of a G domain, an insert region, a hypervariable region, and a functional C-terminal extension, that have been structurally and functionally conserved throughout evolution. The G domain serves as the main functional unit of the GTPase activity and consists of five G motifs made up of five alpha-helices and a 6-stranded mixed beta-sheet. Within the G domain are five G motifs that are highly conserved among all regulatory GTPases and are involved in the binding of the guanine nucleotide, which influence affinity and contribute to the regulation of GTP hydrolysis. Switch I and switch II are functional core elements that undergo conformational changes upon GTP binding (Reiner and Lundquist, 2018). Switch I is essential for the downstream effector signaling function, and when mutated inhibits interaction with downstream partners. Switch II is important for the coordination of both intrinsic and GAP-regulated GTPase activity. The insert region is a helical stretch of 10-15 residues that facilitates Rho signaling through interaction with GEFs to promote guanine nucleotide exchange. Rho GTPases have a C-terminus that includes a hypervariable region that partially functions as a protein binding site and at the C-terminus is a CAAX-box motif that is site of isoprenylation , which is required for membrane binding (Schaefer, 2014).

Rho proteins cycle between active (GTP-bound) and inactive (GDP-bound) states. The cycling is mainly controlled by two classes of regulators, guanine-nucleotide exchange factors

(GEFs) and GTPase activating proteins (GAPs). GEFs promote the exchange of GDP to GTP-bound Rho GTPase. The action of the GEF, which binds to the GTPase, promotes the release of GDP, and is thus the rate-limiting step in the activation process. The GAP can bind the GTP-bound GTPase then activate the intrinsic GTPase activity and hydrolyze GTP to GDP (Schmidt and Hall, et al., 2002). The binding of Rho•GTP to downstream effector proteins results in signal transduction usually mediated through cell surface receptors, including integrins, cadherins, cytokine receptors, Tyr kinase receptors, and G-protein coupled receptors (Rossman et al., 2005). In contrast, GAPs stimulate hydrolysis of GTP to GDP within the small GTPase yielding inactive (GDP-bound) small GTPases. Most small GTPases have weak intrinsic GTPase activity. However, this process is typically very slow and likely is inefficient in the context of the signal transduction necessary for cellular processes, thus requiring the incorporation of GAP regulation to the pathway to speed up hydrolysis (Bernards and Settleman, 2004). Additionally, the third and less characterized class of small GTPase regulators includes the guanine nucleotide dissociation inhibitors (GDI) which sequester GDP-bound GTPases in the cytosol, thus preventing localization to membranes or GEF activation. While the majority of Rho GTPase signaling involves the cycling regulated by GEFs, GAPs, and GDIs, as shown in Figure 1.3 and 1.4) there are some exceptions to consider.

Rho family proteins, consisting of over 20 members are evolutionarily conserved regulators of a wide range of cellular processes. There are 10 Rho proteins that are considered classical GTPases controlled by the GTP-GDP cycling via GEF and GAP proteins. The remaining members are known as ‘atypical’ Rho GTPases characterized as either GTPase deficient or fast-cycling Rho GTPases (Aspenström, 2017). Canonical RhoA, RAC1, and Cdc42 are the most

extensively studied of all Rho family members with each distinctly contributing to the regulation of actin cytoskeleton dynamics in both motile and sessile cell types. RhoA activation promotes the formation of stress fibers made of actin and myosin in addition to focal adhesion assembly. RAC1 promotes the formation of lamellipodia and membrane ruffling, while Cdc42 stimulates the formation of the actin-rich filopodia (Nobes and Hall, 1999). Interestingly, crosstalk between these three Rho GTPases not only regulates each other's activity but also plays a major role in the dynamic coordination of cytoskeleton architecture in cells. CDC42 can activate RAC1, which promotes suppression of RhoA, due to the antagonistic nature of the contractile forces induced by RhoA on the adhesive forces stimulated by RAC1. At the trailing edge of a moving cell (rear of the cell), RhoA-driven retraction of membrane and cell-matrix adhesions occurs, while CDC42 and RAC1-mediated expansion of cellular protrusions and cytoskeleton polarization continue in the direction of migration (the front of the cell) (Iden & Collard, 2008; Nguyen, Kholodenko, and von Kriegsheim, 2018).

Rho•GTP stimulates rapid signal transduction through interactions with downstream effectors such as protein kinases, actin regulators, and adaptor proteins. As previously mentioned, Rho activation is regulated through cell surface receptors like integrins, cadherins, cytokine receptors, tyrosine kinases, and G-proteins coupled receptors (Rossman et al., 2005) and thus have the capacity to promote a wide range of cellular behaviors including the regulation of actin cytoskeleton, cell-cycle progression, and gene transcription. Previous studies have shown Rho proteins to play major roles in cell adhesion, migration, phagocytosis, cytokinesis, neuron development, cell morphology, polarity, growth, and survival. Due to the broad range of cellular processes a single Rho protein can influence depending on the cell type and stimulus, it

is required that these proteins are tightly regulated in a spatiotemporal manner (Hodge and Ridley, 2016). To achieve this level of tight regulation many Rho GTPases, undergo post-translational modifications (PTMs) which in concert with GDP-GTP cycling, G protein regulators, and protein interactions control GTPase specificity and activity. Rho GTPase proteins are regulated by a variety of PTMs including lipid modifications, phosphorylation, sumoylation, and ubiquitylation (Olsen, 2018; Navarro-Lérida, et al., 2021).

Post-translational prenylation and palmitoylation lipid modification of Rho GTPases are important for distinct membrane compartment localizations in addition to mediating interactions with specific RhoGEFs and downstream targets. Prenylation of the C-terminus is among the most common PTM of Rho GTPases that yields the addition of either a farnesyl (C15) or geranylgeranyl (C20) 15- or 20-carbon chain to the cysteine residue in the CAAX motif (Katayama et al., 1991 & Adamson et al., 1992) catalyzed by farnesyltransferase (FT) and geranylgeranyltransferase (GGT) enzymes, respectively. The three C-terminal residues subsequently undergo proteolysis followed by the carboxymethylation of the prenylated cysteine residue. The nature of the C-terminal residue X indicates if a protein is an FT or GGT-1 substrate with FT favoring Met, Ser, Gln, or Cys for X, and GGT-1 preferring Leu or Ile for X. However, in the case of Rho GTPases, a geranylgeranyl (C20) is typically bound to the target protein with some exceptions (Berndt et al., 2011). Palmitoylation is involved in the tethering of G proteins to membrane cytosolic surfaces. This reversible modification yields the thioesterfication of specific cysteine residues of the target protein with a fatty acetyl palmitoyl group, ultimately enabling dynamic membrane interactions and downstream signaling (Wan et al., 2007). Actin polymerization at the plasma membrane via RAC1 mediated stimulation occurs in a specific PTM order, first Cys189 undergoes prenylation

followed by the palmitoylation of Cys178, which increases RAC1 stability, by targeting the protein to the actin cytoskeleton-linked detergent-resistant membrane regions. Furthermore, palmitoylation-deficiency of RAC1 at Cys178 in cells results in defective cell spreading and migration. Consequently, this deficiency also inhibits GTP loading in parallel with reduced activation of the downstream effector PAK at the plasma membrane (Navarro-Lérida et al., 2012). Although this demonstrates lipid modifications significantly affect Rho GTPase activity directly impacting the coordination of cytoskeleton architecture, phosphorylation also have essential roles in mediating these functions.

Phosphorylation provides additional spatiotemporal control to their target G-proteins' functional regulation. This can occur in two ways: (1) residues at the C terminus near lipid modifications can be phosphorylated and alter Rho GTPase localization, and/or (2) residues within the GTPase domain undergo phosphorylation and affect the GTP-GDP cycling, and/or downstream effector interactions. There are several examples of Rho GTPases that are regulated by phosphorylation in various cell types, with RhoA being the first shown to use this mechanism (Lang et al, 1996). Phosphorylation of RAC1 has been shown to ultimately affect cell morphology due to RAC1 mediated actin cytoskeleton and adhesion functionality. Specifically, Tyr64 phosphorylation directly influences endothelial cell spreading on fibronectin in vitro. Inhibiting phosphorylation at this site yields increased cell spreading and increased GTP binding, while a phosphomimic substitution promotes cell rounding and lack of fully developed lamellipodium or focal adhesion complexes, rendering this site as being necessary for negatively regulating RAC1 (Chang et al., 2011). Other examples include phosphorylation of Ser71 via AKT to increase GDP bound RAC1 (Kwon et al., 2000) and Thr108 via ERK resulting in nuclear localization and

preventing RAC1 activation during cell migration (Tong et al., 2013). These examples illustrate the important regulatory pathways that phosphorylation targets to mediate a wide range of Rho GTPase activities to confer specificity in a context-dependent manner.

Ubiquitylation and sumoylation are PTMs that are important for regulating Rho GTPase activity and turnover. In brief, ubiquitylation is a three-step process that results in polyubiquitin chains covalently bound to the Lys48 residues of the target protein facilitated by ubiquitin-activating (E1), ubiquitin-conjugating (E2), and ubiquitin ligase (E3) enzymes. This modification targets the protein for degradation by the 26S proteosome, thus directly regulating protein turnover. However, the mono-ubiquitylation and polyubiquitylation of other lysine residues of Rho GTPases also alter the localization to specific subcellular compartments, due to its role in mediating the precise regulation of GTPases in space and time (Hodge and Ridley, 2016). The ubiquitylation of RhoA is the most characterized of the Rho family and is ubiquitinated by various E3 ligase complexes, further suggesting that this PTM is controlled in a complex manner to facilitate specificity depending on stimuli and cell type. During cell migration, the E3 ligase complex SMURF1 is recruited to the cell's leading edge, and Lys6 and Lys7 of RhoA are ubiquitylated. This results in proteosome-mediated degradation of RhoA preventing its ability to stimulate stress fiber formation, consequently promoting lamellipodia protrusion by RAC (Deng & Huang, 2014) (Wang et al., 2003). Sumoylation is less characterized in the Rho GTPase family with RAC1 being the only one shown to undergo this modification. While the sumoylation of RAC1 is not essential for its activation it has been shown to enhance GTP binding and lamellipodia formation and cell migration (Castillo-Lluva et al., 2010).

Generally, phosphorylation, ubiquitylation, and sumoylation are not essential for the activation of Rho GTPases. However, the conformation changes of small G proteins that result from PTMs directly impact localization, functionality, and specificity. In most cases, the combinatorial effects of multiple PTMs and small GTPase regulators enhance the specificity that is required to coordinate the cytoskeleton architecture that drives essential and dynamic cellular functions that are dependent upon the stimulus and cell type. To date, there are approximately 145 RhoGEF and RhoGAP proteins that regulate 10 classical Rho-family molecular switch-proteins, providing an additional layer of complexity controlling Rho signaling specificity (Müller et al., 2020).

Rho-family Regulators: GEFs & GAPs

GTPase cycling between inactive and active states is tightly controlled and is essential for the dynamic regulation of a wide range of cellular behaviors in a spatiotemporal manner. The cycling effect of small GTPases is generally facilitated by two classes of regulators, including the guanine-nucleotide exchange factors (GEFs) and GTPase activation proteins (GAPs). However, there is a third and less characterized class known as guanine nucleotide dissociation inhibitor (GDIs), which are proposed to have functions that sequester GDP-bound or (inactive) small GTPases to the cytosol via binding to the switch regions of the target protein. However, the functional significance of GDIs is still poorly understood and GDIs are only known for a subset of regulatory GTPase families.

Guanine nucleotide-Exchange Factors (GEF) Regulation

Guanine-nucleotide exchange factors (GEFs) facilitate the exchange of GDP-bound to GTP-bound G protein, cycling from the inactive to the activated state of target small G proteins in response to a wide range of extracellular stimuli. As previously mentioned, Rho GTPases function as molecular switches by undergoing conformational changes in response to binding to GDP or GTP. Rho family GEFs are typically split into two structurally different groups known as DOCK and Dbl families. "**D**edicator **o**f **c**yto**k**inesis" or DOCK RhoGEFs, have two domains, the DOCK homology region (DHR) which is the lipid-binding domain for membrane localization, and the catalytic GEF domain, respectively (Hodge and Ridley, 2016). However, the focus of this section will be the Dbl family as it directly relates to their regulatory role in cytoskeleton dynamics via Rho GTPase interactions.

The Dbl family is the most prevalent of the RhoGEFs that harbor a Dbl-homology (DH) domain and an associated pleckstrin homology (PH) domain, commonly known as a DH-PH motif flanked by regions that have unique sequences rendering them specific to particular Rho GTPases. During activation of a small GTPase by a GEF, GTP is preferentially loaded in the binding pocket during nucleotide exchange because it exists at a greater concentration in cells as compared to GDP. The mechanism of the nucleotide exchange for RhoGEFs harboring DH domains is distinct to the interface established between a RhoGEF and its target Rho GTPase. The interface between various Dbl-proteins and GTPases form an adjacent interval of non-conserved residues that are vastly different between GTPases. This suggests a mechanism that confers the specificity of GEF-GTPase coupling, which is essential for the spatiotemporal regulation and coordination of cellular activities via GTPase activity (Worthylake et al., 2000; Schmidt and Hall, 2002).

The pleckstrin homology or PH domain is hypothesized to control plasma membrane localization and regulation of GEF activity via allosteric mechanisms upon phosphoinositide binding (Rossman et al., 2005). PH domains are located C-terminal to their associated DH domain and seem to be important for increased nucleotide exchange potential as compared to their respective DH domains. However, there is limited evidence to structurally distinguish the PH domain mechanism due to its close structural proximity to the DH domain, in addition to the varied lateral and rotational differences relative to the DH domain among the few solved structures.

Like GTPases, RhoGEFs also undergo PTMs that are essential for temporal regulation of their activities within the cell at specific time points during complex cellular processes. RhoGEFs undergo phosphorylation, ubiquitylation, and acetylation which directly influence the activation of their target GTPase. RhoGEF phosphorylation can occur via different mechanisms that are dependent upon the target RhoGEF and the type of kinase. Phosphorylation causes conformation changes in the catalytic region or regulates binding between a GEF and scaffolding proteins, which directly alter its activity. The majority of RhoGEFs are phosphorylated by tyrosine kinases, which cause activation. For example, phosphorylation of Thr678 of GEF-H1 mediated by ERK stimulates activation and interaction with RhoA. Once phosphorylation of a RhoGEF occurs it is activated and facilitates the exchange of GDP for GTP, and activation of the Rho GTPase ensues, however in some cases this PTM plays an inhibitory role for GEF activity. During early embryogenesis in mice, axon growth is temporally regulated by phosphorylation of RhoGEF DOCK6. During axon extension, protein phosphatase 2A (PP2A) dephosphorylates and activates DOCK6 to promote axon growth through activation of RAC1. Subsequent stimulation of TRKA, a nerve growth factor receptor, drives activation of AKT, phosphorylating DOCK6 thus preventing its GEF activity and

inhibiting axon extension (Miyamoto et al., 2013). RhoGEFs are also degraded via ubiquitylation pathways to maintain the appropriate balancing of certain regulatory pathways, similar to Rho GTPases. Song et al., 2015 provided the first evidence that acetylation of the RhoGEF, Net1A affects its localization and GTPase activity. In brief, Net1A harbors two nuclear localization sequences (NLSs) at the N-terminus, which sequesters it in the nucleus. The acetylation of residues near the more C-terminal NLS promotes its translocation to the cytoplasm to directly activate RhoA. While PTMs of RhoGEFs are necessary for the temporal regulation of the cycling requirement of Rho GTPases at distinct phases of cellular processes, complex formation is also important for controlling GTPase signaling.

The formation of complexes among RhoGEFs plays a significant role in the precise coordination of Rho GTPase regulation in cells. RhoGEFs can interact with specific proteins in response to extracellular stimuli to promote various functions. These assemblages among RhoGEFs can yield functional complexes with Rho GTPase targets, provide protection from degradation, as well as enhance the regulation of nucleotide exchange activity (Hodge and Ridley, 2016). Some well-characterized examples include Rac1/Cdc42-specific GEF, β-PIX forming a complex with the scaffolding Arf GAP GIT-1, and Rac1/Cdc42-target PAK, which promotes focal adhesion turnover and cell motility (Radu et al., 2014). In addition, I have shown (Moody et al., 2020) that the complex formed between Rho GEF PIX-1 and the scaffolding protein GIT-1 is important for the stabilization of PIX-1, as deficiency of GIT-1 yields a significant decrease in the level of PIX-1, in *C. elegans.* P-REX1, a RAC GEF, forms a complex with the RAC-target FLI1 establishing direct interaction with RAC1 to promote cell migration (Mauri et al., 2016). Another example is the stabilization of the GEF VAV1 promoted through the complex it forms with the

GTPase dynamin 2, which when inhibited targets VAV1 for lysosomal degradation (Razidlo, et al., 2013). Lastly, a subfamily of GEFs undergoes oligomerization through their distinct C-terminal RGS-like (RGL) domains. This function is proposed to be a mechanism of inhibitory regulation of GEF activity and GTPase activation. Loss of RGL domain function in these GEFs stimulates enhanced nucleotide exchange activity and RhoA activation (Chikumi et al, 2004). The combination of mechanisms that regulate GEF activity is important for the coordination, specificity, and function of Rho GTPases in a temporally controlled manner.

GTPase Activation Protein (GAP) Regulation

Rho GAPs are required for the inactivation of Rho GTPases. While the Rho GTPase itself has intrinsic hydrolysis activity, the rate at which this occurs is relatively slow, and thus, to meet the demands of rapid cellular signaling, GAPs function to rapidly catalyze this hydrolysis. Interestingly, there are approximately 80 encoded mammalian genes identified to harbor RhoGAP domains, yet there are only ~20 Rho GTPase genes. This suggests that GAP specificity needs to be tightly regulated to temporally control the GTPases they interact with to coordinate a wide range of cytoskeleton dynamics and gene expression. RhoGAPs represent a relatively large and diverse family of functional GTPase regulators, however, they do share some structural and mechanistic similarities.

Most RhoGAPs are typically multidomain proteins that have essential functions in several regulatory pathways, protein-protein interactions in addition to their GTPase activity regulation, thus yielding several subfamilies based on structure and functions. RhoGAPs are defined as proteins that possess a conserved catalytic ~190 residue domain containing a conserved arginine

residue, known as the ‘arginine finger’. This arginine residue is inserted into the active site of the target Rho GTPase and allows for the stabilization of a conformation needed for hydrolysis that leads to the inactivation of the GTPase (Amin et al., 2016). RhoGAP regulation can involve both activation and inhibitory functions that control Rho GTPase signaling.

Similar to Rho GTPases and GEFs, RhoGAPs undergo phosphorylation and ubiquitylation that can modulate their localization and activity. ARHGAP24 becomes activated upon phosphorylation of Ser402, which results in its translocation from the cytoskeleton network to the cytosol where it inactivates RAC1. In the mammalian brain, ubiquitylation of the ARHGAP32 is facilitated by interaction with two separate ubiquitin ligase complexes. First, the APC^{CDH1} complex induces ubiquitylation and ARHGAP32 interacts with the SMURF1 ligase complex which promotes stimulation of axon growth by negatively regulating RhoA (Hodge & Ridley, 2016). RhoGAP PTMs are one of the mechanisms that function in concert to achieve the specificity and tightly controlled regulation required for Rho GTPase signaling at distinct time points within the cell in response to extracellular stimuli in addition to complex formation.

RhoGAP proteins are typically large and contain other domains that regulate the localization and/or protein-protein interactions that play an essential role in controlling the specificity and coordination of interactions with Rho GTPases. The complexes that form between RhoGAPs and scaffolding proteins and/or cytoskeleton regulators provide temporal control of G protein cycling. Interestingly, Rho GTPase cycling dynamics are essential for the control that both classes of regulators (GEFs and GAPs) have in responding to extracellular stimuli as well as downstream target interactions.

Previous studies have demonstrated that the exclusive loss of function of the GEF or GAP of the same molecular pathway yields the same phenotype. For example in *Saccharomyces cerevisiae,* the budding location selection occurs at axial or bipolar sites in a cell-specific manner. This cellular function relies upon the GTPase cycling of the Ras-like GTPase BUD1, the GEF BUD5, and the GAP BUD2. Loss of function mutations in any of these three components results in random spatial patterning of the bud site in yeast (Park, Chant, & Herskowitz, 1993). Another example is embryonic cytokinesis defects found for loss of function for *rho-1* (RhoA), *rga-3* (RhoGAP), *rga-4* (RhoGAP), and *ect-2* (RhoGEF) in *C. elegans* (Morita et al., 2005; Schonegg et al., 2007; Jantsch-Plunger et al., 2000; Canman et al., 2008). Together these results suggest that the small GTPase cycling requires tight regulation to control signaling output to downstream targets. More importantly, this provides a useful genetic tool for the identification of unknown components of a cycling pathway through phenotypic observation.

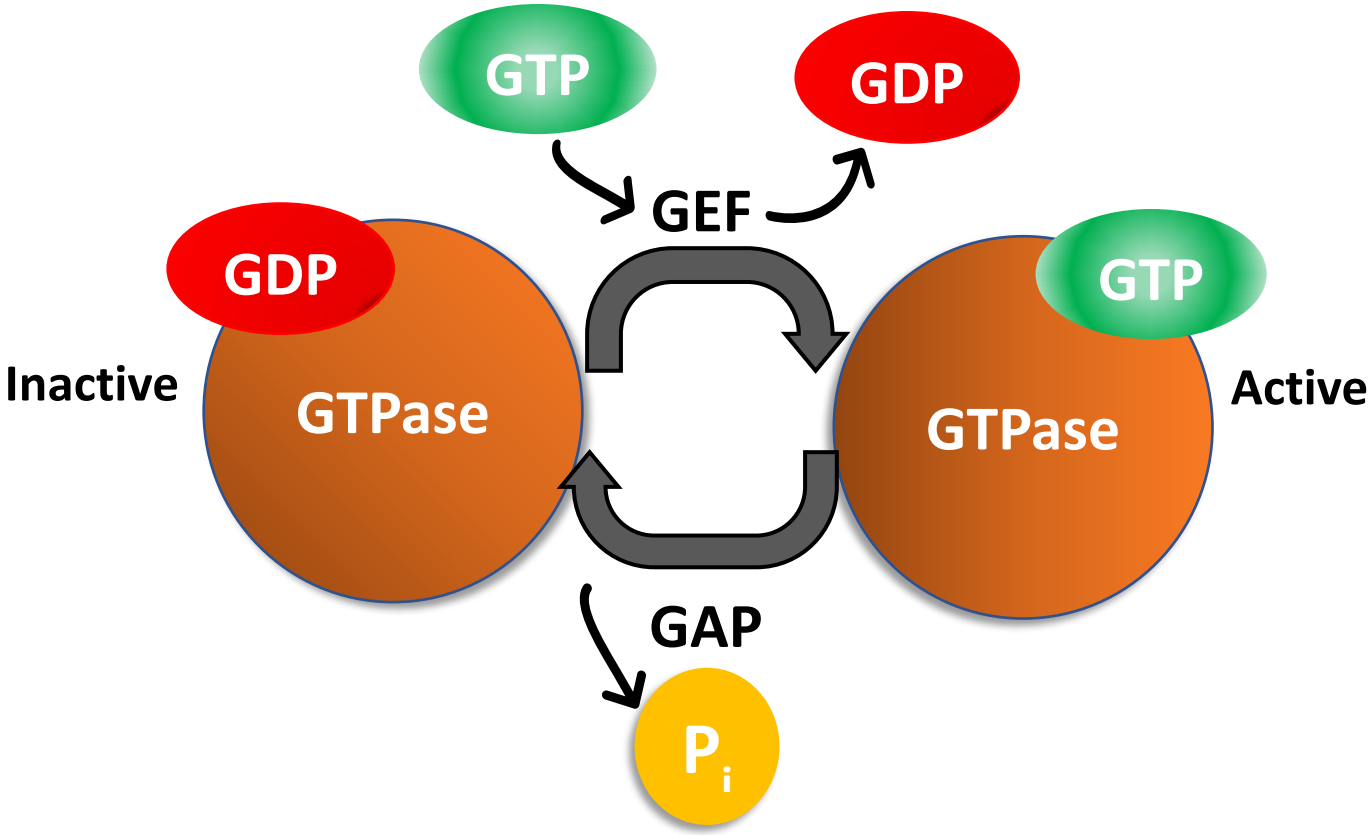

Figure 1.3 GEF and GAP proteins are two main classes regulators of GTPase activity. A simplified diagram showing the cycling mechanism of a Rho GTPase. Most Rho G proteins cycle between active (GTP-bound) and inactive (GDP-bound) states. The cycling is mainly controlled by two classes of regulators, guanine-nucleotide exchange factors (GEFs) and GTPase activating proteins (GAPs). GEFs facilitate the exchange of GDP to GTP-bound Rho GTPase due to increased levels of free GTP as compared to GDP in cells. This difference in concentration promotes GTP loading thus directly activating the small GTPase to participate in downstream signal transduction (Schmidt and Hall, et al., 2002). The binding of Rho•GTP to effector proteins activates signal transduction involving cell surface receptors, including integrins, cadherins, cytokine receptors, Tyr kinase receptors, and G-proteins coupled receptors (Rossman et al., 2005). In contrast, GAPs stimulate hydrolysis of the active (GTP-bound) small GTPase yielding inactive (GDP-bound) small GTPases. The intrinsic activity of the small GTPase suggests that this alone would be sufficient to hydrolyze bound GTP to GDP. However, this intrinsic activity is typically very slow and likely is inefficient in the context of signal transduction necessary for cellular processes, thus requiring the incorporation of GAP regulation in the pathway to speed up hydrolysis.

Reiner DJ, Lundquist EA. Small GTPases. In: WormBook: The Online Review of C. elegans Biology [Internet]. Pasadena (CA): WormBook; 2005-2018. Available from: https://www.ncbi.nlm.nih.gov/books/NBK19741/

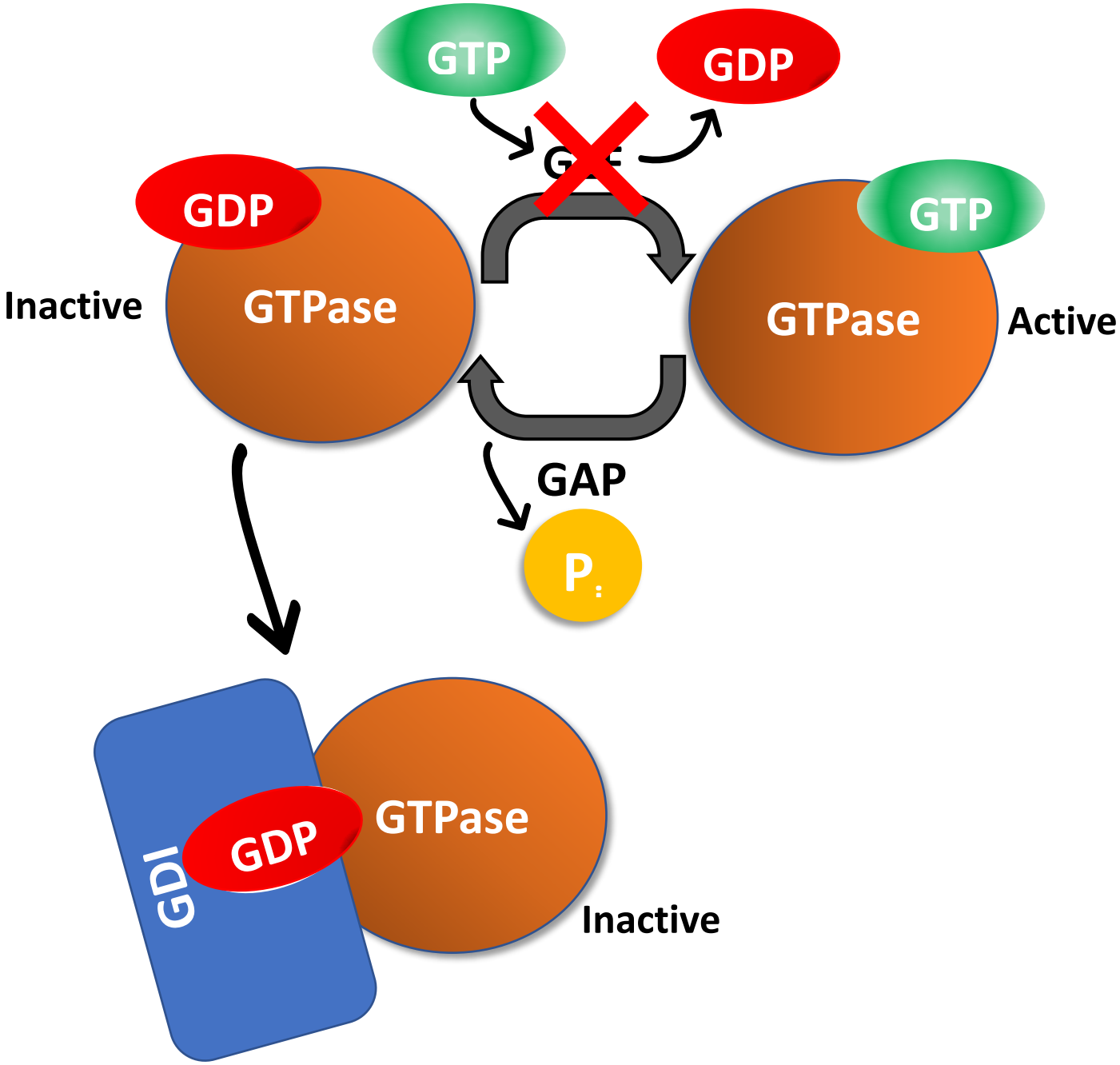
GTP
GDP
GDP
Inactive
GTPase
GTP
GTPase
Active
GAP
P:
GDI
GDP
GTPase
Inactive

Figure 1.4 GDIs are the third and less characterized class of regulators that facilitate GTPase activity. A model figure showing the disruption of classic Rho GTPase activity by a Guanine nucleotide dissociation inhibitor (GDI). This type of regulator functions to sequester GDP-bound GTPases in the cytosol, thus preventing membrane localization or GEF activation by binding to the switch regions of the target GTPase proteins. This activity can be reversed upon the GDI releasing the inactive GTPase upon interacting with additional proteins or in response to external signaling mechanisms.

Reiner DJ, Lundquist EA. Small GTPases. In: WormBook: The Online Review of C. elegans Biology [Internet]. Pasadena (CA): WormBook; 2005-2018. Available from: https://www.ncbi.nlm.nih.gov/books/NBK19741/

V. Integrin adhesion complexes

The adhesion of cells to the ECM is facilitated by a complex network of adhesion receptors and signaling proteins, which form IACs. IAC signaling is necessary for various cellular activities which require precise mechanisms that regulate intracellular signaling pathways in response to specific environmental stimuli. The dynamic nature of IACs involves assembly, disassembly, and specific localization, which are tightly regulated by cell-surface activity, integrin trafficking, intracellular signaling, and mechanotransduction mechanisms (Humphries et al., 2019).

The central component of these networks is the heterodimeric transmembrane protein called integrin. These adhesion receptors link the actin cytoskeleton to the extracellular environment via bi-directional signaling as shown in Figure 1.6C (Peters et al., 2011). IACs (aka focal adhesions or adhesomes) consist of noncovalently-linked α-integrin and β-integrin subunits that consist of short cytoplasmic tails and relatively large extracellular domains that facilitate the formation of hundreds of different proteins in a complex both in the ECM and intracellularly (Iwamoto & Calderwood, 2015). Extracellular integrin interactions trigger a cascade of signaling events that influences cell behaviors such as adhesion, proliferation, survival or death, shape, polarity, motility, gene expression, and differentiation, predominantly via effects on the cytoskeleton (Takeda, Ye, and Simon, 2007). The bi-directional signaling capacity of integrin is dynamic and provides important functions in a wide range of cell types and essential cellular functions.

Studies of platelets, leukocytes, and tissue culture cells indicate that integrins are expressed on the cell surface in a compact-bent or inactive state, unable to bind to their extracellular targets, but can become “activated” to bind via several triggers (chemokine to chemokine receptor

interaction, local increase in PIP_2 or calpain) that lead to binding of the cytoplasmic tail of β-integrin to talin. Talin binding drives integrin to a more open conformation, competent to bind extracellular targets. Kindlin is similar in domain composition to talin and is also involved in integrin activation by clustering of talin-activated integrins, at least mammalian platelets (Ye et al., 2013). Not only do the conformational changes that facilitate the activation of integrins they also increase the affinity for binding to ECM ligands and ultimately the formation of specialized adhesion structures.

The adhesion of cells to the ECM via IACs is a complex process that is essential for cellular functions including tissue formation and cell migration. The conformational activation of integrin is followed by the downstream interactions with several multivalent substrates that form large networks of protein complexes that establish cellular adhesions. In stationary cells like muscle cells, these complexes are rather stable, but in motile cells, they are dynamic, with new complexes assembled at the leading edge and older complexes disassembled at the trailing edge as illustrated in Figure 1.5 (Frame et al., 2002; Ananthakrishnan and Ehrlicher, 2007). IACs of migrating cells can be categorized into different classes based on their maturation and morphology. Nascent adhesions are characterized as small complexes with a turnover rate of about 1 minute. They are found at the edge of the lamellipodium, and consist of integrin, paxillin, and talin. A small portion of nascent adhesions will mature into focal complexes with a larger size and slower turnover. Subsequently, these focal complexes will mature into focal adhesions which are larger and more stable structures. In some cell types such as fibroblasts and platelets, focal adhesions become fibrillar adhesions the largest and most stable type of IACs. Each of these classes functionally regulates force transmission from the actin cytoskeleton to the

ECM. The spatial organization of IAC components plays an important role in controlling the assembly and coordination IACs with a multitude of protein-protein interactions involved in signal transduction (Chastney et al., 2021). Although we understand the steps involved in the formation of IACs, we do not know how the composition of an IAC is determined or what determines where an IAC forms.

Based on previous studies in the Benian lab and other labs, distinct IAC protein complexes have been identified to localize at three locations in *C. elegans* muscle as shown in Fig. 1.7 (Qadota et al., 2017). These sites include the M-lines, dense bodies, and attachment plaques between adjacent muscle cells also known as muscle cell boundaries. Figure 1.6A is a schematic diagram illustrating the structure of vertebrate muscle costameres attaching the most peripheral myofibrils to the cell membrane (Ervasti et al., 2003). These costameres facilitate the transmission of lateral forces during muscle contraction from the cell membrane to the ECM. *C. elegans* myofibrils are anchored to the cell membrane at both the dense bodies and M-lines, thus serving a similar function to vertebrate costameres. Previous work involving a combination of cloning genetically identified genes, mutant analysis, yeast two-hybrid screens, assays, in vitro biochemical binding experiments, and immunolocalization, we understand complex protein interactions at each site. Also note that at each site, the IAC begins with the same set of core proteins (UNC-52 (perlecan), PAT-2 and PAT-3 (integrins), UNC-112 (kindlin), PAT-4 (ILK), PAT-6 (α-Parvin), (etc. shown in yellow in Figure 1.7, and then deeper into each structure, the proteins are specific for those structures (red for the M-line, and green for the dense body) (Qadota et al., 2017). IACs of the muscle cell boundary consist of a subset of proteins found at the dense body.

In *C. elegans* muscle cell boundary (MCB) is characterized by a zipper-like structure that lies between adjacent muscle cells divided by a very thin layer of ECM (Qadota et al., 2017). In Moody et al., 2020 we provide the first evidence for the site-specific assembly of IACs at MCBs requiring the function of the RhoGEF PIX-1. Assessment of loss of function *pix-1* mutants exhibits loss of core IAC components, PAT-6, UNC-112, UNC-52, and PAT-3 only at the muscle cell boundary and reduced whole animal locomotion in swimming and crawling assays. Furthermore, several studies have provided evidence that mutations of several of these IAC components are associated with cardiomyopathies and muscular dystrophies.

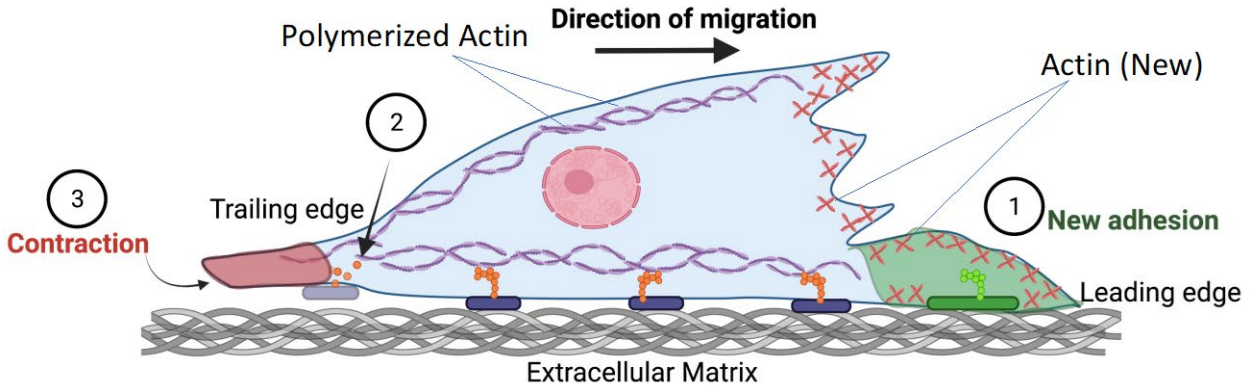

Figure 1.5 Integrin adhesion complexes (IACs) are assembled and disassembled via a dynamic, stepwise mechanism in motile cells. A schematic representation of integrin adhesion complex regulation during cell migration. Protrusion of the cell occurs in the direction of cell migration at the leading edge proceeded by (1) the formation of new contacts or adhesions (green highlighted region) between the leading edge of the cell and the extracellular matrix via the assembly of new complexes. This quickly results in tension created in the actin cytoskeleton, followed by (2) the release of adhesion complexes between the cell and the ECM at trailing edge due to the disassembly of IACs in the opposite direction of cell migration. Finally, the release of adhesion contacts between the cell and the ECM causes (3) contraction at the trailing edge (red highlighted region), ultimately allowing the cell to progress in the direction of migration (Frame et al., 2002; Ananthakrishnan and Ehrlicher, 2007). *Made using BioRender

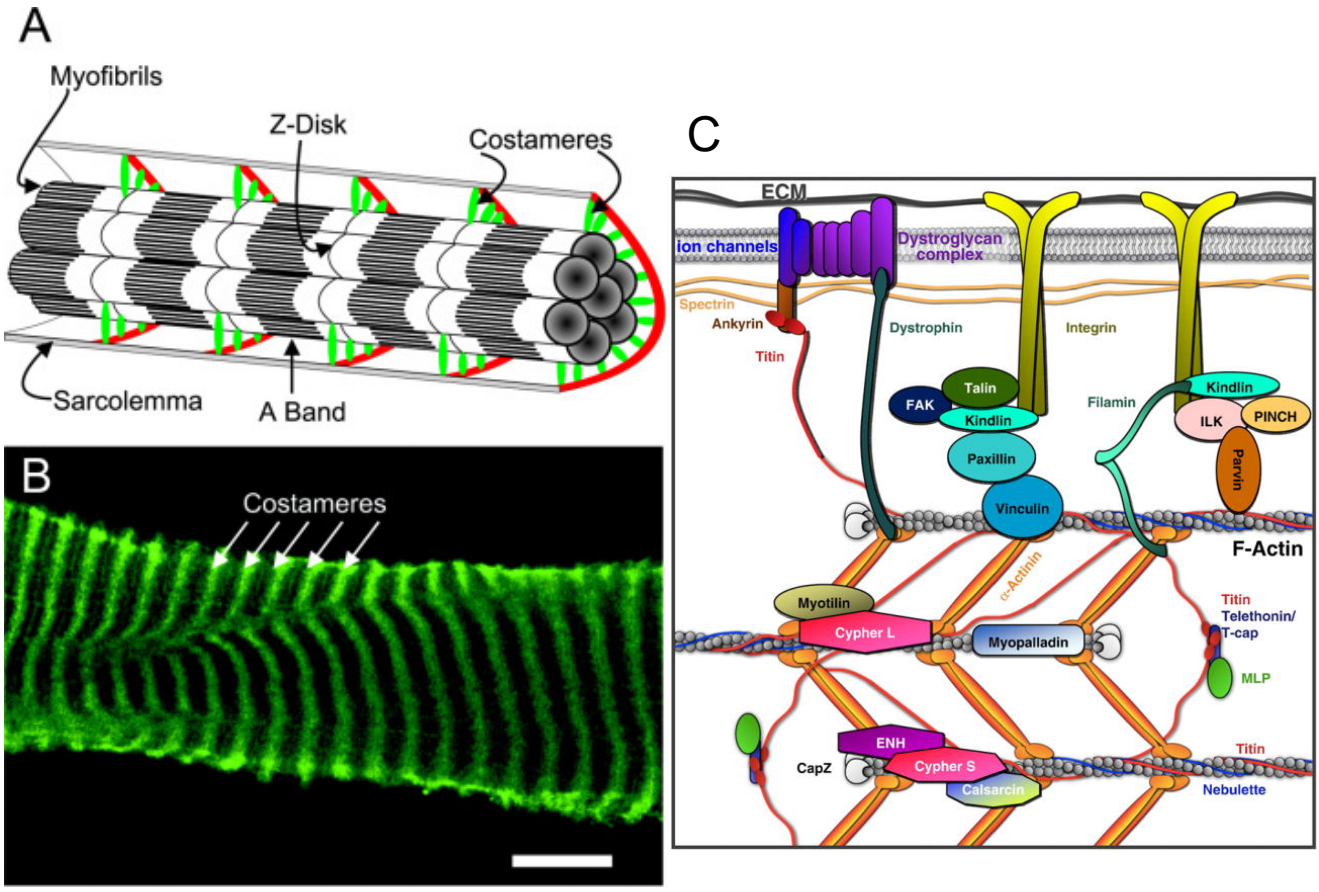

Figure 1.6 Costameres are IACs in vertebrate striated muscle (skeletal and heart muscle). **A.** The centrally located myofibrils in mammalian striated muscle are anchored together via intermediate filaments (not shown). The myofibrils at the periphery of the cell are attached to the sarcolemma, or muscle cell membrane (red lines) via costameres (green lines) , which are structurally and functionally analogous to focal adhesions in non-muscle cells. **B.** Muscle cell membrane mechanically removed from the human skeletal muscle cell immunostained with a costamere marker, that are arranged in register with the Z-disks (A and B from J.M. Ervasti, 2003). **C.** Simplified depiction of protein complexes at costameres that are associated with Z-line. The dystrophin glycoprotein complex and integrin–vinculin–talin complex are two the major protein complexes (left to right) that act as bridges between the ECM and actin filaments of the Z disks in muscle. The two integrin complexes are based on current knowledge in the field, however currently there is not one consensus complex (from Peter et al., 2011).

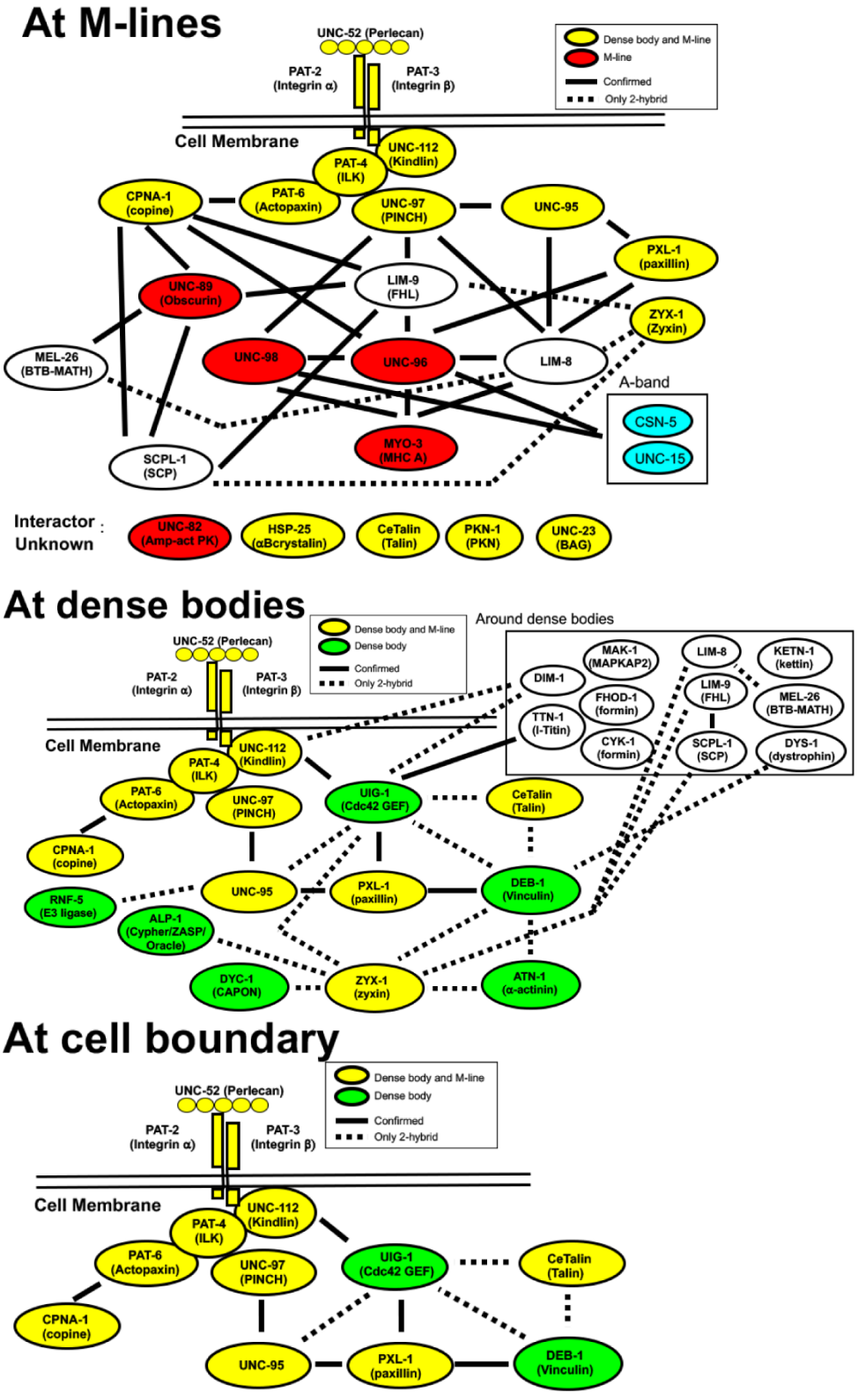
At M-lines
UNC-52 (Perlecan)
PAT-2 (Integrin α)
PAT-3 (Integrin β)
Dense body and M-line
M-line
Confirmed
Only 2-hybrid
Cell Membrane
UNC-112 (Kindlin)
PAT-4 (ILK)
CPNA-1 (copine)
PAT-6 (Actopaxin)
UNC-97 (PINCH)
UNC-95
PXL-1 (paxillin)
UNC-89 (Obscurin)
LIM-9 (FHL)
ZYX-1 (Zyxin)
MEL-26 (BTB-MATH)
UNC-98
UNC-96
LIM-8
A-band
CSN-5
UNC-15
MYO-3 (MHC A)
SCPL-1 (SCP)
Interactor : Unknown
UNC-82 (Amp-act PK)
HSP-25 (αBcrystalin)
CeTalin (Talin)
PKN-1 (PKN)
UNC-23 (BAG)
At dense bodies
Dense body and M-line
Dense body
Confirmed
Only 2-hybrid
Around dense bodies
UNC-52 (Perlecan)
PAT-2 (Integrin α)
PAT-3 (Integrin β)
Cell Membrane
UNC-112 (Kindlin)
PAT-4 (ILK)
PAT-6 (Actopaxin)
UNC-97 (PINCH)
UIG-1 (Cdc42 GEF)
CeTalin (Talin)
CPNA-1 (copine)
UNC-95
PXL-1 (paxillin)
DEB-1 (Vinculin)
RNF-5 (E3 ligase)
ALP-1 (Cypher/ZASP/ Oracle)
DYC-1 (CAPON)
ZYX-1 (zyxin)
ATN-1 (α-actinin)
MAK-1 (MAPKAP2)
LIM-8
KETN-1 (kettin)
DIM-1
LIM-9 (FHL)
FHOD-1 (formin)
MEL-26 (BTB-MATH)
TTN-1 (I-Titin)
CYK-1 (formin)
SCPL-1 (SCP)
DYS-1 (dystrophin)
At cell boundary
Dense body and M-line
Dense body
Confirmed
Only 2-hybrid
UNC-52 (Perlecan)
PAT-2 (Integrin α)
PAT-3 (Integrin β)
Cell Membrane
UNC-112 (Kindlin)
PAT-4 (ILK)
PAT-6 (Actopaxin)
UNC-97 (PINCH)
UIG-1 (Cdc42 GEF)
CeTalin (Talin)
CPNA-1 (copine)
UNC-95
PXL-1 (paxillin)
DEB-1 (Vinculin)

Figure 1.7 Integrin adhesion cells are localized at M-lines, dense bodies, and muscle cell boundaries in *C. elegans* body wall muscle. Previously published work including the cloning of mutationally defined genes, conducting yeast 2 hybrid screens, localizing proteins with antibodies and GFP fusions, and characterization of mutants have identified complex protein interactions required to assemble M-lines, dense bodies, and adhesion plaques at the muscle cell membrane. Each of these structures begin with the transmembrane heterodimer protein, integrin. Notice how the proteins near the cell membrane are the same in M-lines, dense bodies, and adhesion plaques (shown in yellow), and then become more specific deeper into the cell, in which the M-line-specific proteins are red, and dense body specific proteins are green. Adhesion plaques at the muscle cell boundaries consist of a subset of proteins found in dense bodies. Proteins in parentheses are the human orthologs. Solid lines indicate protein-protein interactions that have been verified by biochemical binding experiments using purified proteins, while the dashed lines indicate those interactions that have only been suggested by yeast 2-hybrid screens or assays.

Gieseler, K., Qadota, H., & Benian, G. M. (2017). Development, structure, and maintenance of C. elegans body wall muscle. *WormBook : the online review of C. elegans biology*, *2017*, 1–59. https://doi.org/10.1895/wormbook.1.81.2.

Chapter 2

The Rho-GEF PIX-1 Directs Assembly or Stability of Lateral Attachments Structures between Muscle Cells

The contents of this chapter were published in Moody et al., Nat. Comm., October 2020.

Introduction

In striated muscle, sarcomeres are attached end to end to create myofibrils that extend the length of the elongated muscle cell. The myofibrils are tightly packed and connected to each other via intermediate filaments. Myofibrils in both skeletal and cardiac muscle cells are connected at the periphery of the muscle cell to the cell membrane and extracellular matrix (ECM) via costameres, muscle-specific integrin adhesion complexes (IACs). Although detectable beneath the entire sarcolemma of skeletal muscle, the dystrophin-glycoprotein complex (DGC) is enriched at costameres. (Ervasti et al., 2008) Genetic deficiencies of dystrophin and a number of DGC proteins result in muscular dystrophies. Deficiency of costameric component integrin α7, results in a congenital myopathy. (Hayashi et al., 1998) Heterozygous mutations in several other costameric proteins result in dilated and hypertrophic cardiomyopathy including vinculin, α-actinin-2, four and a half LIM protein-2 (FHL2), and ILK. (Benian and Epstein, 2011)

C. elegans is an excellent genetic model organism in which to learn new principles of sarcomere assembly, maintenance, and regulation. (Gieseler et al., 2017) The major striated muscle of *C. elegans* is found in the body wall and is required for locomotion. Similar to striated muscle in other animals, the thin filaments are attached to Z- disks (called dense bodies), and the thick filaments are attached to M-lines. However, the myofibrils are restricted to a narrow ~1.5 μm zone adjacent to the cell membrane along the outer side of the muscle cell, and all the dense bodies and M-lines are anchored to the muscle cell membrane and ECM. This architecture, together with what is known about the molecular com- position of these structures, indicates that nematode dense bodies and M-lines also act as costameres. *C. elegans* body wall muscle also has

IACs at the muscle cell boundaries, (Qadota et al., 2017) where they form attachment plaques that anchor the muscle cell to a thin layer of ECM that lies between adjacent muscle cells.

IACs (aka focal adhesions or adhesomes) consist of the transmembrane protein integrin and hundreds of different proteins in a complex both in the ECM and especially intracellularly. (Anthis and Campbell, 2011), (Bachir et al., 2014), (Sun et al., 2014) and (Horton et al., 2015) IACs are important for many cell types. The adhesion of cells to a matrix is crucial for both tissue formation and for cell migration. In stationary cells like muscle, these complexes are rather stable, but in motile cells they are dynamic, with new complexes assembled at the leading edge and older complexes disassembled at the trailing edge. (Anthis and Campbell, 2011) Studies of platelets, leukocytes, and tissue culture cells indicate that normally when integrins are expressed on the cell surface they are in a compact or bent or inactive state, unable to bind to their extracellular targets, but can become "activated" to bind via several triggers (chemokine to chemokine receptor interaction, local increase in PIP2 or calpain) that lead to binding of the cytoplasmic tail of β-integrin to talin. Talin binding drives integrin to a more open conformation, competent to bind extracellular targets. (Todokoro et al., 2003) Kindlin, which is similar in domain composition to talin, is also involved in integrin activation by clustering of talin-activated integrins, at least in mammalian platelets. (Ye et al., 2013) Although we understand the steps involved in the formation of IACs, (Bachir et al. 2014), (Sun et al., 2014) and (Horton et al., 2015) we do not know how the composition of an IAC is determined, and we do not know what determines where an IAC forms. This question is especially important for skeletal muscle cells, in which one type of IAC (the costamere) forms at regular intervals and anchors the peripherally located myofibrils to the sarcolemma and ECM at the level of Z-disks.

Here, we show that through a genetic screen in *C. elegans*, identification of a signaling molecule, PIX-1 (orthologous to β- PIX in mammals), that is required for assembly or stability of IACs only at muscle cell boundaries. PIX proteins consist of SH3 and RhoGEF domains, and a coiled-coil region, and are known to act as guanine exchange factors (GEFs) for activation of the small GTPases, Rac1 and/or Cdc42. Antibodies to PIX-1 localize to all three types of muscle IAC-muscle cell boundaries, M-lines and dense bodies. A biochemical pathway for PIX-1 can be inferred from studies of PIX proteins in mammals and pix-1 in several non-muscle tissues *in C. elegans.* Analysis of loss of function mutants for genes encoding proteins at all known steps of this pathway show defects of muscle cell boundaries similar to *pix-1* mutants. As compared to wild type, a *pix-1* null mutant and a *pix-1* missense mutant show reduced levels of activated (GTP bound) Rac in muscle. Both deficiency and overexpression of wild-type PIX-1 protein result in disrupted muscle cell boundaries and decreased whole nematode locomotion, suggesting that the level of PIX-1 protein needs to be tightly regulated. Our results demonstrate that the PIX signaling pathway has an important function in muscle.

Results

We screened the Million Mutation Project (MMP) (Thompson et al., 2013) mutant strains for defects in integrin adhesion complex organization. After screening 574 strains, we identified one strain, VC20386, that by immunostaining showed lack of localization of one IAC component, PAT-6 (α-parvin), at muscle cell boundaries, but normal localization of PAT-6 at M-lines and dense bodies (Fig. 1a). Using a combination of outcrossing to wild-type and SNP mapping, we determined that this phenotype is due to a nonsense mutation in a single gene, *pix-1* (see "Methods"), with allele designation *gk299374*. We then obtained six additional strains from the *Caenorhabditis* Genetics Center (CGC) that contained mutations in *pix-1*. Two are intragenic deletions, one is a nonsense mutation, and three are missense mutations. Except for the deletions, these additional *pix-1* alleles come from the MMP. WormBase indicates that there are 17 MMP alleles of *pix-1*, but the ones we chose to study either have nonsense mutations (the original one from our immuno-screening, and one more), or have missense mutations residing in conserved protein domains (see below for PIX-1 domain structure). By immunostaining, we found the absence of PAT-6 at the muscle cell boundaries in four out of six of these additional strains (Fig. 1b; Supplementary Fig. 1). The two intragenic deletion alleles, *gk416* and *ok982,* and the additional nonsense allele, *gk299384*, show the same boundary defect phenotype as the original allele, *gk299374,* thus confirming that loss of function of pix-1 is responsible for the phenotype. One of the three missense alleles, *gk893650*, shows a similar phenotype, but two of the missense alleles, *gk406361* and *gk713465*, display a wild-type boundary phenotype. Perhaps these two missense mutants, *gk406361* and *gk713465*, showing no phenotype are affecting residues in PIX-

1 that are not essential for function. Indeed, *gk713465* is an R212Q substitution in a residue that is not conserved in the RhoGEF domain (see below).

Additional evidence that *pix-1* is responsible for the muscle boundary phenotype, is that we were able to rescue the phenotype by expressing a wild-type version of *pix-1* cDNA under the control of a muscle-specific promoter (Fig. 2.1c). By immunostaining, we found that in the nonsense mutant, *pix-1(gk299374),* other IAC components are missing from the muscle cell boundaries, including UNC-52 (perlecan) in the ECM, PAT-3 (β-integrin) at the muscle cell membrane, UNC-112 (kindlin), and UNC-95 (Fig. 2.1d). Thus, we conclude that PIX-1 is required for the assembly or stability of IACs at the muscle cell boundary.

The standard view of integrin adhesion sites is that they act as a physical link between the ECM and cell membrane to cortical actin filaments. Like other cells, muscle cells are known to have cortical actin, however, this has not been previously reported for *C. elegans* muscle cells. Our attempts to visualize actin filaments near the muscle cell boundary using phalloidin staining were not successful for unknown reasons. As an alternative, we imaged F- actin using strain KAG547 that expresses in body wall muscle both GFP-myosin (MHC A) and LifeAct-mCherry. LifeAct is a 17 amino acid peptide that binds to F-actin and does not interfere with actin dynamics. (Riedl et al., 2008) In wild-type animals, as shown in Fig. 2.2 (top row), there is clearly a thin band of F-actin that lies near the muscle cell boundary (indicated by yellow arrow), which can be identified by three criteria: (1) its location between two adjacent spindle-shaped body wall muscle cells (Supplementary Fig. 2.2S), (2) being thinner than a typical I-band which alternates with myosin A-bands, and (3) not projecting throughout the depth of the myofilament lattice (Qadota et al., 2017) like a typical I-band, which can be discerned by observing less

intense signal when the optical slice is taken deeper into the lattice (the label of deeper part in Fig. 2.2 and Supplementary Fig. 2.2S). If there is cortical actin underneath the cell membranes of each adjacent muscle cell, why do we not observe two closely spaced lines? The likely reason is that the cells are very close to each other and these lines are not resolvable by the light microscope. We crossed the KAG547 strain into *pix-1 (gk299374)*. In this pix-1 nonsense mutant, the muscle cell boundaries clearly have two separated F-actin lines at the muscle cell boundary (bottom two rows in Fig. 2.2 and Supplementary Fig. 2.2S). Therefore, although *pix-1* is required for assembly or maintenance of IACs at the muscle cell boundary, it is not required for the assembly of cortical F-actin to which it likely interacts. The fact that two clearly separated F-actin lines can be observed in the *pix-1* nonsense mutant indicates that the cells are separated from each other, likely due to less adhesion to the ECM lying between adjacent cells.

A BLAST search reveals that C. elegans PIX-1 is most similar to mammalian β-PIX and α-PIX. Mammals have 2 PIX proteins, α-PIX and β- PIX, encoded by separate genes, whereas *C. elegans* has a single gene encoding a single PIX protein[14,15]. Our sequence and domain analysis of PIX-1 and human α-PIX and β-PIX proteins indicates that PIX-1 is quite similar to both α-PIX and β-PIX, but more similar to β-PIX because PIX-1, like β-PIX, is missing the CH domain found in α-PIX, and the SH3, RhoGEF and coiled- coil regions of PIX-1 are slightly more identical to those in β-PIX (Fig. 2.3a).

In *C. elegans* muscle, the force of muscle contraction that bends the worm and thus propels locomotion (swimming, crawling, burrowing), is transmitted through all three integrin attachment sites, the M-lines, the dense bodies and the adhesion plaques at the muscle cell boundaries. Thus, mutants that are defective in these structures, in many cases, show reduced

whole animal locomotion[18]. As shown in Fig. 2.4a and b, the pix-1 nonsense mutant, gk299374, the pix-1 intragenic deletion, gk416 (each outcrossed 5× to wild type) and the pix-1 intragenic deletion, ok982 (outcrossed 3X to wild type), show reduced locomotion in swimming in buffered water and in crawling along an agar surface. However, pix-1 (gk893650) (outcrossed 5× to wild type) which has the missense mutation P190S, and has a more subtle boundary defect (see below), displays normal swimming and crawling motility (Fig. 2.4a, b). We next wondered whether the pix- 1 rescued strain would show normal or near normal locomotion. To our surprise, in both swimming and crawling, the integrated transgene expressing wild-type pix-1 cDNA from the muscle- specific promoter for myo-3, [pix-1(gk299374); sfIs20], was slower than wild type (Fig. 2.4c, d). One possibility is that the integration occurred in a gene essential for normal locomotion, for example, a muscle or neuronal Unc gene. However, this does not appear to be the explanation for slow movement: Slow movement was observed even in a strain in which the extrachromosomal array was expressed in a wild-type background, [wild type; sfEx61] (Fig. 2.4c, d). Thus, the most likely explanation for reduced motility shown by the strains carrying the transgene, is overexpression of PIX-1, which is typical for extrachromosomal or integrated arrays. Indeed, quantitative western blotting using an antibody to PIX-1 (described below) shows that the integrated array expresses six times the amount of PIX-1 as found in wild type (Fig. 2.5a, b). In addition to a motility defect, overexpression of PIX-1 results in a defective muscle cell boundary (Fig. 2.5c). Finally, although we found a motility defect in three independently generated loss of function mutants, we were concerned that the motility defect might result from a mutation in a gene closely linked to PIX-1. In order to eliminate this possibility, we used CRISPR/Cas9 to correct the TAA stop codon in *pix-1(gk299374)*, to the

wild-type sequence of a CAA Gln codon. As shown in Fig. 2.4c, d, this strain, *pix-1 (syb2137gk299374)* displays normal swimming and crawling motility, and as shown in Fig. 2.5d, normal muscle cell boundaries. We conclude that either loss of function or overexpression of pix- 1 results in reduced locomotion and a muscle cell boundary defect.

The sarcomeres of pix-1 mutants are normally organized: thin filaments (phalloidin), thick filaments (anti-MHC A), dense bodies (anti-α-actinin), and M-lines (anti-UNC-89 (obscurin)) show the same localization in *pix-1(gk299374)* as they do in wild- type muscle (Supplementary Fig. 2.3S). Therefore, the defects in locomotion in pix-1 mutants might be attributed to a defect in force transmission through a lack of IACs at the lateral muscle cell boundaries, thus demonstrating both the functional importance of these structures and the importance of PIX-1 in establishing or maintaining these structures.

We developed two sets of polyclonal antibodies to PIX-1. WormBase predicts that pix-1 encodes two protein isoforms, PIX- 1a (646 residues) and PIX-1b (450 residues) (Fig. 2.6a). The first immunogen chosen (#1) was expected to generate antibodies that could detect both of these isoforms. The resulting rabbit poly- clonal antibodies were of low titer and allowed western blot detection of PIX-1a but not PIX-1b. Also, these antibodies to immunogen #1 failed to localize in muscle by immunostaining experiments. We then generated antibodies to a second immunogen (#2). As shown in Fig. 2.6b, this higher-titer antibody detected a protein of ~80 kDa, close to the expected size for PIX- 1a (73.2 kDa) from wild type, but not from the nonsense or two intragenic deletion alleles of pix-1. Interestingly, these antibodies detect a PIX-1 protein of normal size and abundance from *pix-1 (gk893650)*, which expresses PIX-1 with the missense mutation P190S in the RhoGEF domain. The expression of normal levels of intact PIX-1 protein likely explains

why the muscle cell boundary defect is more subtle in *pix-1(gk893650)*. (Supplementary Figs. 1; Fig. 2.6c; Fig. 2.9b, c).

We next used these anti-PIX-1 antibodies (to immunogen #2) to immunostain body wall muscle. As shown in Fig. 6c, anti-PIX- 1 localizes to muscle cell boundaries, to M-lines and dense bodies, and this staining is not detectable in the *pix-1* nonsense, *gk299374*, and intragenic deletion, *gk416*, mutants. However, consistent with the immunoblot results anti-PIX-1 staining is detectable at muscle cell boundaries in *pix-1(gk893650)* P190S.

Based on studies of β-PIX in mammals and some studies of pix-1 in C. elegans (but not in muscle), we hypothesized that PIX-1 functions in the biochemical pathway shown in Fig. 2.7a: that it activates a Rac/Cdc42 family member, perhaps via the scaffold protein GIT-1 (or additional or another scaffold protein), and this Rac/Cdc42 family member acts through a PAK protein kinase. C. elegans has 3 Rac proteins, CED-10, MIG-2, and RAC-2; one Cdc42, CDC-42; and 3 PAK protein kinases, PAK-1, PAK-2, and MAX-2. There are loss or reduction of function mutants available for all of the proteins indicated in Fig. 2.7a, except for CDC-42. As shown in Fig. 2.7b (and summarized in Fig. 2.7a), loss of function mutants in GIT-1, CED-10, PAK-1, and PAK-2, but not MIG-2, RAC-2 or MAX-2, result in the absence or reduced accumulation of PAT-6 at muscle cell boundaries. The defect in *pak-2(ok332)* is more subtle than the other mutants (Fig. 2.7b, bottom row); although there is not complete absence of PAT-6, PAT-6 appears less concentrated or more discontinuous at the cell boundaries than it does in wild type. Also, as shown in Supplementary Fig. 2.4, we obtained similar results for an additional allele of *rac-2, gk281*, and an additional allele of *ced-10, n1993*. However, the disruption of PAT-6 organization at muscle cell boundaries is less severe for *ced-10(n1993)* than

it is for *ced-10(n3246)*. This is consistent with the nature of the mutations: *ced-10(n3246)* is a G60R mutation at a highly conserved residue in the middle of the protein, whereas *ced-10(n1993)* is a V128G mutation at the penultimate residue that is only moderately conserved.

We next asked whether the level of PIX-1 protein might be affected by the deficiency of other pathway proteins. As shown in Fig. 2.8, using anti-PIX-1 in a quantitative western, we found that in either *git-1(ok1848)* or *pak-1 (ok448)*, but not *ced-10(n3246),* there are reduced levels of PIX-1 as compared to wild type. These data suggest that GIT-1 and PAK-1 are required for PIX-1 stabilization.

PFAM alignment of RhoGEF domains from PIX proteins across 10 different species shows that P190 is absolutely conserved (Fig. 2.9a). This conservation suggests that P190 is required for RhoGEF activity, and that the P190S missense mutation results in reduced RhoGEF activity. Our alignment of these RhoGEF domains also indicates that PIX-1 R212 is not conserved, and this might explain why *pix-1(gk713465*) R212Q has no obvious phenotype (Fig. 2.1Sb, Supplementary Fig. 1). Closer examination of confocal images of *pix-1(gk893650)* shows that the boundary defect is more subtle in this mutant than in the non- sense and intragenic deletion pix-1 mutants. In Qadota et al. 2017, we reported that by structured illumination microscopy (SIM), in wild-type muscle, the boundaries appear like a zipper, in which the two sides of the zipper are closely opposed to each other (as if the zipper were closed). Zoomed-in confocal views of muscle (Fig. 2.9b) using antibodies to two different IAC components, UNC-95 and PAT-6 (α-parvin), show a closed zipper in wild type, whereas in *pix-1(gk893650)* the zipper appears open. This result is also revealed by SIM imaging of PAT-6 staining (Supplementary Fig. 2.5S). A similar “open zipper” appears with anti- UNC-112 (kindlin) staining (Fig. 2.9c),

although anti-UNC-52 (perlecan) and anti-PAT-3 (β-integrin) staining show only less of these proteins at the boundaries of *gk893650* (Fig. 9c). In summary, the immunoblot and immunolocalization results using anti-PIX-1 show that PIX-1 P190S is a stable protein that localizes to the general vicinity of the muscle cell boundaries, but examination of other IAC components show that although each half of the zipper is formed, these halves are abnormally separated from each other. Taken together with the conservation of P190 in the RhoGEF domain, this suggests that RhoGEF activity is required for proper muscle cell boundary organization.

We predicted the structure of the RhoGEF domain of PIX-1 by homology modeling using the NMR structure of human β-PIX (Aghazadeh et al., 1998) as a template. We also predicted the structure of a complex between PIX-1 and both GDP- and GTP-bound forms of Rac1 GTPase, using GEF-Rac1 complexes as templates. We analyzed the helical conformation in PIX-1 molecular dynamic (MD) simulations to predict structural effects of the P190S mutation. In PIX-1 simulations, we observed that the serine eliminates the helical kink at the P190 position (Fig. 2.10a, left pair). This same effect is not observed in Rac1 complexes (Fig. 2.10a, right pair). The presence of the GTPase appears to maintain the kinked con- formation at the 190 position, even with the serine substitution.

However, further investigation of the complexes in MD simulations reveals that the mutation modulates the interaction of PIX-1 with Rac1 in complexes. We evaluated the (i) contact surface area, (ii) van der Waals interactions at the interface, and (iii) root mean square fluctuations (RMSF) of protein residues. Our analyses reveal that the introduction of the P190S mutation stabilizes a putative complex between PIX-1 and GTP-bound Rac1. We observe an increase in the contact surface area between the two proteins in the mutant compared to the wild-

type PIX-1 complex (Fig. 2.10b). We examined a predicted van der Waals interaction on the interface between A186 (PIX-1) and L70 (located in the Switch II region of Rac1). This interaction, which lies in the vicinity of P190, exists in the mutant P190S complex but not in the wild-type complex. In addition, RMSF analysis reveals that the interface is more stabilized in the P190S complex (Supplementary Fig. 2.6S). RMSF values are lower around the interface of the mutant complex, indicative of reduced fluctuations and a more stable interaction.

All the trends that are observed here are reversed in the PIX-1 complexes with GDP-bound Rac1. Contact surface area between PIX-1 and Rac1 is decreased in the mutant complex relative to wild type (Fig. 2.10b). Consistent with this observation, the van der Waals interaction shown in Fig. 2.10c is lost in the mutant complex, but present 24.4% of the simulation in wild type. Combined, MD analyses suggest that the P190S mutation enhances GTP-bound Rac1 interaction with PIX-1.

To understand how the P190S mutation results in a normal level of PIX-1 protein but disrupted muscle cell boundary structures, *pix- 1(gk893650)* [P190S] was crossed into the transgenic line in which HA-tagged CED-10 is expressed in body wall muscle cells, made whole worm lysates and used GST-PAK-PBD to pull down GTP- bound CED-10. As shown in Fig. 2.10d, less activated CED-10 was pulled out from *pix-1(gk893650)* [P190S] than from wild type. Repeating this experiment three times, the mean level of activated CED-10 from P190S was 52.9 +/− 5.7% (mean and standard deviation) of the level from wild type. Therefore, the P190S mutation in the RhoGEF domain of PIX-1 reduces its GEF activity.

Figures

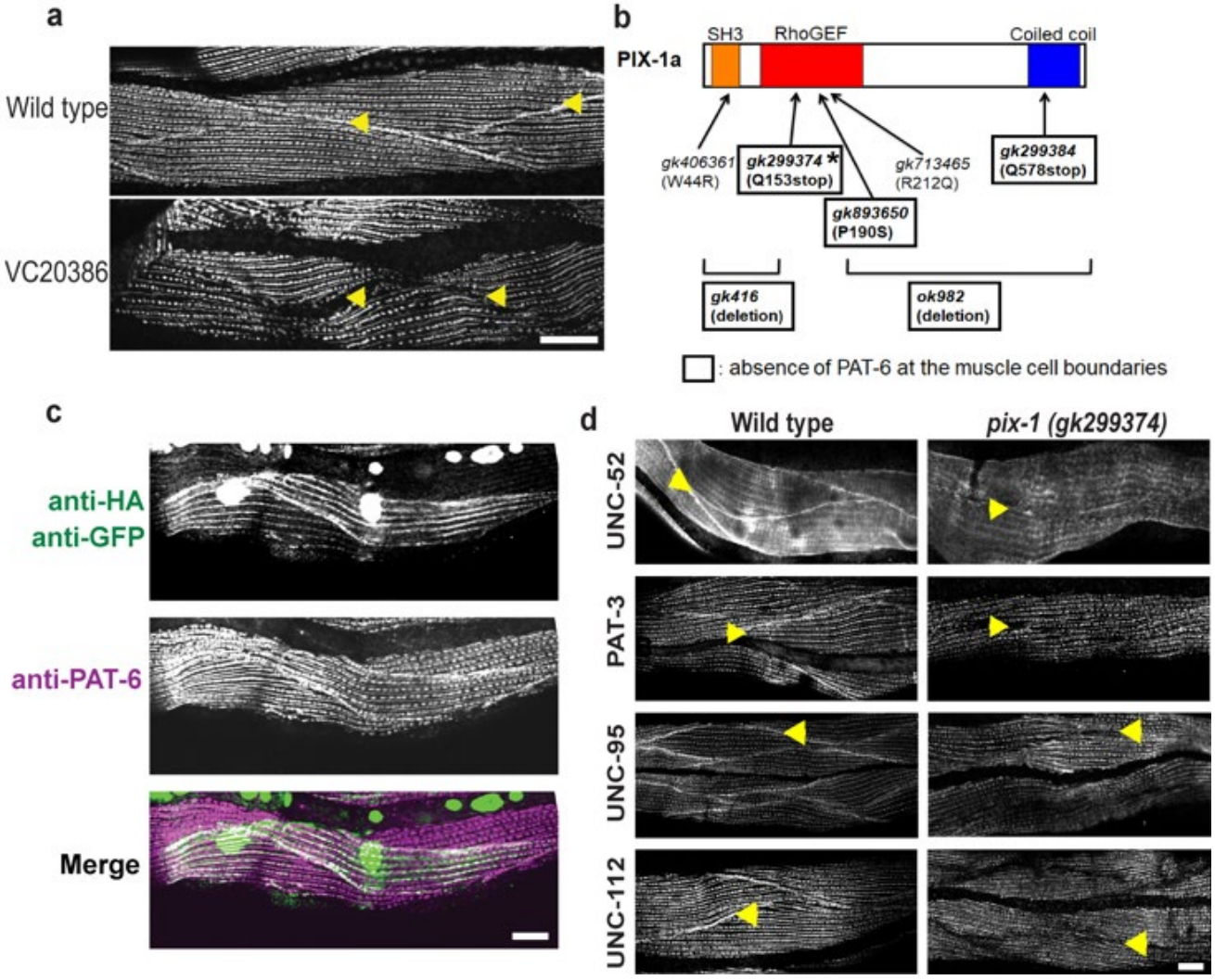
a
Wild type
VC20386
b
PIX-1a
SH3
RhoGEF
Coiled coil
gk406361
(W44R)
gk299374 *
(Q153stop)
gk713465
(R212Q)
gk299384
(Q578stop)
gk893650
(P190S)
gk416
(deletion)
ok982
(deletion)
: absence of PAT-6 at the muscle cell boundaries
c
anti-HA
anti-GFP
anti-PAT-6
Merge
d
Wild type
pix-1 (gk299374)
UNC-52
PAT-3
UNC-95
UNC-112

Figure 2.1 Identification of pix-1 as a gene required for the assembly of IACs at the muscle cell boundaries. a.) Confocal images of several body wall muscles immunostained with antibodies to PAT-6 (α-parvin) from wild type and the strain VC20366 identified by screening 574 MMP strains. Arrowheads point to the boundaries between muscle cells. **b.**) Schematic representation of domains in C. elegans PIX-1a, and the location and nature of 7 *pix-1* mutants and evaluation of their phenotypes. The asterisk denotes the pix-1 mutant allele found in the original strain VC20366. **c.**) Muscle-specific expression of a wild-type cDNA for PIX-1 tagged with HA rescues the phenotype of *pix-1(gk299374).* The transgene is *sfEx61*[myo-3p::HA-PIX-1;sur-5::nls::GFP], in which sur-5::nls::GFP is the transformation marker showing GFP in the nuclei. Note that PAT-6 has been restored to the muscle cell boundaries (indicated by arrowheads), and that HA-tagged PIX-1 localizes to muscle cell boundaries, dense bodies and M-lines. **d.**) Comparison of wild type vs. *pix-1(gk299374)* immunostained with antibodies to the indicated IAC proteins and imaged by confocal microscopy. Arrowheads denote muscle cell boundaries. Note that all four proteins ae present in wild type but missing from muscle cell boundaries in *pix-1* mutant. Each image is a representative image obtained from at least 2 fixation and immunostaining experiments =, and imaging at least three different animals. Scale bars in (**a**), (**c**), and (**d**), 10μm.

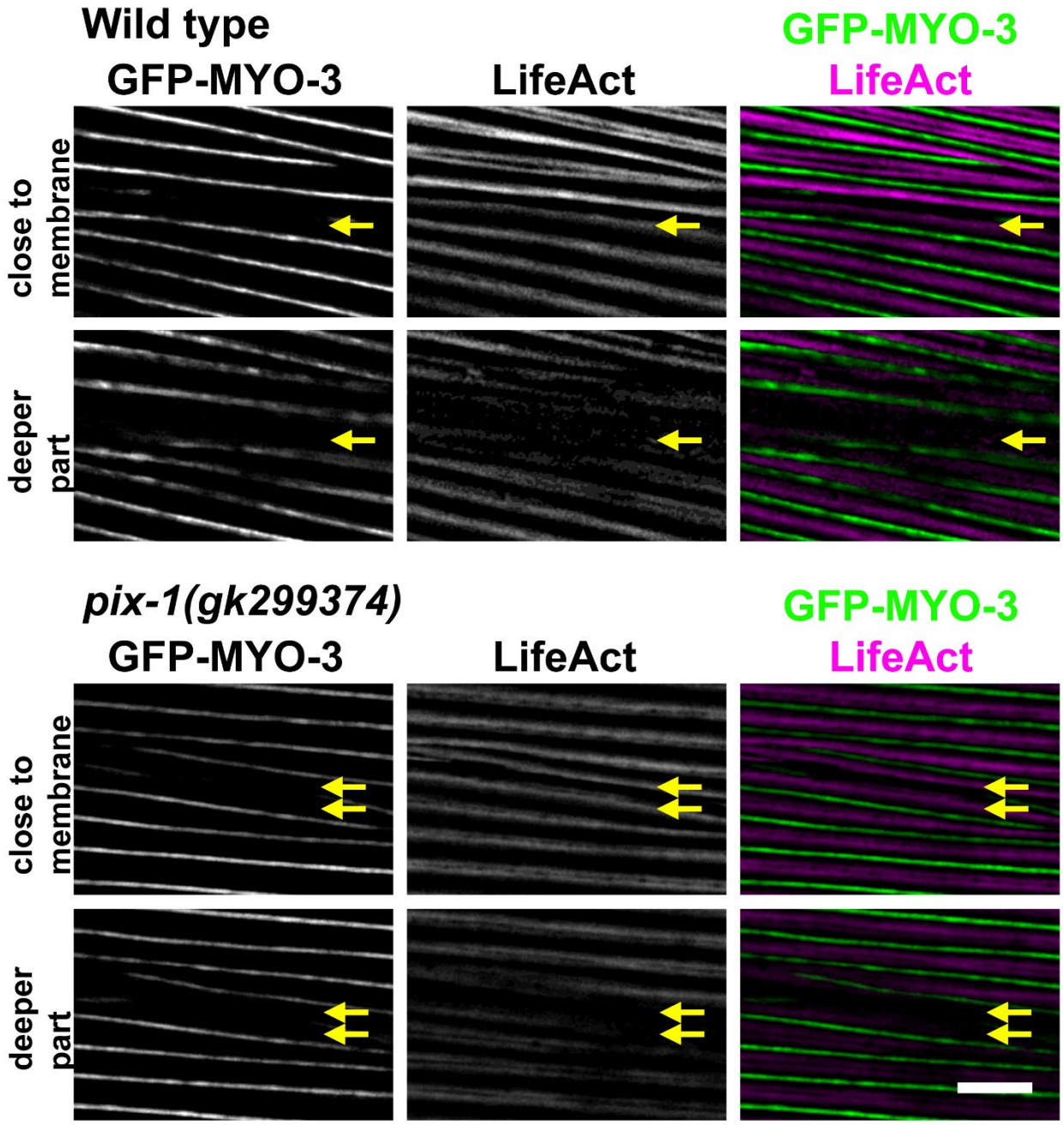
Wild type
GFP-MYO-3
LifeAct
GFP-MYO-3
LifeAct
close to membrane
deeper part
pix-1(gk299374)
GFP-MYO-3
LifeAct
GFP-MYO-3
LifeAct
close to membrane
deeper part

Figure 2.2 Live imaging of cortical F-actin at muscle cell boundaries. SIM images of portions of two adjacent body wall muscle cells from a nematode strain which is a muscle myosin MHC A was tagged with GFP by CRISPR and LifeAct-mCherry was expressed in muscle cells from a transgene. GFP-MYO-3 (MHC A) labels the middle of the sarcomeric A-bands, and LifeAct-mCherry labels I-bands, except for F-actin at the boundary between two adjacent muscle cells (indicted by yellow arrows). Note how the signal from the F-actin at the boundary diminishes as the focal plane changes from close to the outer muscle cell membrane to deeper into the myofilament lattice whereas F-actin signal from I-bands does not change. Also note that in pix-1, nonsense mutant, *gk299374,* there as two bands of cortical F-actin at the boundary. Each image is a representative image obtained from imaging in three different animals of each strain. Scale bar, 5μm.

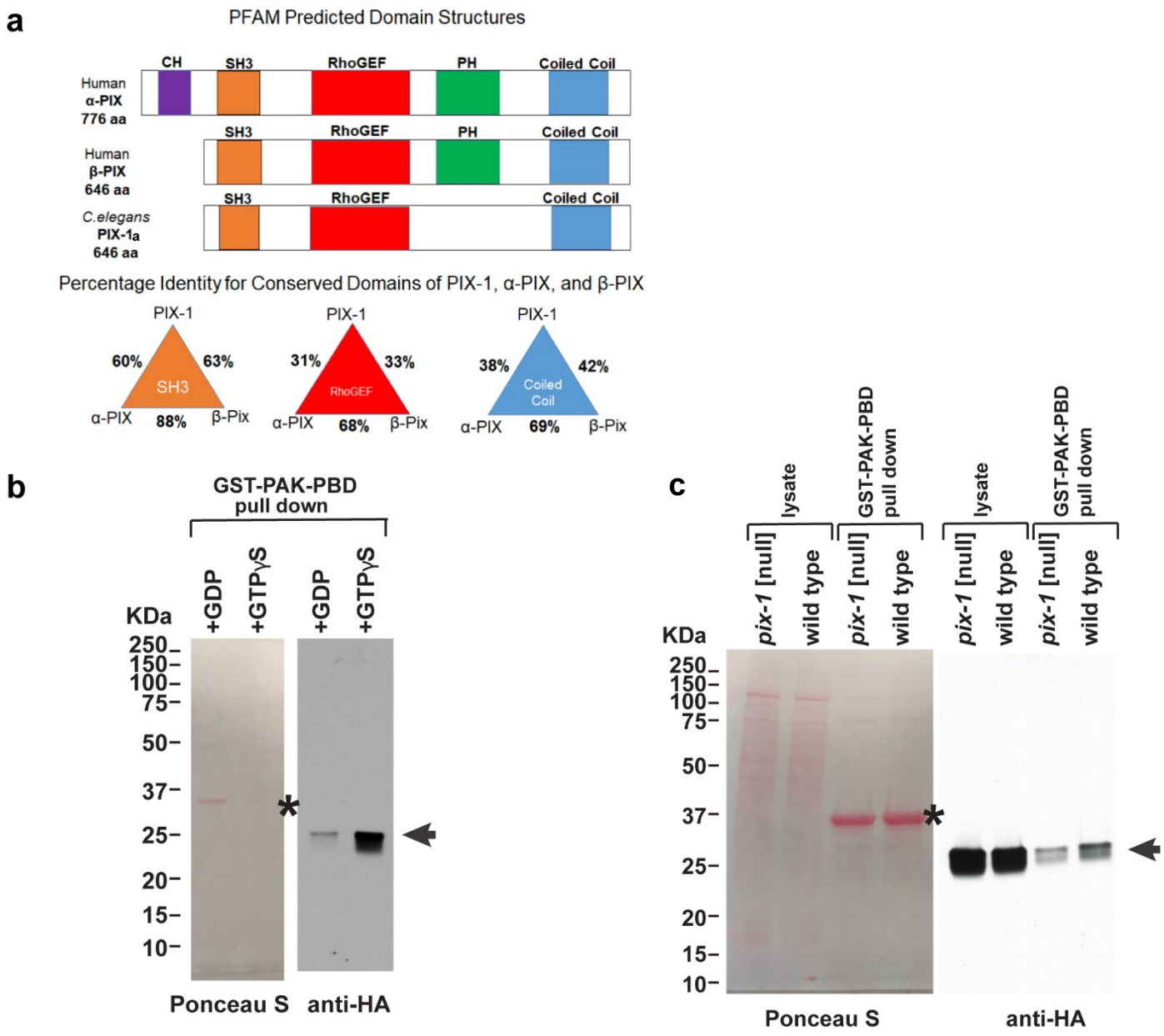
a
PFAM Predicted Domain Structures
CH
SH3
RhoGEF
PH
Coiled Coil
Human α-PIX 776 aa
Human β-PIX 646 aa
C.elegans PIX-1a 646 aa
Percentage Identity for Conserved Domains of PIX-1, α-PIX, and β-PIX
PIX-1
60%
63%
SH3
α-PIX
88%
β-Pix
31%
33%
RhoGEF
68%
38%
42%
Coiled Coil
69%
b
GST-PAK-PBD pull down
+GDP
+GTPγS
KDa
250
150
100
75
50
37
25
20
15
10
Ponceau S
anti-HA
c
lysate
GST-PAK-PBD pull down
pix-1 [null]
wild type
KDa
Ponceau S
anti-HA

Figure 2.3 PIX-1 is most similar to human β-PIX and acts as a GEF for CED-10 (Rac) in muscle. a.) Schematic representation of predicted domains in C.elegans PIX-1a, human α-PIX and human β-PIX. The bottom triangles show a comparison of percentage identities for SH3, RhoGEF, and coiled-coil regions. **b.**) Validation of activation assay. Lysates were prepared from nematodes expressing HA-CED-10 in body wall muscle using a muscle specific promoter, an excess of GDP or GTPγS, was added, and then beads coupled with GST-PAK-PBD were used to pull down activated CED-10 (i.e. bound to GTP or GTP + GTPγS). Samples were separated on a gel, blotted and incubated with antibodies to HA. The asterisk indicates the position GST-PAK-PBD on the blot. Arrow indicates the position of HA-CED-10-GST•GTP/GTPγS on the western blot. **c.**) Deficiency of PIX-1 results in a reduced level of activated CED-10. Lysates were prepared from two strains each expressing HA-CED-10 in body wall muscle: wild type, and *pix-1 (gk299374),* a nonsense mutation that results in no detectable PIX-1. These lysates were incubated with beads coupled to GST-PAK-PBD, and is used to pull down activated CED-10. Both Ponceau stained blot, and the result of the western using anti-HA are shown. The western shows, from left to right: total HA-CED-10 in *pix-1* mutant and HA-CED-10•GTP in wild type. Asterisk indicates the position of GST-PAK-PBD on the blot. Arrow indicates the position of HA-CED-10 from the lysates, or HA-CED-10•GTP from the pulldown.

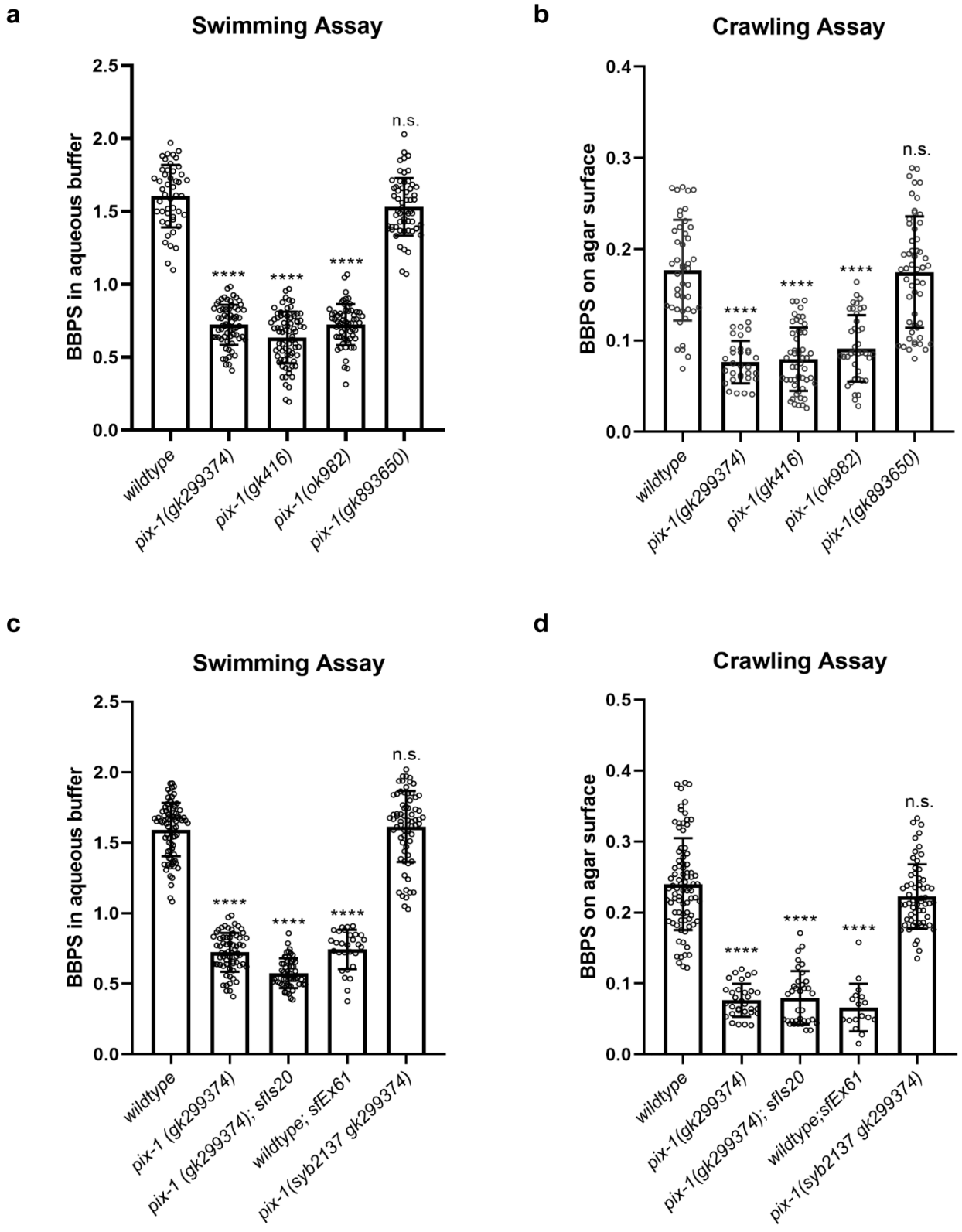
a
Swimming Assay
BBPS in aqueous buffer
2.5
2.0
1.5
1.0
0.5
0.0
****
****
****
n.s.
wildtype
pix-1(gk299374)
pix-1(gk416)
pix-1(ok982)
pix-1(gk893650)
b
Crawling Assay
BBPS on agar surface
0.4
0.3
0.2
0.1
0.0
****
****
****
n.s.
wildtype
pix-1(gk299374)
pix-1(gk416)
pix-1(ok982)
pix-1(gk893650)
c
Swimming Assay
BBPS in aqueous buffer
2.5
2.0
1.5
1.0
0.5
0.0
****
****
****
n.s.
wildtype
pix-1 (gk299374)
pix-1 (gk299374); sfIs20
wildtype; sfEx61
pix-1(syb2137 gk299374)
d
Crawling Assay
BBPS on agar surface
0.5
0.4
0.3
0.2
0.1
0.0
****
****
****
n.s.
wildtype
pix-1(gk299374)
pix-1(gk299374); sfIs20
wildtype;sfEx61
pix-1(syb2137 gk299374)

Figure 2.4 Both loss of function and overexpression of *pix-1* results in reduced locomotion. **a.**) Swimming and **b.**) crawling assays show that loss of function mutations in *pix-1* result in reduced locomotion compared to wild type. **c.**) Swimming and **d.**) crawling assays show that both integrated rescued strain, *pix-1(gk299374); sfIs20,* and wild type expressing the rescue transgene from an extrachromosomal array, *sfEx61,* have reduced locomotion. In contrast, CRISPR/Cas9 repair of the nonsense mutation in *pix-1(gk299374)*, called *pix-1(syb2137 gk299374),* results in normalization of locomotion. In the graphs, each open circle represents the result from an independently selected animal. The exact n values vary, and these data can be found in the Source Data Files. Student's two-sided t test was used to test for significance. Error bars: standard deviations; **** $p \leq 0.0001$; n.s.: no significant difference.

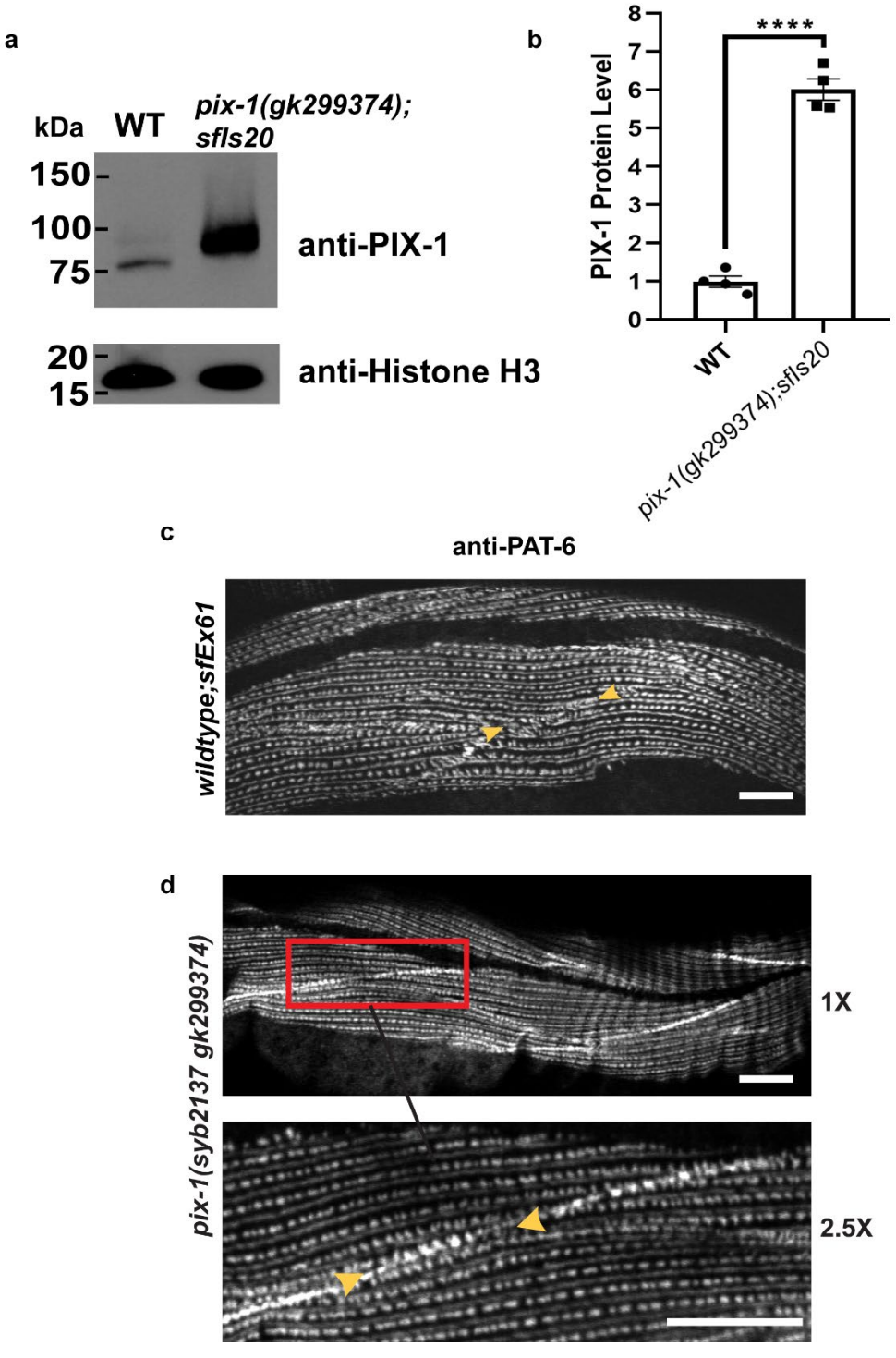
a
kDa
WT
pix-1(gk299374); sfIs20
150
100
75
anti-PIX-1
20
15
anti-Histone H3
b
PIX-1 Protein Level
****
WT
pix-1(gk299374);sfIs20
c
anti-PAT-6
wildtype;sfEx61
d
pix-1(syb2137 gk299374)
1X
2.5X

Figure 2.5 Overexpression of pix-1 results in disruption and CRISPR repair of *pix-1(gk299374)* results in normalization of muscle cell boundaries. a, b.) Western blot analysis showing overexpression of PIX-1 in the strain [*pix-1(gk299374);sfIs20]* in which the muscle cell boundary defect observed in *pix-1(gk299374)* has been rescued by an integrated array of wild-type *pix-1* expressed from a muscle specific promoter (see Fig.1c) **a.**) A representative western blot is shown reacted with antibodies to PIX-1 and to the loading control histone H3. **b.**) Graphical summary of four independent western blot reactions for wild type vs. *pix-1(gk299374);sfIs20.* Means and standard errors of the means are shown. Two strains show statistically different levels of PIX-1 using a two-sided student t test with $p<0.0001$(indicated by ****). Images of the entire western blots are provided in the Source Data Files. **c.**) The same array when expressed in a wild-type background [wild-type;*sfEX61*] disrupts the muscle cell boundary. **d.**) *pix-1(syb2137 gk2993374)* is *pix-1(gk299374)* after CRISPR/Cas9 was used to repair the nonsense mutation. Confocal microscopy images of anti-PAT-6 are shown and reveal that the muscle cell boundary is normal. This is further evidence that the muscle cell boundary defect is specifically due to mutation in the *pix-1* gene. Arrowheads point to the muscle cell boundaries visualized by immunostaining with anti-PAT-6. Each image is a representative image obtained from at least two fixation and immunostaining experiments, and imaging at least three different animals. Scale bars, 10μm.

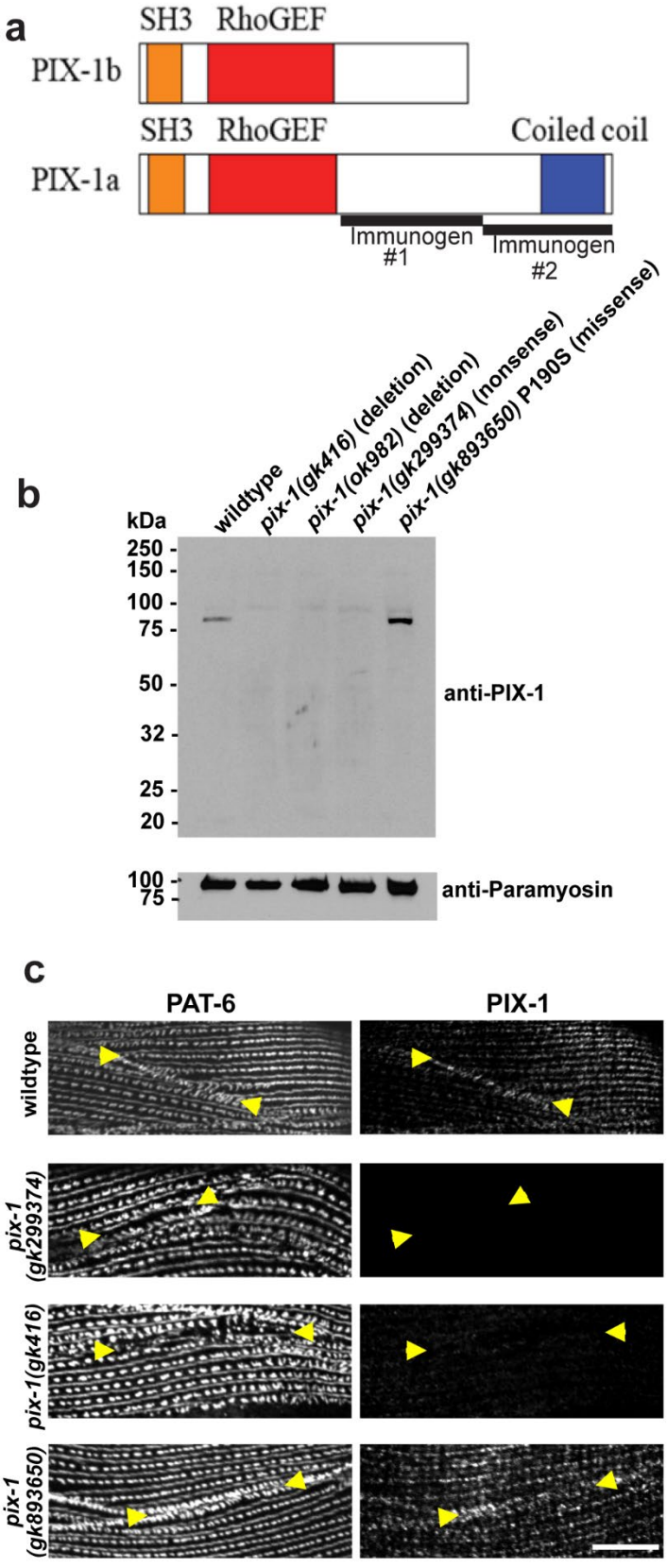
a
SH3
RhoGEF
PIX-1b
SH3
RhoGEF
Coiled coil
PIX-1a
Immunogen #1
Immunogen #2
b
wildtype
pix-1(gk416) (deletion)
pix-1(ok982) (deletion)
pix-1(gk299374) (nonsense)
pix-1(gk893650) P190S (missense)
kDa
250
150
100
75
50
32
25
20
anti-PIX-1
100
75
anti-Paramyosin
c
PAT-6
PIX-1
wildtype
pix-1 (gk299374)
pix-1(gk416)
pix-1 (gk893650)

Figure 2.6 Antibodies to PIX-1 detect PIX-1a on western blot and localize to muscle cell boundaries, M-lines, and dense bodies. a.) Schematic representation of domains in the predicted isoforms PIX-1a and PIX-1b and regions used as immunogens to generate antibodies. **b**.) Western blot detection of protein of expected size for PIX-1a from wild type and from *pix-1(gk893650)* [P190S] but not from the deletion or nonsense *pix-1* mutants. Anti-paramyosin was used as a gel loading control. An image of the entire blot reacted with anti-paramyosin is available in the Source Data Files. **c.**) Antibodies to PIX-1 localize to muscle cell boundaries and stained with less intensity to the M-lines and dense bodies. Each strain stained with antibodies to PAT-6 and PIX-1 and imaged by confocal. Note the lack of PIX-1 immunostaining in the nonsense and deletion *pix-1* mutants, but strong and disorganized muscle cell boundary staining in *pix-1(gk893650)* [P190S]. Arrowheads point to a muscle cell boundary. Each image is a representative image obtained from at least two fixation and immunostaining experiments., and imaging of at least three different animals of each strain. Scale bar, 10μm.

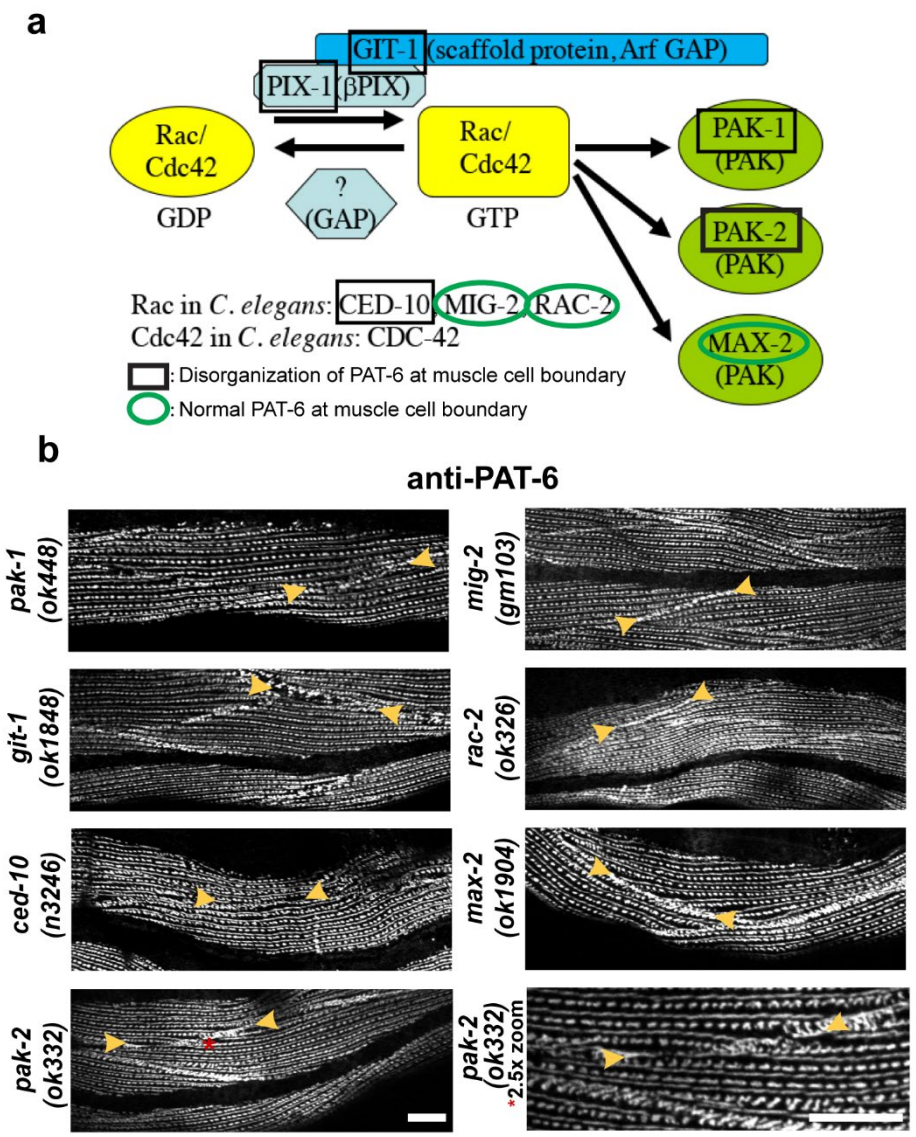

Figure 2.7 Mutations in genes encoding known proteins of a PIX-1 pathway result in muscle cell boundary disruption. a.) Putative PIX-1 biochemical pathway based on what is known of PIX proteins in mammals and other cell types in *C. elegans*. Also indicated is summary of the results shown in **b. b.**) Confocal images of body wall muscle from the indicated mutants immunostained with anti-PAT-6. Note reduced or disorganized PAT-6 localization at muscle cell boundaries (indicated by arrowheads) *pak-1*, *git-1*, *ced-10*, and *pak-2* mutants, but normal PAT-6 localization in *mig-2, rac-2, max-2* mutants, Results on second alleles for *rac-2* and *ced-10* are shown in Supplementary Figure 3. Each image is a representative image obtained from at least 2 fixation and immunostaining experiments, and imaging at least three different animals of each strain. Scale bar, 10μm.

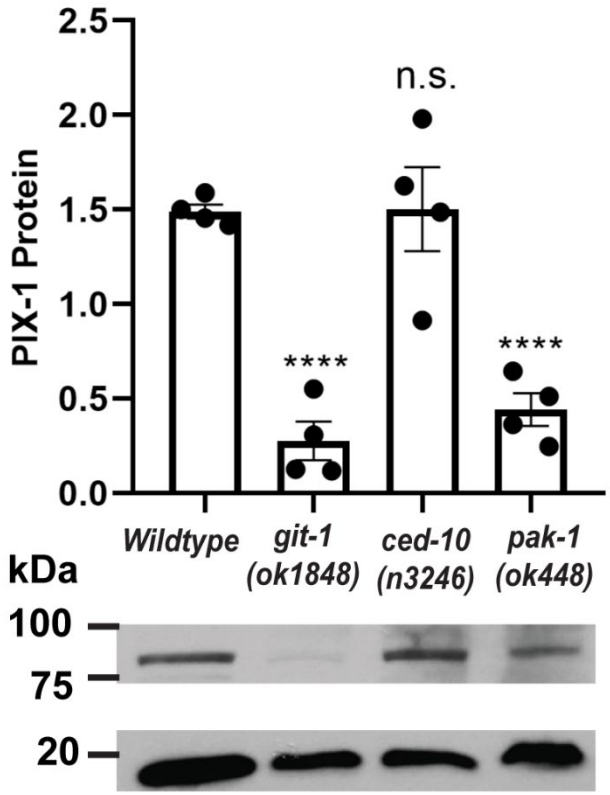

Figure 2.8 PIX-1 levels are reduced in *git-1* and *pak-1* mutants. Equal quantities of total SDS-soluble proteins from wild type, *git-1(ok1848), ced-10 (n3246), and pak-1(ok448)*, were resolved on a gel, blotted to the membrane and reacted with anti-PIX-1, and as loading control with anti-histone H3, the levels of PIX-1 in the normalization to the amount of histone H3, the levels of PIX-1 in the mutants were compared to the level of PIX-1 in wild type. Representative immunoblot results are shown below the graph. N=4 independent western blot reactions from each strain; means and standard error of the means are shown; *git-1* and *pak-1* mutants show statistically different levels from wild-type based on a two-sided student's t test at p≤0.0001 (indicated by ****). Images of the entire western blots are provided in the Source Data Files.

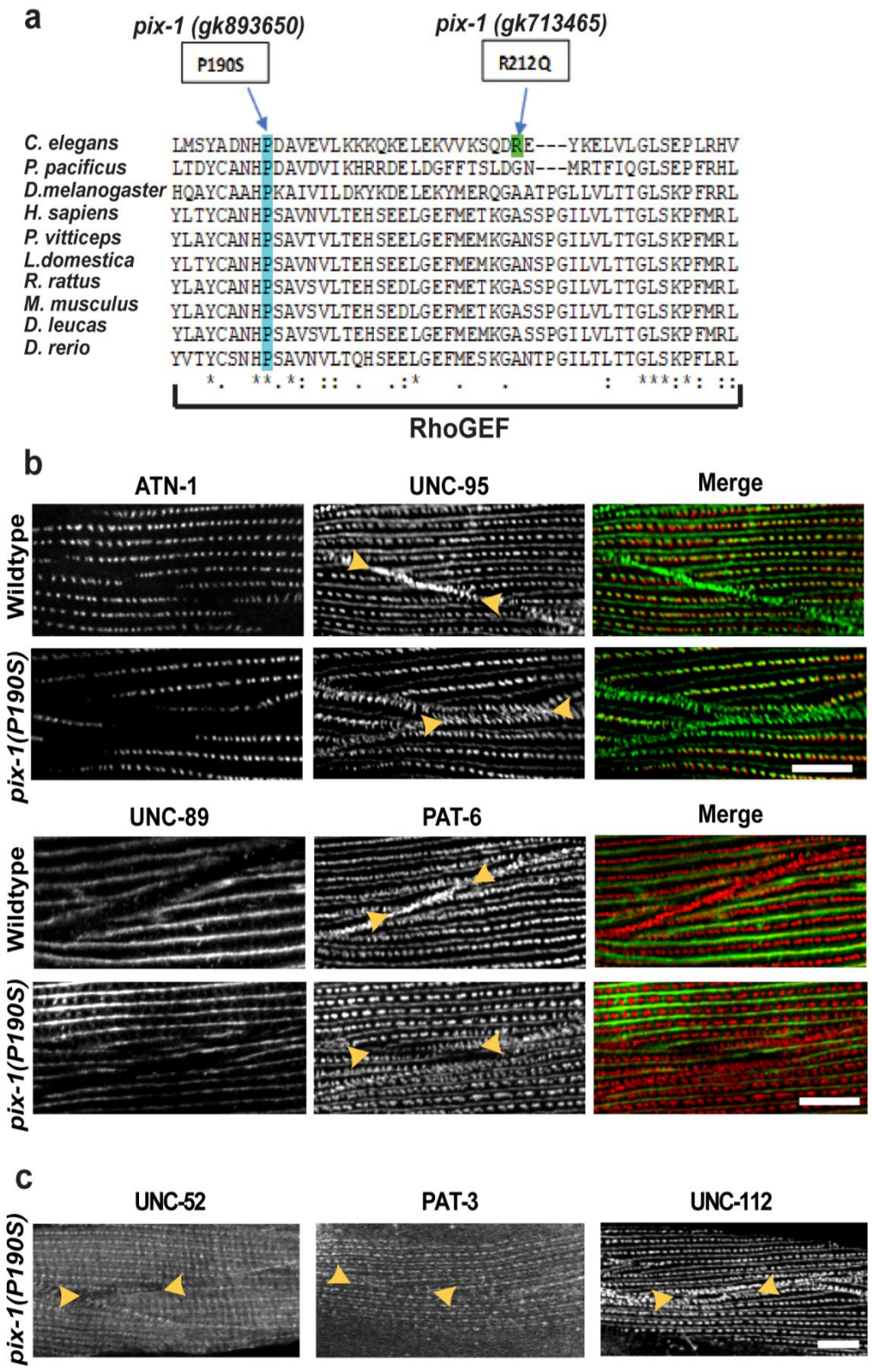
a
pix-1 (gk893650)
P190S
pix-1 (gk713465)
R212Q
C. elegans LMSYADNHPDAVEVLKKKQKELEKVVKSQDRE---YKELVLGLSEPLRHV
P. pacificus LTDYCANHPDAVDVIKHRRDELDGFFTSLDGN---MRTFIQGLSEPFRHL
D.melanogaster HQAYCAAHPKAIVILDKYKDELEKYMERQGAATPGLLVLTTGLSKPFRRL
H. sapiens YLTYCANHPSAVNVLTEHSEELGEFMETKGASSPGILVLTTGLSKPFMRL
P. vitticeps YLAYCANHPSAVTVLTEHSEELGEFMEMKGANSPGILVLTTGLSKPFMRL
L.domestica YLTYCANHPSAVNVLTEHSEELGEFMEMKGANSPGILVLTTGLSKPFMRL
R. rattus YLAYCANHPSAVSVLTEHSEDLGEFMETKGASSPGILVLTTGLSKPFMRL
M. musculus YLAYCANHPSAVSVLTEHSEDLGEFMETKGASSPGILVLTTGLSKPFMRL
D. leucas YLAYCANHPSAVSVLTEHSEELGEFMEMKGASSPGILVLTTGLSKPFMRL
D. rerio YVTYCSNHPSAVNVLTQHSEELGEFMESKGANTPGILTLTTGLSKPFLRL
RhoGEF
b
ATN-1
UNC-95
Merge
Wildtype
pix-1(P190S)
UNC-89
PAT-6
Merge
Wildtype
pix-1(P190S)
c
UNC-52
PAT-3
UNC-112
pix-1(P190S)

Figure 2.9 P190 is conserved in PIX RhoGEF domains and required for PIX-1 function at muscle cell boundaries. a.) PFAM alignment of RhoGEF sequences of PIX proteins from 10 species showing that P190 is absolutely conserved. In contrast, R212 is not conserved, which might explain why *pix-1(gk713465)* [R212Q] has no obvious phenotype. **b.**) Confocal microscopy of wild type and *pix-1(gk893650)* [P190S] mutant co-stained with antibodies to ATN-1 (α-actinin) and UNC-95 (top two rows), and co-stained with UNC-89 (obscurin) and PAT-6 (α-parvin) (bottom two rows). Note that in *pix-1(gk893650),* at the muscle cell boundary, the two halves of the zipper are separated, whereas the in the wild type they are together. **c.**) Confocal imaging of *pix-1(gk893650)* [P190S] stained with antibodies to UNC-52 (perlecan), PAT-3 (β-integrin) or UNC-112 (kindlin). Note that these IAC proteins also show reduced or disrupted localization at muscle cell boundaries. Arrowheads bracket a muscle cell boundary. Each image is a representative image obtained from two fixation and immunostaining experiment, and imaging at least three different animals of each strain. Scale bar, 10μm.

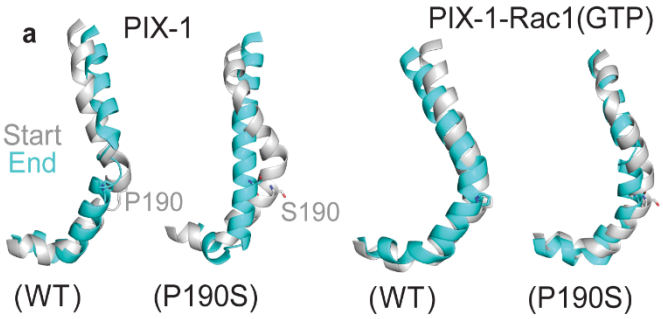

b

	Contact area (Å^2)
WT-Rac1 (GTP)	1298.3
P190S-Rac1 (GTP)	1742.0
WT-Rac1 (GDP)	2047.2
P190S-Rac1 (GDP)	1597.4

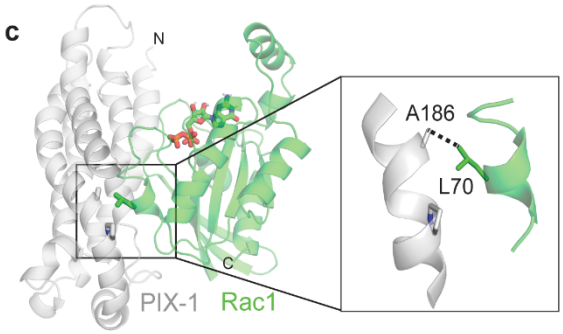

	Distance (Å)	Interaction %
WT-Rac1 (GTP)	9.8	1.2
P190S-Rac1 (GTP)	4.4	65.5
WT-Rac1 (GDP)	5.1	24.4
P190S-Rac1 (GDP)	9.1	0.4

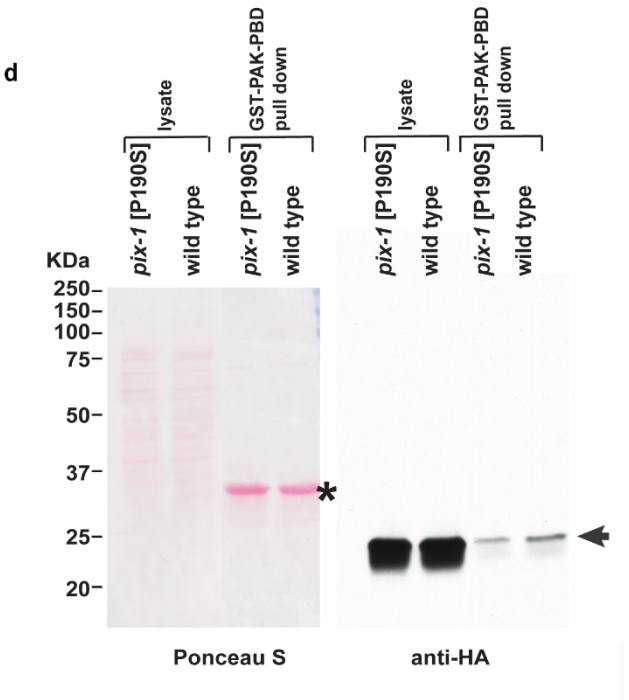

Figure 2.10 P190S may alter RhoGEF structure and interaction with Rac, and in muscle there is a reduction in activated Rac. a.) Comparison of helical conformations at the start (gray) and end (cyan) of PIX-1 and PIX-1-Rac1 complex MD simulations. Wild type PIX-1 maintains the predicted kinked helical conformation near P190. (This proline is on helix F in the β-PIX structure.) Mutant PIX-1 reveals a loss of the kink in the helix by the end of the simulation. In simulations of PIX-1 complexed with GTP-bound Rac1, the kinked conformation is maintained in the mutant complex. The same result is observed with GDP-bound Rac1 (not shown). **b.**) **Contact** surface areas were calculated for wild type and mutant PIX-1-Rac1 complexes. In GTP-bound Rac1 complexes, the mutation leads to an increase in contact surface area. In GDP-bound Rac1 complexes, the mutation leads to a decrease in the contact surface area. **c.**) The predicted PIX-1-Rac1 complex reveals an interaction on the interface near the P190 position. This interaction between A186 of PIX-1 with L70 of Rac1 (Switch II region) is quantified as an average distance between the residues and percentage of time the residue distance is <4.5 Å over the simulation. In GTP-bound Rac1, the interaction is lost in wild type but maintained in the mutant. The trend is reversed in GDP-bound Rac1. **d.)** Comparison of the level of activated CED-10 (Rac) in wild type vs. P190S mutant muscle. Nematode lysates were prepared from two strains, each expressing HA-CED-10 in body wall muscle: wild type, and *pix-1(gk893650)* which expresses approximately normal levels of P190S mutant PIX-1 protein. The lysates were incubated with beads coupled to GST-PAK-PBD to pull down activated CED-10. The Ponceau S stained blot, and the result of the western using anti-HA are shown. Asterisk indicates the position of GST-PAK-PBD on the blot. Arrow indicates the position of HA-CED-10 from the lysate, or HA-CED-10•GTP from the pulldown.

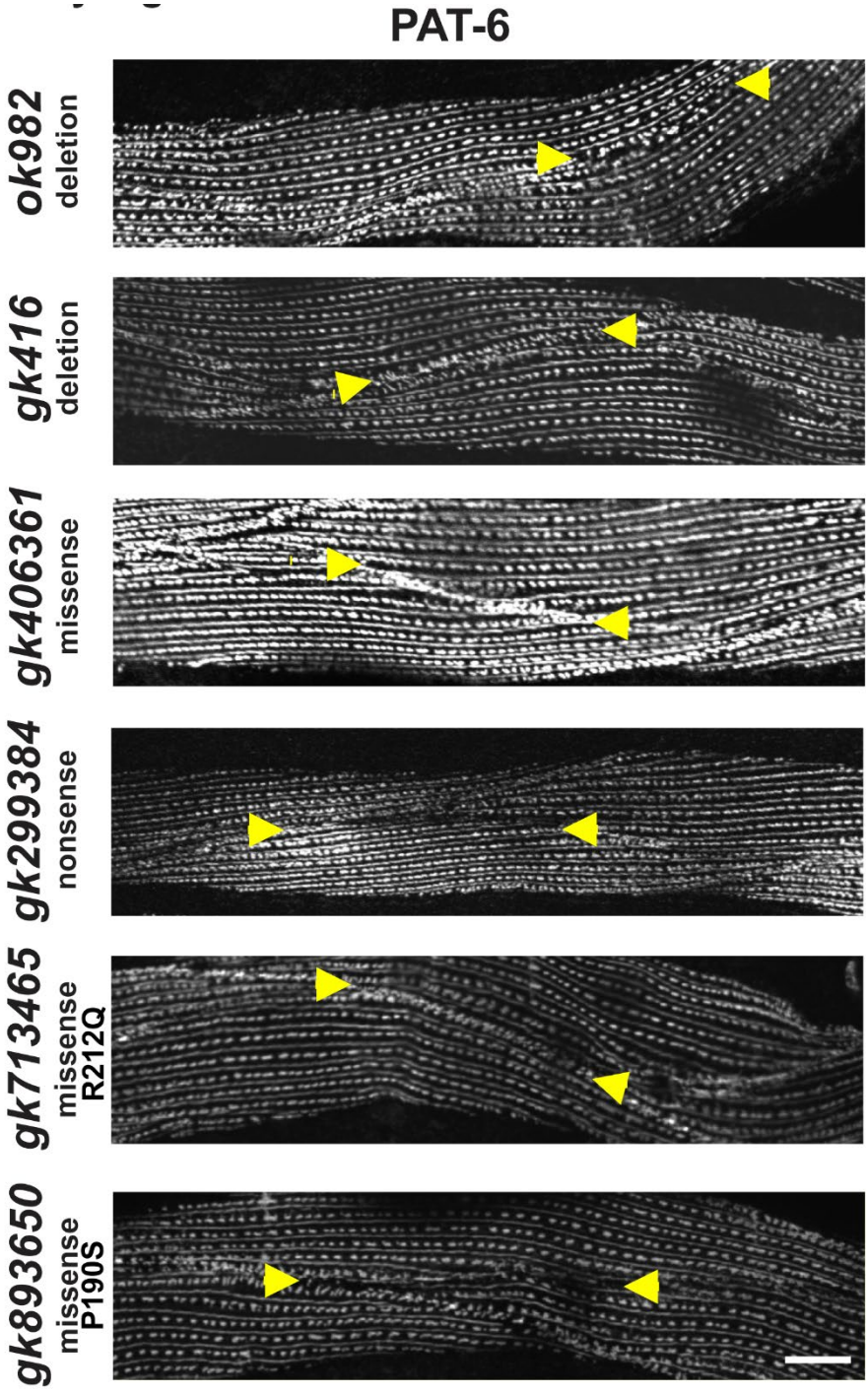

Figure 2.1S. Immunostaining of 6 *pix-1* mutant alleles using antibodies to PAT-6. The results are summarized in Figure 1b. Each image is a representative image obtained from at least two fixation and immunostaining experiments, and imaging of at least three different animals from each strain. Scale bar, 10 μm.

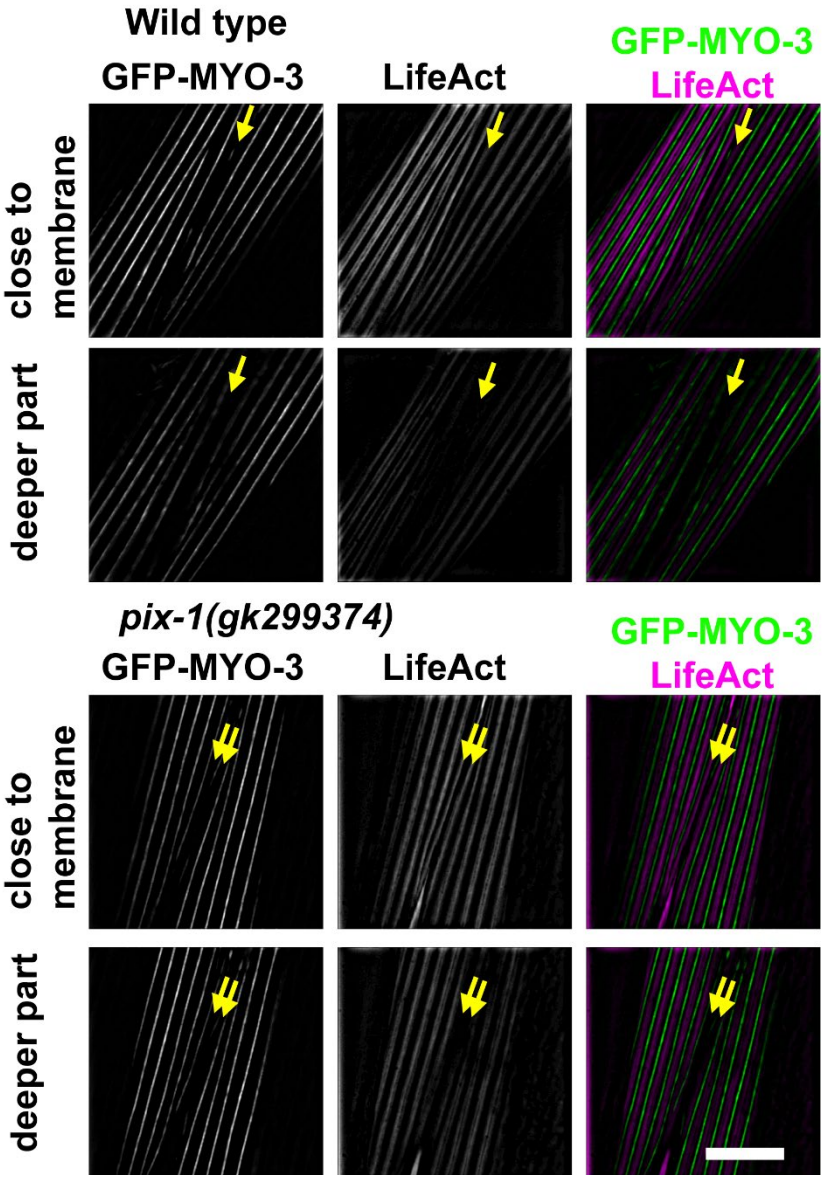

Figure 2.2S. Live imaging of cortical F-actin at muscle cell boundaries. SIM images of portions of two adjacent body wall muscle cells from a nematode strain in which a muscle myosin was tagged by GFP by CRISPR and LifeAct-mCherry was expressed in muscle cells from a transgene. GFP-MYO-3 labels the middle of sarcomeric A-bands, and LifeAct-mCherry labels I-bands, except for F-actin at the boundary between two adjacent muscle cells (indicated by yellow arrows). The signal from the F-actin at the boundary diminishes as the focal plane changes from close to the outer muscle cell membrane to deeper into the myofilament lattice whereas the F-actin signals from I-bands does not change. In the *pix-1* nonsense mutant, *gk299374*, there are two bands of cortical F-actin at the boundary. Each image is a representative image obtained from at least two fixation and immunostaining experiments and imaging at least three different animals. Scale bar, 10 μm. These images are the same as shown in Figure 2, except that they are shown here at lower magnification. This broader perspective allows better observation of the spindle shape of the body wall muscle cells and thus the location of the boundary between these cells.

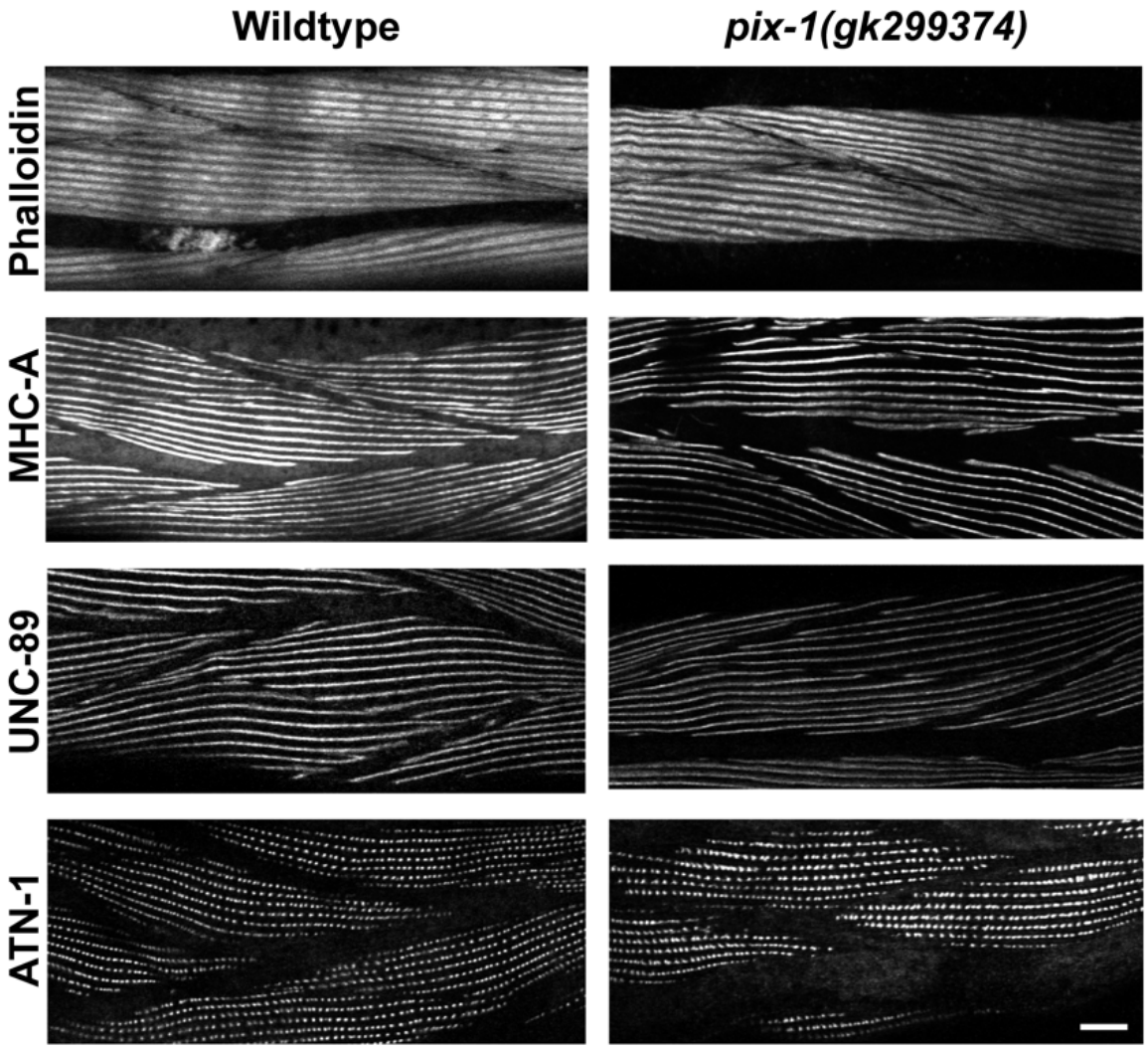

Figure 2.3S. A *pix-1* mutant has normally organized sarcomeres. Confocal microscopy of wild type and *pix-1(gk299374)* reacted with rhodamine-phalloidin (thin filament), and antibodies to sarcomere proteins MHC-A (thick filaments), UNC-89 (M-lines) and ATN-1 (dense bodies). Note that with each of these markers, *pix-1 (gk299374)* appears the same as wild type. Each image is a representative image obtained from at least two fixation and immunostaining experiments, and imaging of at least three different animals from each strain. Scale bar, 10 μm.

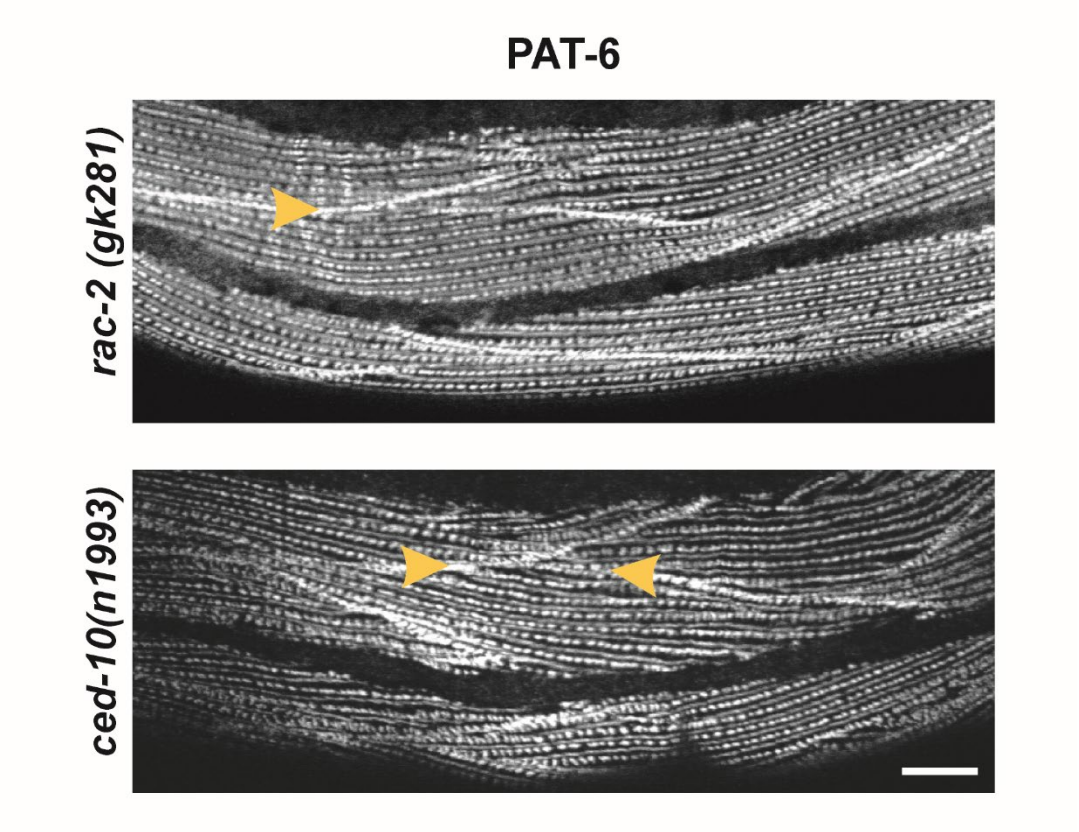

Figure 2.4S. PAT-6 immunostaining of two additional alleles of rac-2 and ced-10. Note that the muscle cell boundaries appear normal om *rac(gk281),* in agreement with the result presented in Figure 7b of *rac-2(ok326)*. Th disruption of PAT-6 organization at muscle cell boundaries is less severe for *ced-10(n1993)* shown here in comparison to ced-10(n3246) (shown in Figure 7b). Each image is a representative image obtained from at least two fixation and immunostaining experiments, and imaging of at least three different animals from each strain. Scale bar, 10 μm.

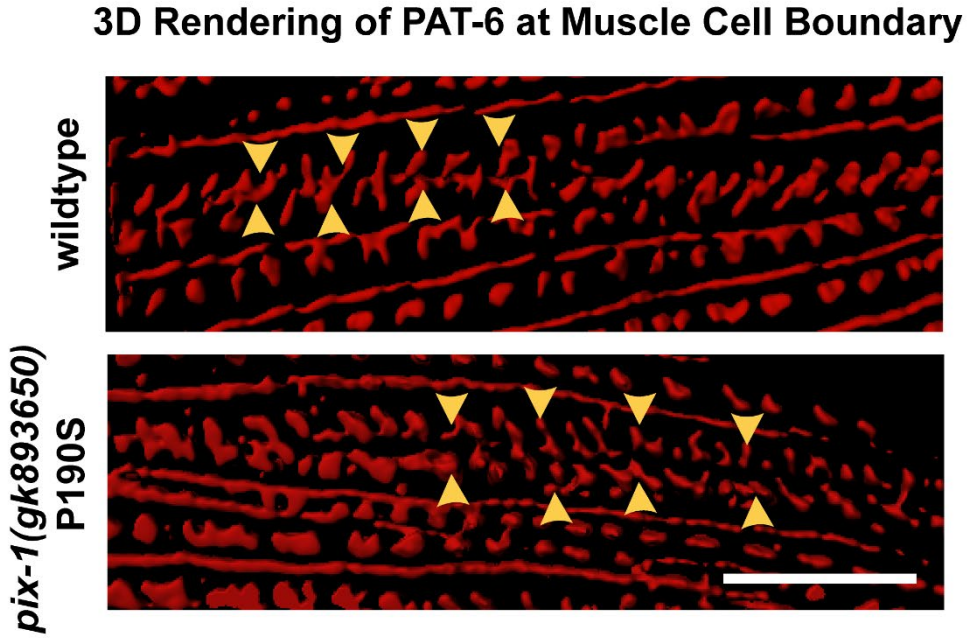

Figure 2.5S. 3D rendering of SIM images of PAT-6 muscle boundary localization of wild type compared with *pix-1(gk893650).* The higher resolution of SIM compared to confocal allows clear delineation of the two sides of the "zipper-like" structure at the muscle cell boundary (arrowheads pointing down and up). In wild type the two sides of the zipper appear close together, whereas in pix-1(gk893650) P190S, although both sides of the zipper are present, they are more separated. Each image is a representative image obtained from at least two fixation and immunostaining experiments and imaging at least three different animals. Scale bar, 5 μm.

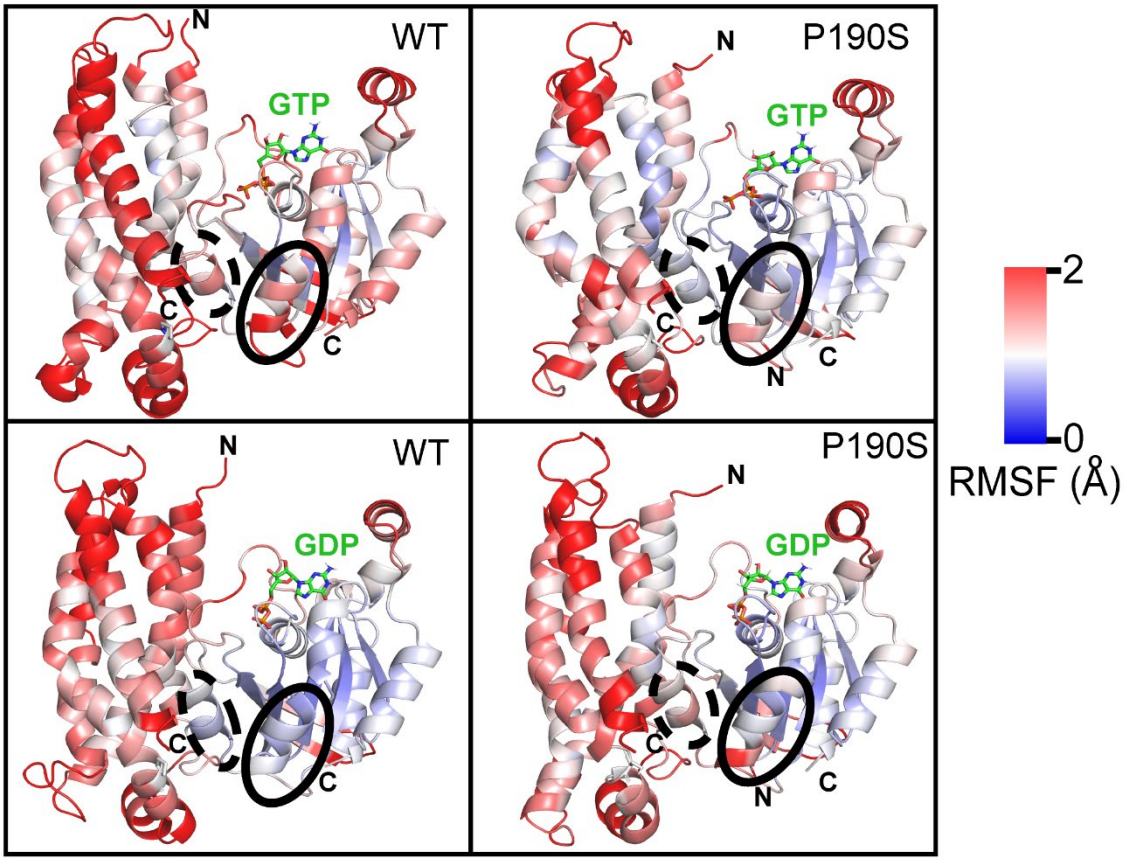

Figure 2.6S. Root mean square fluctuation analysis (RMSF) of PIX-1-Rac complexes indicate that the P190S mutation alters stability at the interface. Proteins are colored by RMSF as indicated. All regions colored red indicate RMSF > 2 angstroms over the simulation. To describe fluctuations on the interface, we focused on the indicated helical segments (dashed line = PIX-1, solid line = Rac) that are predicted to be in contact. In GTP-Rac complexes, the P190S mutation stabilizes the interaction between the two helices, as RMSF values on the two helices decrease. In GDP-Rac complexes, RMSF values show a net increase, indicating that the P190S mutation increases fluctuations compared to WT.

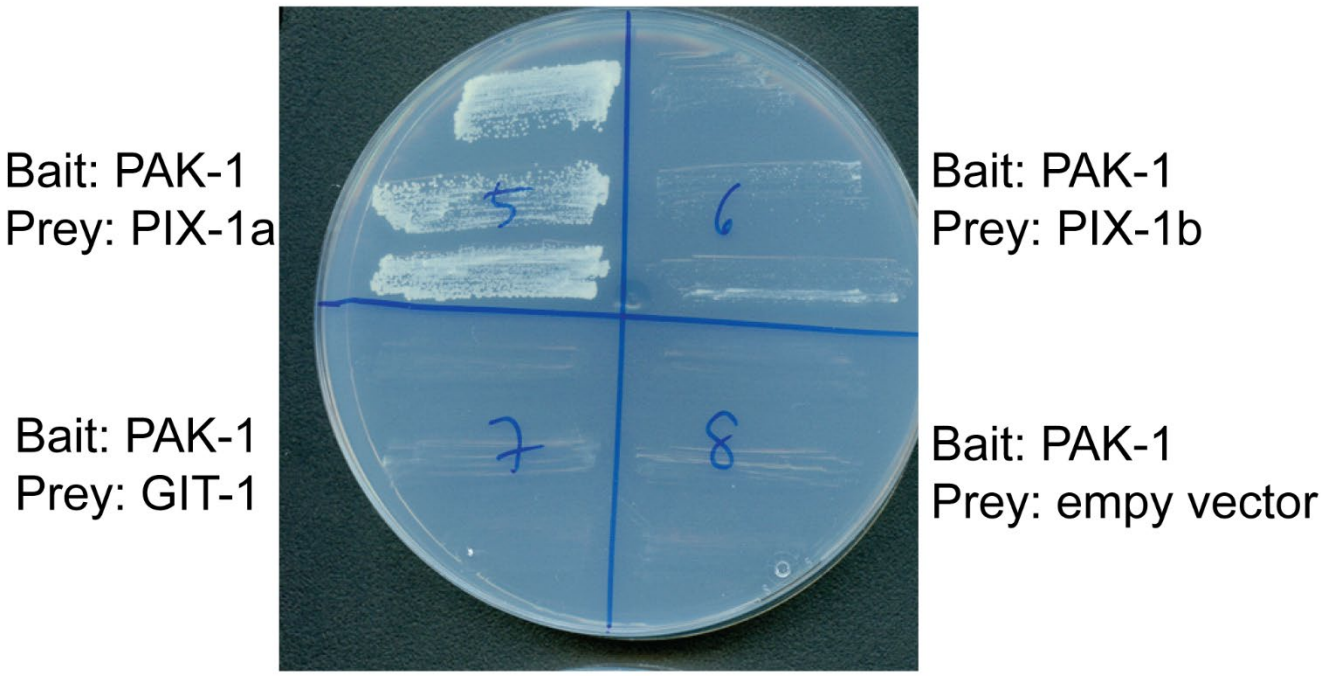

Figure 2.7S. Yeast two-hybrid assays showing that full length PAK-1 interacts specifically with full length PIX-1a but not full-length PIX-1b or full-length GIT-1. Yeast colonies containing the indicated bait and prey plasmids were streaked on -Histidine + 2mM 3AT plates and incubated at 30 degrees for 3 days. For reproducibility, as indicated, three independent yeast colonies were streaked out for each experiment, and they show the same result.

Supplemental Table 1. DH domain proteins in *C. elegans* muscle

***C. elegans* protein**	**human ortholog**	**notes**
CGEF-1	MCF2 & MCF2L	
ECT-2	ECT2	
EPHX-1	ARHGEF16	
EXC-5	FGD2 & FGD4	
FRM-3	FARP1 & FARP2	
OSG-1	ARHGEF17	
PIX-1	β-PIX	Rac GEF; localized to M-lines, dense bodies & MCBs
RHGF-1	ARHGEF11	
RHGF-2	PLEKHG5	
SOS-1	SOS1	
TAG-52	ARHGEF39	
TIAM-1	TIAM2	Rac GEF
UIG-1	PLEKHG1	Cdc42 GEF; localized to dense bodies
UNC-73	KALRN	Rac GEF & Rho GEF domains
UNC-89	obscurin	Rho GEF; localized to M-lines
VAV-1	VAV1 & VAV2	
Y37A1B.17	DNMBP	

Discussion

By screening a collection of adult-viable *C. elegans* mutants by immunostaining, we identified a strain in which IAC components are missing from the muscle cell boundaries but present and normally localized at M-lines and dense bodies. These boundaries consist of cell to ECM to cell attachments. The defect in the strain was mapped to a single mutant gene, *pix-1*, which encodes a PIX protein, known from previous studies to be a RhoGEF for Rac/ Cdc42. As compared to wild type, a *pix-1* null mutant shows an ~50% reduction in the level of activated (GTP bound) Rac in muscle. Despite having normally organized sarcomeres, multiple pix-1 mutants display reduced whole-animal locomotion. We hypothesize that this reduced motility results from decreased transmission of lateral forces between muscle cells. Interestingly, in addition to deficiency of PIX-1, muscle-specific overexpression of PIX-1 protein also results in decreased locomotion and disrupted muscle cell boundaries. Perhaps these results reflect the requirement for PIX-1 signaling to be set at just the optimal level for proper assembly or maintenance of IACs at the muscle cell boundary.

Antibodies to PIX-1 localize to all 3 IACs–muscle cell boundaries, M-lines and dense bodies—and yet PIX-1 is only required at muscle cell boundaries. One possibility is genetic redundancy, that is, there is a second PIX protein that is localized to M-lines and dense bodies that compensates for loss of PIX-1 at these sites. This does not seem to be the case however, since no PIX-1 paralogs can be found by querying the *C. elegans* proteome. Another possibility is that there are additional RhoGEF- containing proteins with RacGEF activity like PIX-1 that are present at M-lines and dense bodies, but not at muscle cell boundaries. We find that there are a total of 17 proteins in C. elegans that contain RhoGEF (DH) domains and are expressed in

muscle, based on the query of SAGE data (Supplementary Table 2.1S). (Meissner et al., 2009) These 17 proteins include PIX-1, and UIG-1 and UNC- 89 that have been studied previously. (Hikita et al. 2005) and (Qadota et al., 2020) UNC-89 is specifically localized to M-lines (Benian et al., 1996) and (Small et al., 2004) and the DH domain of UNC-89 specifically activates RHO-1(RhoA), (Qadota et al., 2008) and is thus not relevant here. The properties of UIG-1 somewhat support this hypothesis: UIG- 1 is localized to dense bodies and is a GEF for Cdc42. TIAM-1 is reported on WormBase to activate Rac. UNC-73 has two RhoGEF domains, one that activates Rac and one that activates RhoA. (Steven et al., 1998) The muscle intracellular locations of TIAM-1 and UNC-73 are unknown.

Another possible reason that PIX-1 is required at muscle cell boundaries but not at M-lines dense bodies can be envisioned. We observe the loss of IACs at muscle cell boundary when either the PIX-1 pathway is reduced or increased in activity; there are boundary defects in loss of function for *pix-1, git-1, ced-10,* and *pak-1*, and from overexpression of *pix-1*. These results could be interpreted as indicating a requirement for cycling of the Rac GTPase rather than its absolute activity. If IAC assembly required the PIX-1 pathway, then IACs that are assembling and disassembling at faster rates would be more sensitive to PIX-1 cycling. Therefore, we have considered the hypothesis that PIX-1 is required at MCBs because muscle cell boundaries are more dynamic that M-lines and dense bodies. However, our preliminary FRAP experiments with GFP tagged PAT-6 and UNC-97, show no differences in turnover rates at muscle cell boundaries vs. dense bodies, so this idea does not seem viable.

It should be emphasized that prior to our study, there were no known genes that when mutated resulted in loss or disorganization of IACs specifically at muscle cell boundaries. This

easily scorable phenotype allowed us to determine that each component of the known PIX-1 signaling pathway is required for the assembly or stability of IACs at muscle cell boundaries. Although *C. elegans* has a single PIX protein, in mammals, there are two PIX proteins, α-PIX and β-PIX, and these have been shown to be important for the development and function of nervous and immune systems. (Ranmakers et al., 2012) and (Missy et al., 2008) In *C. elegans*, PIX-1 has been shown to be required for several events during development: control distal tip cell shape and migration (important for germ cell formation) (Steven et al., 1998), migration of Q neuroblasts that give rise to sensory and inter-neurons (Dyer et al., 2010), tension-dependent morphogenesis of epidermal cells (Zhang et al., 2011), and for proper early embryonic elongation (Martin et al., 2014). However, until our results, no study had demonstrated a function for a PIX protein in striated muscle, in any organism.

By quantitative western blot, we showed that the level of PIX-1 is reduced in loss of function mutants for the scaffold protein GIT-1 and the effector protein kinase, PAK-1, but not for loss function for the Rac protein CED-10. These data suggest that GIT-1 and PAK-1 are required for the stabilization of PIX-1. The GIT-1 result is consistent with the known high-affinity complex formed between PIX and GIT proteins in mammals. (Schlenkerbet et al., 2009) It is also consistent with the reports that GIT1 deficient mice have reduced levels of α-PIX and β-PIX in the brain (Won et al., 2011) , and that GIT2 deficient mice have reduced levels of α-PIX in immune cells (Hao et al., 2015). Our finding that PIX-1 is reduced in a *pak-1* mutant is consistent with our finding that by yeast 2 hybrid assays, PIX-1 interacts with PAK-1 (see Supplementary Fig. 2.7S). It is also compatible with the known interaction of the SH3 domain of β-PIX with PAK1-3 in mammals. (Manser et al., 1998)

We have also shown that deficiency of either *pak-1* or *pak-2* results in the muscle cell boundary defect. In the future, we would like to determine if protein kinase activity of PAK-1 or PAK-2 is required for this function, and if so, to identify the key substrates in muscle. Zhang et al. (2011) have demonstrated that in *C. elegans*, PAK-1 phosphorylates several intermediate filament proteins in epidermal cells and this is required for maturation of hemidesmosomes in these cells. However, *C. elegans* muscle does not seem to express intermediate filament proteins, and this suggests the existence of additional PAK substrates, at least in muscle.

We were able to find that the MMP collection contains a most informative *pix-1* mutant allele, P190S. This mutation results in a stable full-length PIX-1 protein that localizes in the vicinity of muscle cell boundaries, but yet the boundaries are not properly formed. These data together with the absolute conservation of proline at this position in the RhoGEF domain of PIX proteins, suggest that the GEF activity of PIX-1 is crucial for its function. By expressing CED-10 (Rac) specifically in muscle, we were able to show that using a pull-down assay, worms carrying this PIX-1 P190S mutation have a ~50% reduction in the level of activated (GTP bound) CED-10(Rac) in muscle. This was approximately the same level of reduction in activated CED-10 that we observed in a *pix-1* null mutant. This suggests that, indeed, the P190S mutation completely inactivates the RacGEF activity of PIX-1. In the future, biochemical GEF assays using purified proteins will be necessary to determine if this prediction is true. Nevertheless, the muscle cell boundary defect of *pix-1* null and P190S mutants are different; whereas the null mutants result in the absence of IACs, the P190S mutant results in a defect in which components of the IAC localize to muscle cell boundaries, but the boundary appears split, such that the IACs are formed but are less functional, perhaps less able to anchor cells to the ECM. The fact that the P190S

mutant shows some IAC formation and an abundant full-length protein, and is still likely to have zero RacGEF activity, suggests that perhaps PIX-1 has a function in addition to its RacGEF activity.

Finally, our analysis of a homology model of the RhoGEF domain of PIX-1 bound to Rac1 reveals that the P190S mutation likely increases the affinity of GTP-bound Rac1 with PIX-1. We suggest that this enhanced interaction will slow the release of GTP-bound Rac from the RhoGEF of PIX-1, consequently, reduce the probability of GDP-bound Rac from binding to PIX-1, reduce the rate of the GTPase cycle, and thus result in less IAC formation. Again, in the future, we hope to conduct biochemical assays to test this prediction.

Materials and Methods

C. elegans strains. All nematode strains were grown on NGM plates using standard methods and maintained at 20° unless otherwise noted. The following mutant and transgenic strains were used: N2 (wild type, Bristol) (Brenner 1974), VC20386 [*pix-1 (gk299374)*], GB291 [*pix-1(gk299374)*; outcrossed 5X to N2], VC863 [*pix-1(gk416)*], GB292 [*pix-1(gk416)*; outcrossed 5X to N2], VC651 [*pix-1(ok982)*], GB294 [*pix-1 (ok982)*; outcrossed 3X to N2], VC30034 [*pix-1(gk406361)*], VC30094 *[pix-1 (gk299384)*], VC40598 [*pix-1(gk713465)*], VC40945 [*pix-1(gk893650)*], GB286 [*pix- 1(gk299374)*; *sfEx61[myo-3p:*::HA::PIX-1a; sur-5::NLS::GFP], GB288 [*pix-1 (gk299374)*; sfIs20[myo-3p::HA::PIX-1a; sur-5::NLS::GFP], GB290 [*pix-1(gk299374)*; *sfIs20[myo-3p*::HA::PIX-1a*; sur-5*::NLS::GFP; outcrossed 1X to *pix-1(gk299374)*], RB689 [*pak-1(ok448)*], RB1540 [*git-1(ok1848)*], MT9958 [*ced-10(n3246)*; received as outcrossed 4X to N2], VC259 [*pak-2(ok332)*; temperature sensitive (ts)], NG103 [*mig-2(gm103)*; received as outcrossed 2X to N2], VC126 [*rac-2(ok326)*], and VC1462 [*max-2(ok1904)*; received as outcrossed 1X to N2]. The ts allele *pak-2 (ok332)* was grown at 15°, embryos prepared, allowed to hatch to L1, and then shifted to 25° for growth to adulthood.

WormBase notes that *git-1(ok1848)* is an ~1 kb deletion. By PCR and sequencing, we determined that *git-1(ok1848)* is an 891 bp deletion that begins after the codon for amino acid 550 and continues into the 3'UTR, where, after an additional 29 codons occur in-frame a premature stop codon is encountered. This results in a mutant GIT-1 protein that is the missing the normal C-terminal 120 residues (normally GIT-1 is 670 residues long) but has 29 residues of novel sequence at its C-terminus.

CRISPR/Cas9 correction of *pix-1(gk299374)* to wild-type sequence. The conversion of the 153rd codon of pix-1 from the TAA stop codon in GB291, *pix-1 (gk299374)* 5X o.c., to a CAA Gln codon (as found in wild-type strain N2), was conducted by SunyBiotech (http://www.sunybiotech.com) using the following sgRNA and repair template to generate strain PHX2137, *pix-1(syb2137gk299374*): sgRNA, AACTGGAGCGTGAGCAAAAg(tga) (parentheses bracket the "NGA" site); repair template: ACGTTGGTTGGGAATTTCGAAGTAATTTACACTCTGAAACGTGA TCTTTTTGAGCAATTGGAGCGCGAGCAAAAgtgagttttaatttctccaaccttcttcaactttctt atttcagTGAG Since there were no suitable "NGG" sequences close to the sgRNA for the editing site, an "NGA" was used together with mutant Cas9 (D1135V R1335Q T1337R). PHX2137 was then outcrossed 3X to generate strain GB317, which was used for locomotion assays.

Immunostaining of body wall muscle. Adult nematodes were fixed and immu- nostained using the method described by Nonet et al. (1993) with further details pro- vided in Wilson et al. (2012). In brief, synchronized adults were washed free from E. coli by multiple washes in M9 buffer and ~50 µl of packed worms were fixed with 810 µl of fixative (50% Bouin's fixative, 50% methanol, 1.2% β-mercaptoethanol) at room temperature for 30 min, then frozen in liquid nitrogen for 5 min, thawed and continuing incubation at room temperature for an additional 30 mins. The worms were pelleted and washed 3× with 1.4 ml of BTB solution (20 mM sodium borate pH 9.5, 0.5% Triton X-100, 2% β-mercaptoethanol), and then resuspended in 1 ml of BTB and continuing incubation with mixing for 1 h. The worms were pelleted again and resuspended in 1 ml of BTB and incubated for 3 hrs with mixing at room temperature. The worms were pelleted and washed with 1 ml of BT (20 mM sodium borate pH 9.5, 0.5% Triton X-100),

pelleted, and washed 2× with 1 ml of AbA buffer (PBS, 1% bovine serum albumin, 0.5% Triton X-100, 1 mM sodium azide, 1 mM EDTA), pelleted, resuspended in 1 ml of AbA and incubated with mixing for 30 mins, pelleted and resuspended in 100 µl of AbA. Immunostaining was conducted using 5 µl of a suspension of these fixed worms together with 20 µl of primary antibody in AbA and incubating overnight with mixing. The animals were pelleted and washed 4X with PBS + 0.5% Triton X-100, pelleted, removing as much supernatant as possible and incubating with 20 µl of secondary antibody in AbA for 2 h, followed by washing 4× with PBS + 0.5% Triton X-100, and finally removing as much supernatant as possible and mounting 5 µl of resuspended worms with 5 µl of DAPCO solution (20 mM Tris-HCl pH 8.0, 0.2 M 1,4-diaza-bicyclo-2,2,2-octane (DABCO), 90% glycerol) on a glass slide with a coverslip and sealed with nail polish. The following primary antibodies were used at 1:200 dilution except as noted: anti-PAT-6 (rat polyclonal) (Warner et al., 2013), anti-UNC-52 (mouse monoclonal MH2) (Mullen et al., 1999), anti-PAT-3 (1:100 dilution; mouse monoclonal MH25) (Francis and Waterston, 1985) and (Gettner et al., 1995), anti-UNC-95 (rabbit polyclonal Benian-13) (Qadota et al., 2007), anti-UNC-112 (1:100 dilution) (Hikita et al., 2005), anti-MHC A (mouse monoclonal 5–6) (Miller et al., 1983), anti-UNC-89(rabbit polyclonal EU30) (Benian et al., 1996), anti-ATN-1 (mouse monoclonal MH35) (Francis and Waterston, 1991), anti-HA (mouse monoclonal; H3663; Sigma-Aldrich), and anti-GFP (rabbit polyclonal; Thermo Fisher, A11122). Secondary antibodies, used at 1:200 dilution, included anti-rabbit Alexa 488, anti-rat Alexa 594, and anti-mouse Alexa 594, all purchased from Invitrogen. Fixation and phalloidin-rhodamine staining was conducted as described. (Waterston et al., 1984) Images were captured at room temperature with a Zeiss confocal system (LSM510) equipped with an Axiovert 100 M microscope and an Apochromat

x63/1.4 numerical aperture oil immersion objective, in 1× and 2.5× zoom mode. For the images presented in Fig. 2, and Supplemental Figs. 2 and 5, super-resolution microscopy was performed with a Nikon N-SIM system in 3D structured illumination mode on an Eclipse Ti-E microscope equipped with a 100×/1.49 NA oil immersion objective, 488- and 561-nm solid-state lasers, and an EM-CCD camera (DU-897, Andor Technology). Super-resolution images were reconstructed using the N-SIM module in NIS-Elements software. For all the images, confocal, and SIM, the color balances were adjusted by using Adobe Photoshop (Adobe, San Jose, CA).

Mapping the phenotype to *pix-1*. The original MMP strain VC20386 (Thompson et al., 2013) has outcrossed to wild type N2 Bristol three times, each time selecting for the PAT-6 muscle boundary defect. Comparison of genomic sequences of VC20386 and N2 allowed the selection of SNPs on each chromosome arm to distinguish the two strains. PCR and Sanger sequencing of these 12 segments from the third outcrossed strain revealed that only the left arm of chromosome III and the right arm of X were derived from VC20386. For III and X, we identified genes known to be expressed in muscle (Meissner et al., 2009), and of these identified four genes on III and three genes on X, that had nonsense or non-conservative missense mutations in VC20386. RNAi for three of them failed to reveal the PAT-6 boundary defect. One of the 7 genes, pix-1 on X, had a nonsense mutation. Six additional mutant alleles of pix-1 were obtained from CGC, and four of these six mutants also showed the PAT-6 boundary defect (detailed in Results).

Transgenic rescue. An HA-tagged cDNA encoding full-length PIX-1a was amplified by PCR using the RB2 cDNA library (provided by Robert Barstead) as template and was cloned into vector pPD95.86 (provided by Andrew Fire) designed to express HA-PIX-1a in muscle by the

myo-3 muscle-specific promoter. This plasmid, pPD95.86-HA-PIX-1a at 10 ng/µl together with plasmid pTG96 which expresses SUR-5-NLS-GFP as a transformation marker at 90 ng/µl was micro- injected into *pix-1(gk299374)* 5X o.c. to generate the strain GB286, *pix-1(gk299374)*; *sfEx61[myo-3p*::HA::PIX-1a; *sur-5*::NLS::GFP]. This extrachromosomal array was integrated into the genome by ultraviolet irradiation (Mitani 1995) with modifications (Peter Barrett, personal communication). The resulting nematode strain is called GB288, *pix-1(gk299374)*; *sfIs20 [myo-3p*::HA::PIX-1a; *sur-5*::NLS::GFP]. To remove back- ground mutations induced by UV, GB288 was backcrossed to *pix-1(gk299374)* 1X, recovering strain GB290, and this strain was tested in locomotion assays. The extrachromosomal array *sfEx61 [myo-3p*::HA::PIX-1a; *sur-5*::NLS::GFP], was also crossed into N2 to generate the strain GB295.

Imaging of F-actin at the muscle cell boundary. We used strain KAG547 kindly provided by Kathrin Gieseler (Universite Claude Bernard Lyon): GFP::MYO-3; *Ex [myo-3p::LifeAct::mCherry*]. Animals were washed off plates and washed free from bacteria using M9 buffer and then immobilized by incubation in 10 µM levamisole in M9 for 10 min. Approximately 50–100 animals in 3 µl were added to 7 µl of ice-cold 25% Pluronic F127 in M9 (Hwang et al., 2014) lying on a cold glass slide, to which was added a cover slip and it was sealed with nail polish. After incubation at room temperature for 5–10 min to solidify, images were taken using a Nikon N-SIM microscope system, as described above.

Protein sequence analysis. Nematode PIX-1a protein sequence was obtained from Wormbase. A BLAST homology search identified human orthologs of the nematode protein using the NCBI PubMed database. The domain organization for PIX-1 and its orthologs were analyzed via

PFAM. Human α-PIX and β-PIX amino acid sequences were aligned with PIX-1 using pBLAST to determine percent identities for each domain (Fig. 3a). PIX-1 RhoGEF domains from 10 organisms were compared also using pBLAST (Fig. 9a).

Measurement of CED-10 activation state in body wall muscle. An HA-tagged cDNA encoding full-length CED-10 was amplified by PCR using the RB2 cDNA library as template and was cloned into vector pKS-HA8(Nhex2), the DNA sequence verified, and then the NheI fragment was excised and inserted into pPD95.86 designed to express HA-CED-10 in muscle from the myo-3 muscle specific promoter. This plasmid, pPD95.86-HA-CED-10, at 10 ng/µl together with plasmid pTG96 which expresses SUR-5-NLS-GFP as a transformation marker at 90 ng/µl was microinjected into wild-type animals to generate a transgenic strain GB314, sfEx63[myo-3p::HA::CED-10; sur-5::NLS::GFP]. This extrachromosomal array was integrated into the genome by ultraviolet irradiation (Mitani, 1995) with modifications (Peter Barrett, personal communication). The resulting nematode strain is called GB315, sfIs22 [myo-3p::HA::CED-10; sur-5::NLS::GFP]. This strain was crossed into pix-1(gk299374) 5X OC, to generate strain GB316, pix-1(gk299374); sfIs22, and crossed into pix-1(gk893650) [P190S] 5X OC, to generate strain GB318, pix-1 (gk893650); sfIs22. After growing several grams of worms from GB315, GB316, and GB318, worm powders were prepared by grinding in a mortar and pestle under liquid nitrogen on a bed of dry ice. We modified the Rac1 Activation Assay Biochem Kit (cat. #BK035, Cytoskeleton, Inc.) as follows: One small spatula-full of worm powder was added to 3ml of ice-cold Cell Lysis Buffer containing protease

inhibitor cocktail, vortexing for 1 min, and centrifuging at maximum speed in a microcentrifuge for 10 min at 4°. A small portion supernatant was used for protein concentration determination using the BCA Assay (cat. #23225, ThermoScientific), and multiple 200 µl aliquots of the remainder were snap frozen in liquid nitrogen and stored at −70°. The protein concentrations of the lysates varied from 1.25 to 3.4 mg/ml. Positive and negative controls were created by adding to 250 µg of total protein of wild-type worm lysate, GTPγS to a final concentration of 0.20 mM, or GDP to a final concentration of 1 mM, respectively. 250 µg of total protein from each lysate were added to 10 µg of GST-PAK-PBD Beads, and incubated with mixing for 1 h, 15 min, at 4°. Then, the beads were pelleted at 4° by spinning at 4000 Å~ g for 1 min, supernatant carefully removed, and the beads were washed 1Å~ with Wash Buffer, and the beads pelleted. After removing as much supernatant as possible, 20 µl of 2Å~ Laemmli were added, vortexed for 5 s, heated at 95° for 3 min, centrifuged at top speed for 3 min, and then 20 µl of each supernatant were run on a 12% SDS-PAGE and transferred to nitrocellulose. HA-CED-10 was visualized by incubating with rabbit monoclonal antibodies to HA at 1:1000 dilution (cat. #C29F4, Cell Signaling Technology), and reacting with ECL reagents and exposed to film. We used a flat-bed scanner to image the Ponceau S staining of the blot using the “reflective” mode in 24-bit color, and to image the ECL reactions recorded on film using the “film scan” mode in gray scale. The images were opened in AdobePhotoshop, and after inverting the ECL images, both the ECL bands (HACED-10) and the Ponceau S bands (GST-PAK-PBD) “mean” and “pixel” values

were recorded. The absolute intensity of each band was a product of these two values. The HA-CED-10 band products were normalized by dividing by the GSTPAK-PBD bands for each lane.

Swimming and crawling assays. For swimming assays, day 2 adults from two, 6 cm NGM OP50 seeded plates were washed off the plates, washed free from bacteria and collected into M9 buffer such that the ratio of worms to buffer was 1:1. 2ml of M9 buffer was added to an unseeded 6 cm NGM plate where upon 5 µl of worm suspension was added to the center of the plate. Worms were allowed 5 min to adapt before a video recording of their swimming motions was made using a dissecting stereoscopic microscope fitted with a CMOS camera (Thorlabs). Ten, 10 s videos were recorded for each nematode strain from different sections of the plate, each video tracking the motion of ~10 worms. The video data were analyzed by Image J FIJI WrmTracker software (Nussbaum-Krammer et al., 2015) to obtain body bends per second (BBPS). After removing outliers and animals that had moved out of frame, ~30 animals were analyzed for each strain. The resulting BBPS values for each mutant strain were compared to wild type and differences were tested for statistical significance using a Student T-test.

For crawling assays, day 2 adults were harvested as above, except that all washing steps used M9 buffer containing 0.2 g/L gelatin. Five microliters of worm suspension was added to the center of a 6 cm unseeded NGM plate, and the excess liquid was removed. After 5 min for adaptation, worm crawling was recorded using the above-mentioned strategy for extraction of BBPS for individual worms in each video. The resulting values for each strain were compared to wild type for statistical analysis using a Student T-test for significance.

PIX-1 antibody generation. Rabbit polyclonal antibodies were generated to two different immunogens from PIX-1a. Immunogen #1 consists of residues 268–449, and immunogen #2 consists of residues 441–646. The coding sequences for each immunogen were cloned into vectors pGEX-KK1 and pMAL-KK1, respectively to express glutathione S-transferase (GST) and MBP fusion proteins in E. coli. (Mercer et al., 2006) In brief, to express each fusion protein, the plasmids were transformed into Esherichia coli Rosetta 2 (DE3) (Millipore Corporation, cat. no. 71397-4) and grown in Luria-Bertani medium containing 10 μg/ml ampicillin at 37° to OD_{600}=0.6–0.8, followed by induction of protein expression with 0.5mM isopropyl β-D-1-thiogalactopyranoside, and further growth at 20° for 5 h. Cell pellets were harvested by centrifugation and resuspended in 50mM Tris-HCl pH 8.0 supplemented with 100mM phenylmethylsulfonyl fluoride (PMSF) and cOmplete Mini protease inhibitor cocktail (Roche, Inc., cat. no. 11836170001), and then broken in a French pressure cell at 1000 pounds inch−2, addition of Triton X-100 to 1%, followed by spinning out debris by centrifugation at 12,000 Å~ g for 20min. The cleared lysates were added to either a slurry of glutathione-agarose beads (Sigma, cat. no. G-4510) or amylose resin (New England BioLabs, cat. no. E8021L), and incubated with shaking for 30min at 4°. The beads were then washed 5Å~ with 50mM Tris-HCl pH 8.0 containing 1% Triton X-100 and 100mM PMSF, and then 4Å~ with 50mM Tris-HCl pH 8.0 containing 100mM PMSF. The beads/resin were placed onto mini columns and then eluted with either 10mM free glutathione or 10mM maltose in 50mM Tris-HCl pH 8.0. The GST fusions were shipped to Noble Life Sciences (Sykesville, Maryland) for the production of rabbit antibodies. Antibodies were affinity-purified using Affigel (BioRad)-conjugated MBP fusions, as described. (Mercer et al., 2003) In brief, the MBP fusion proteins were dialyzed against 100mM

3 morpholinopropane-1-sulfonic acid (MOPS) pH 7.0, and then 3–10mg were covalently coupled to ~1ml of a 50:50 mixture of Affi-Gel 10 and Affi-Gel 15 beads (Bio-Rad Laboratories, cat. nos. 1536099 and 153-6051) according to the manufacturer's procedure. These columns were then used to affinity purify ~2ml of antiserum and the antibodies eluted with low and high pH and concentrated with a centrifugal filter (Centriprep 10, Millipore, cat. no. 4304). The method of Hannak et al. (2002) was used to prepare total protein lysates from wild-type, *5X pix-1(gk416)* o.c., *pix-1(ok982*), *pix-1(gk299374)* 5X o.c., *pix-1(gk893650*), *git-1(ok1848), ced-10(n3246)*, and *pak-1(ok448)* mixed-stage animals. In brief, we grew worms on 2–4, 10 cm NGM plates seeded with E. coli OP50, washed the worms off with M9 buffer and continued washing until the supernatant was clear of bacteria, yielding ~100 µl of worms after centrifuging briefly in a microfuge. To make protein lysates, an equal volume of 2Å~ Laemmli sample buffer containing EDTA and a protease inhibitor cocktail was added, vortexed 1min, and sonicated for 10mins in a water bath sonicator containing 80 °C water. After a quick pop spin, the material was heated in a boiling water bath for 5min, and then debris was pelleted by spinning for 5min at top speed in a microfuge. Equal amounts of total protein were separated on 10% polyacrylamide-SDS- Laemmli gels, transferred to nitrocellulose membranes, reacted with affinity purified, E. coli OP50-absorbed anti-PIX-1a at 1:200 (for immunogen #1) or at 1:5000 (for immunogen #2), reacted with goat anti-rabbit immunoglobulin G conjugated to HRP (GE Healthcare) at 1:10,000 dilution, and visualized by ECL. For total protein loading control, we used reaction to either paramyosin (monoclonal 5–23 (Miller et al., 1991); 1:5000 dilution), or to histone H3 (rabbit polyclonal ab1791, Abcam, Inc.; 1:40,000 dilution).

Model construction for molecular dynamics simulations. Six complexes were prepared for MD simulations. (1) A PIX-1 homology model prepared using PDB 1BY1 (human beta-PIX) as a template. (Aghazadeh et al., 1998) Our model aligned PIX-1 residues 89-272 with the beta-PIX DBL homology domain. (2) A PIX-1-Rac1 complex prepared using PDB 5O33 (GEF Kalirin DH domain in complex with GDP-bound Rac1 GTPase) as a template. (3) PIX-1-Rac1 complex with GTP-bound Rac1, obtained from PDB 6BC1. For consistency, Rac1 sequences were restored to wild type in both GDP- and GTP-bound forms. Complexes 4–6 were P190S mutants of complexes 1–3 respectively. All mutations were introduced in silico.

Molecular dynamics simulations. The complexes were solvated in an octahedral box of TIP3P water with a 10 Å buffer around the protein complex. Na+ and Cl− ions were added to neutralize the protein and achieve physiological buffer concentrations. Xleap in AmberTools 18 (Case et al., 2018) was used to prepare systems for simulation with the parm99-bsc0 forcefield (Pérez et al., 2007). Parameters for GDP and GTP in Rac1 complexes were created using Antechamber (Wang et al., 2006) Minimizations and simulations were performed with Amber18 (Case et al., 2018). Systems were minimized with 5000 steps of steepest descent followed by 5000 steps of conjugate gradient minimization with 500 kcal/mol Å2 restraints on all atoms. In PIX-1-Rac1 complexes, an extra minimization step (5000 steps of steepest descent, 5000 steps of conjugate gradient) was performed, with restraints retained on protein residues lying on the interface between PIX-1 and Rac1. Restraints were then removed from all atoms and both conjugate gradient and steepest descent minimization were repeated.

Following minimization, the systems were heated from 0 to 300 K with a 100-ps run, 5 kcal/mol Å2 restraints on all protein/nucleotide atoms and using constant volume periodic boundaries. MD equilibration was performed for 10ns with 10 kcal/mol Å2 restraints on all solute atoms, using the NPT ensemble. Restraints were reduced to 1 kcal/mol Å2 which was followed by an additional 10ns of MD. Restraints were then removed and 500ns production simulations obtained for each system. All bonds between heavy atoms and hydrogens were fixed with the SHAKE algorithm (Ryckaert et al., 1977) permitting the use of a 2-fs timestep. Long-range electrostatics and van der Waals forces were calculated with a 10 Å cutoff distance. *Analysis.* 25,000 evenly spaced frames were obtained from each simulation and used for analysis. Structural averaging and analysis were performed with the CPPTRAJ module of AmberTools. (Roe and Cheatham, 2013) RMSF analysis was performed on Cα atoms of protein residues to calculate atomic deviations over the course of the simulation. RMSF was computed relative to the starting structure. CPPTRAJ was used to calculate distances between heavy atoms of residue pairs over trajectories. Solvent accessible surface areas (SASA) of proteins were calculated using the molsurf algorithm in AmberTools. Contact surface areas in protein complexes were calculated using the formula ($SASA_{PIX\text{-}1} + SASA_{Rac1}$) - $SASA_{complex}$.

Chapter 3

The RhoGAP RRC-1 is a member of the PIX pathway and controls the assembly or stability of integrin adhesion complexes in muscle

The contents of this chapter will be submitted for publication in March 2022.

Introduction

Integrin adhesion complexes (IAC), also known as focal adhesions, consist of the transmembrane heterodimeric proteins α/β integrin as well as hundreds of other proteins that are associated both from the extracellular matrix (ECM) and especially intracellularly (Anthis and Campbell, 2011; Sun et al., 2014; Bachir et al., 2014; Horton et al., 2015). IACs are important for many cell types. The adhesion of cells to a matrix is crucial for both tissue formation and for cell migration. In stationary cells like muscle, these complexes are rather stable, but in motile cells they are dynamic, with new complexes assembled at the leading edge and older complexes disassembled at the trailing edge (Anthis and Campbell, 2011). When integrins are expressed on the cell surface they are in a compact or bent or inactive state, unable to bind to their ECM targets, but can become activated to bind via several triggers (e.g. chemokines, local increase in $P(4,5)IP_2$) that lead to binding of the cytoplasmic tail of β-integrin to talin. Binding to talin results in integrin assuming a more open conformation, able to bind to extracellular targets (Tadokoro et al., 2003). Kindlin is also involved in integrin activation by clustering of talin-activated integrins, at least in platelets (Ye et al., 2013). Although we understand the steps involved in the formation of IACs, we do not know how the composition of an IAC is determined or regulated, and we do not know what determines where an IAC forms, how many IACs form, and what their spacing will be.

In striated muscle, which includes both skeletal and cardiac muscle, myofibrils at the periphery of the cell are attached to the cell membrane and ECM via “costameres”(Ervasti, 2003; Henderson et al., 2017), muscle-specific IACs. Costameres are involved in anchorage of the muscle cell to the ECM, and transmission of force. *C. elegans* is an outstanding genetic model

organism in which to learn new principles about muscle (Gieseler et al., 2017). The major striated muscle is found in the body wall and is used for locomotion (Benian and Epstein, 2011). Similar to striated muscle in other animals, the thin filaments are attached to Z-disk like structure (dense bodies), and the thick filaments are attached to M-lines. The sarcomeres are restricted to a narrow ~1.5 mm zone adjacent to the cell membrane along the outer side of the muscle cell, and all the dense bodies and M-lines are anchored to the muscle cell membrane and ECM. The base of dense bodies and M-lines contain integrin adhesion complexes (IACs) and much is known about their protein composition (Gieseler et al., 2017). Additional IACs are located at the muscle cell boundaries, where they form attachment plaques that anchor the muscle cell to a thin layer of ECM that lies between adjacent muscle cells (Qadota et al., 2017). Thus, in *C. elegans* muscle IACs are located at M-lines, dense bodies and muscle cell boundaries (MCBs), and although the base of each consists of integrins and a set of core proteins, they also contain proteins specific for each site (Gieseler et al., 2017). IACs at MCBs consist of a subset of proteins that are found at dense bodies (Qadota et al., 2017).

Recently, we reported that a protein in *C. elegans*, PIX-1 (orthologous to β-PIX in mammals), is required for the assembly or stability of IACs at MCBs (Moody et al., 2020). A PIX signaling pathway is important for the mammalian nervous (Schmalxigaug et al., 2009; Ramakers et al., 2012; Huang et al., 2011) and immune systems (Volinsky et al., 2006; Missy et al., 2008), and for the control of distal tip cell shape and migration (important for formation of the germline) (Lucanic and Cheng, 2008), and for epithelial morphogenesis (Zhang et al., 2011) in *C. elegans*. However, no prior study had demonstrated a function for PIX in striated muscle in any organism. PIX proteins contain an SH3 domain, and a Rho GEF domain that activates the

small GTPases Rac and Cdc42. In *C. elegans*, PIX-1 is localized to the IACs present at the muscle boundaries and the IACs at M-lines and dense bodies. As compared to wild type, a *pix-1* null mutant shows reduced levels of activated, GTP-bound Rac in muscle. Interestingly, either deficiency or overexpression of PIX-1 results in disrupted MCBs and decreased nematode muscle function, suggesting that the level of PIX-1 needs to be tightly controlled. The Rho GEF domain of PIX proteins promote the exchange of GDP for GTP, thus converting inactive to active Rac or Cdc42. In the PIX pathway, the active GTP bound Rac or Cdc42 binds to and activates a PAK family protein kinase, which then phosphorylates one or more unknown substrates to somehow promote assembly of IACs.

Rho family GTPases (Rho, Rac, Cdc42) cycle between active (GTP-bound), and inactive (GDP-bound) states. Activation occurs via guanine-nucleotide exchange factors (GEFs)(e.g. PIX) that promote exchange of GDP with GTP, and inactivation occurs via GTPase-activating proteins (GAPs), which promote the hydrolysis of GTP to GDP. Perhaps because of the cycling requirement, the terminal phenotypes of loss of function for a GEF and loss of function for a GAP (for a particular GTPase and cellular function), are often the same. For example, in yeast, loss of function of the GTPase Bud1p (similar to mammalian RapGTPases) has a similar phenotype to loss of function of its GEF, BUD5, and its GAP, BUD2 (Michelitch and Chant, 1996). In *C. elegans*, the same embryonic cytokinesis defect is found for loss of function for *rho-1* (RhoA), *rga-3* (Rho GAP), *rga-4* (Rho GAP), and *ect-2* (Rho GEF)(Morita et al., 2005; Schonegg et al., 2007; Jantsch-Plunger et al., 2000; Canman et al., 2008). For the PIX pathway in *C. elegans*, the GEF is PIX-1, and the GAP is unknown. In fact, a GAP for the PIX pathway has not been reported for any organism. We hypothesized that for the PIX pathway in nematode

muscle, the loss of function for the GEF, PIX-1, and an unknown GAP, would be the same. Using an easily scorable phenotype (i.e. loss of IAC components at the MCB), we screened for mutations in genes predicted to encode Rho GAP proteins, and identified one protein, RRC-1, which is required for assembly or stability of IACs at MCBs. RRC-1 contains an SH3 domain and a Rho GAP domain, and is localized to the IACs of MCBs, like PIX-1. Loss of function mutants of *rrc-1* show reduced whole animal locomotion, and genetic interaction with *pix-1* consistent with the idea that they function in the same pathway.

Results

The output of the PIX signaling pathway in mammals and nematodes is that p21-activated kinases (PAKs) which are serine/threonine protein kinases are activated by binding to GTP-bound Rac or Cdc42. Because activation of PAK requires that a GEF first activates Rac or Cdc42, and inactivation occurs by a GAP, we hypothesized that a PAK-1 kinase-dead and a PAK-1 kinase constitutively active mutant might have the same phenotype. We have an easily scorable muscle phenotype for the status of the PIX-1 pathway, i.e., deficiency of any component results in disorganization of integrin adhesion complexes (IAC) at the muscle cell boundary (MCB), including a deficiency of *pak-1* (Moody et al., 2020). We used CRISPR/Cas9 to generate mutant worms carrying either a catalytically dead or constitutively activating mutations for *pak-1*. For the catalytically dead mutant, we replaced K324 with A. In nearly all protein kinases, a K at this position is found in the small lobe of the kinase domain and coordinates ATP and helps transfer γ-phosphate. Mutation of this K to A or several other amino acids inactivates most known kinases (Iyer et al., 2005).

In the absence of GTP-Rac or GTP-Cdc42, PAKs exist in a closed conformation due to binding of an N-terminal (67-150) autoinhibitory domain (AID) with the more C-terminal kinase catalytic domain (Zenke et al. 1999). Binding of GTP-Rac or Cdc42 to this AID leads to an opening of the PAK structure and activation of its phosphotransferase activity. A constitutively active human PAK has been generated by substituting the highly conserved L107 to F in this AID (Brown et al., 1996). In the nematode protein, the homologous residue is L99, and this was mutated to F as described under Methods. As shown in Figure 1, the catalytically dead mutant, *pak-1(syb632)* which has a K324A mutation, and a constitutively active mutant, *pak-1(syb647)*

which has a L99F mutation, each have a similar defect at the MCBs. Specifically, each mutant shows less accumulation of PAT-6 and increased spacing between adjacent muscle cells. This result demonstrates that either decreased or increased activity of the PIX-1 pathway can have the same terminal phenotype. Thus, we hypothesized that increased activity of the PIX-1 pathway by inactivation of a Rho GAP would have the same phenotype as decreased activity of the PIX-1 pathway by inactivation of its Rho GEF, PIX-1.

Our homology search has revealed that there are 32 genes in *C. elegans* that encode proteins harboring Rho GAP domains. Of these 32, 18 of them are expressed in body wall muscle based on SAGE data (Meissner et al., 2009). We obtained mutants for all 18 genes from the Caenorhabditis Genetics Center (see Methods) and screened them for the MCB defect using anti-PAT-6 (α-parvin) immunostaining. Mutants for two genes, *hum-7* and *rrc-1* (Supplementary Figure 1, Supplementary Table 1) each demonstrated defects of the MCB. *hum-7* encodes a 1880 residue protein containing an RA domain, a class IX myosin motor domain, 2 IQ domains, and a Rho GAP domain, and will be described elsewhere. The *rrc-1* gene encodes an approximately 750 residue protein that contains a Rho GAP domain and an SH3 (Figure 2a). Because RRC-1 is a simpler protein, we decided to focus our efforts on RRC-1. We are just beginning the analysis of HUM-7 and it will be described elsewhere. Alternative splicing of *rrc-1* produces three protein isoforms containing both domains and of approximately the same size (742-759 aa) (Figure 3.2b). A Rho GTPase effector pull-down assay of nematode RRC-1 in mammalian tissue culture cells demonstrates that RRC-1 has GAP activity towards mammalian Rac1 and Cdc42 but not RhoA (Delawary et al. 2007). Our BLAST search revealed that the closest human ortholog to RRC-1 is ARHGAP33, and the two proteins are 35% identical in sequence

throughout their lengths. The Rho GAP domains are 49% identical, and the SH3 domains are 28% identical (Figure 3.2c).

The original allele that we characterized, *rrc-1(ok1747)*, is a frame-shifting deletion that removes exons 7 and 8 (Figure 3.2a). We obtained 3 more *rrc-1* mutant alleles from the Caenorhabditis Genetics Center, the first being *tm1023*, which is also a frame-shifting deletion removing exons 3 and 4. Inspection of the Million Mutation Project collection (Thompson et al., 2013) revealed 16 *rrc-1* mutants, one being a splicing defect, and 15 being missense mutations. We ordered the splicing defect mutant, and the four missense mutants that have nonconservative amino acid changes. Unfortunately, two of these strains were too difficult to grow, and one had background mutations in *pak-1* and in *unc-89,* which would confound our analysis, and thus were not pursued. Therefore, we had a collection of four *rrc-1* mutant alleles, including two deletions, one missense mutant, and one splicing acceptor mutant (Figure 3.2a). We outcrossed each mutant to wild type five times, to remove most of the background mutations. Figure 3.2d shows results from immunostaining of the four *rrc-1* alleles with antibodies to PAT-6 (a-parvin) to visualize IACs at the MCBs. All four show MCB defects, but the deletion alleles, *ok1747* and *tm1023*, are more severely affected.

By immunostaining, we found that in the deletion mutant, *rrc-1(ok1747)*, other IAC components are missing or mis-localized at MCBs (Figure 3.3). These IAC components include UNC-52 (perlecan) in the ECM, PAT-3 (β-integrin) at the muscle cell membrane, UNC-95 and UNC-112 (kindlin). We conclude that the Rho GAP RRC-1 is required for the assembly or stability of IACs at the MCB.

In *C. elegans*, the force of body wall muscle contraction that bends the worm and thus permits locomotion of the animal, is transmitted through all three IAC sites, including the M-lines, the dense bodies and the adhesion plaques at the MCBs. We previously showed that in *pix-1* mutants, which have defective MCBs but normal M-lines and dense bodies, there is reduced whole animal locomotion (Moody et al., 2020). Because *rrc-1* mutants show a similar defect to *pix-1* mutants at the MCBs, we conducted worm motility assays. As shown in Figure 3.4a, both deletion alleles, *ok1747* and *tm1023*, and the splicing mutant, *gk290525*, display reduced swimming when compared to wild type. However, the missense mutant, *gk859353*, displays swimming that is not significantly different from wild type. Although *gk859353* is a non-conservative G to E change, it resides outside of a recognizable domain and thus may not have a critical function. Crawling may be a more stringent test of the ability of a worm to move because it is likely that the worm needs to overcome the surface tension lying between itself and the agar surface. Thus, as shown in Figure 3.4b, all four *rrc-1* mutants exhibit reduced crawling as compared to wild type. Moreover, for all four alleles, the trends in both swimming and crawling are similar, with the deletion alleles and splicing mutant showing slower movement than the missense mutant. Overall, this data is consistent with the idea that RRC-1 supports normal muscle function.

We first attempted to make antibodies to RRC-1. Unfortunately, using two different immunogens regions we failed to generate specific antibodies in rabbit. Therefore, to localize RRC-1 in muscle, we used CRISPR/Cas9 to create a worm strain, *rrc-1(syb4499)*, in which the endogenous *rrc-1* gene expresses RRC-1 with an HA tag fused to its C-terminus. As shown in Figure 3.5a, by western blot using anti-HA antibodies, we detect an RRC-1-HA fusion of

expected size (approximately 90 kDa) from this strain but not from wild type. We then used HA antibodies to perform immunostaining. As indicated in Figure 3.5b, these antibodies localize RRC-1-HA to the MCB, co-localizing with antibodies to PAT-6 (α-parvin). We also observed weak localization of RRC-1-HA to the same focal plane as the base of the M-lines and dense bodies where PAT-6 is localized, in a generally striated pattern, but in a more diffuse, less organized manner. This weak staining is not background staining, as the same dilution of anti-HA antibodies and the same gain with our confocal microscope detects no fluorescence in wild type animals (Figure 3.5b, left column). The pattern of RRC-1-HA is somewhat similar to the pattern of UNC-52 (perlecan) immunostaining (Qadota et al., 2017). These results show that RRC-1 is localized to the MCB which is consistent with playing a role in the lateral transmission of force between adjacent muscle cells.

Given the similarity in phenotype between *rrc-1* and *pix-1* mutants, and the similar localization of RRC-1 and PIX-1 to the MCB, we sought to determine if there are genetic interactions between these two genes. By genetic recombination, we created a strain that expresses the HA-tagged RRC-1 in a *pix-1* mutant background, which we designate, RRC-1::HA *pix-1(gk299374)*. In Figure 3.6a, we compare the immunolocalization of PAT-6, and RRC-1::HA in a wild type vs. the *pix-1* mutant background. As shown in Figure 3.6a, PAT-6 is normally localized to the MCB in the strain expressing RRC-1::HA, but missing in the strain RRC-1::HA *pix-1(gk299374)*, as expected for this *pix-1* mutant (Moody et al., 2020). When we immunostained for RRC-1::HA, we found that RRC-1::HA is mostly missing from the MCB in RRC-1::HA *pix-1(gk299374)*. However, the total protein levels of RRC-1::HA is not affected by

pix-1 deficiency, as shown by a quantitative western blot (Figure 3.6b). These data suggest Pix-1 is required for RRC-1 localization to the MCB.

We next asked whether rrc-1 deficiency could affect the localization of PIX-1. We compared the localization of PIX-1 in wild type vs. *rrc-1(ok1747)*. As shown in Figure 3.7a, the localization of PIX-1 is not affected by loss of RRC-1. In addition, the total level of PIX-1 is also not affected (Figure 3.7b). Finally, we asked whether GIT-1 is required for the localization or stability of RRC-1. Previously, we reported that GIT-1, a scaffold for PIX-1, is required for the assembly or stability of IACs at the MCB, and showed that GIT-1 is required for the stability of PIX-1, by using a *git-1* deletion allele, *git-1(ok1848)*(Moody et al., 2020). We now show that *git-1* is also required for the localization of PIX-1 to the MCBs, as shown in Figure 3.8a. To examine the localization of RRC-1::HA in a *git-1* mutant required a recombinant, but because the two genes are so close together on the X chromosome (<0.5 cM apart), we employed *git-1* RNAi, instead. As shown in Figure 3.8b, knock down of *git-1* results in a reduced level of PAT-6 at MCBs. However, the level of RRC-1::HA does not seem to be reduced in *git-1* RNAi compared to empty vector RNAi. Nevertheless, git-1 RNAi does result in a significant reduction in the level of RRC-1::HA by western blot. Overall, our results indicate that PIX-1 is required for the proper localization of RRC-1 but not its stability, that RRC-1 is not required for the localization or stability of PIX-1, and that GIT-1 is not required for the localization of RRC-1 but is required for its stability.

To further explore genetic interaction of *rrc-1* and *pix-1*, we used double mutant analysis in two ways. In the first way, we created a worm strain, *rrc-1(ok1747); sfIs20*, which is both deficient in RRC-1 and overexpresses PIX-1 in muscle. As indicated in Figure 3.9a, MCB

organization is at least partially rescued in *rrc-1(ok1747); sfIs20*; the localization of PAT-6 at the MCB is nearly normal. This is in contrast to overexpression of PIX-1 in a wild type background, in which PAT-6 is missing from the MCB (Moody et al., 2020).

In the second approach, we generated by genetic recombination, the worm strain, *rrc-1(ok1747) pix-1(gk299374)*, which is deficient in both *rrc-1* and *pix-1*. As shown in Figure 3.9b, the MCB was affected in this double mutant to a variable extent. In some worms (example, top panel), the MCB defect was as severe as *rrc-1(ok1747)* itself; in other worms (example, middle panel), the MCB was partially restored; and in other worms (example, lower panel) the MCB was fully restored. The locomotion assays on the single and double mutants are presented in Figure 3.9c and d. As shown in Figure 3.9c, there is partial rescue of the swimming defect; the double mutant, although not restored to the wild type level, shows statistically improved swimming compared to either single mutant. However, as shown in Figure 3.9d, the double mutant did not show an improvement in crawling. The partial improvement in swimming but not in crawling, is likely explained by the greater demands on muscle function required for crawling along an agar surface as compared to swimming in a liquid. Overall, however, both approaches provide additional evidence for a genetic interaction between *rrc-1* and *pix-1*.

Figures

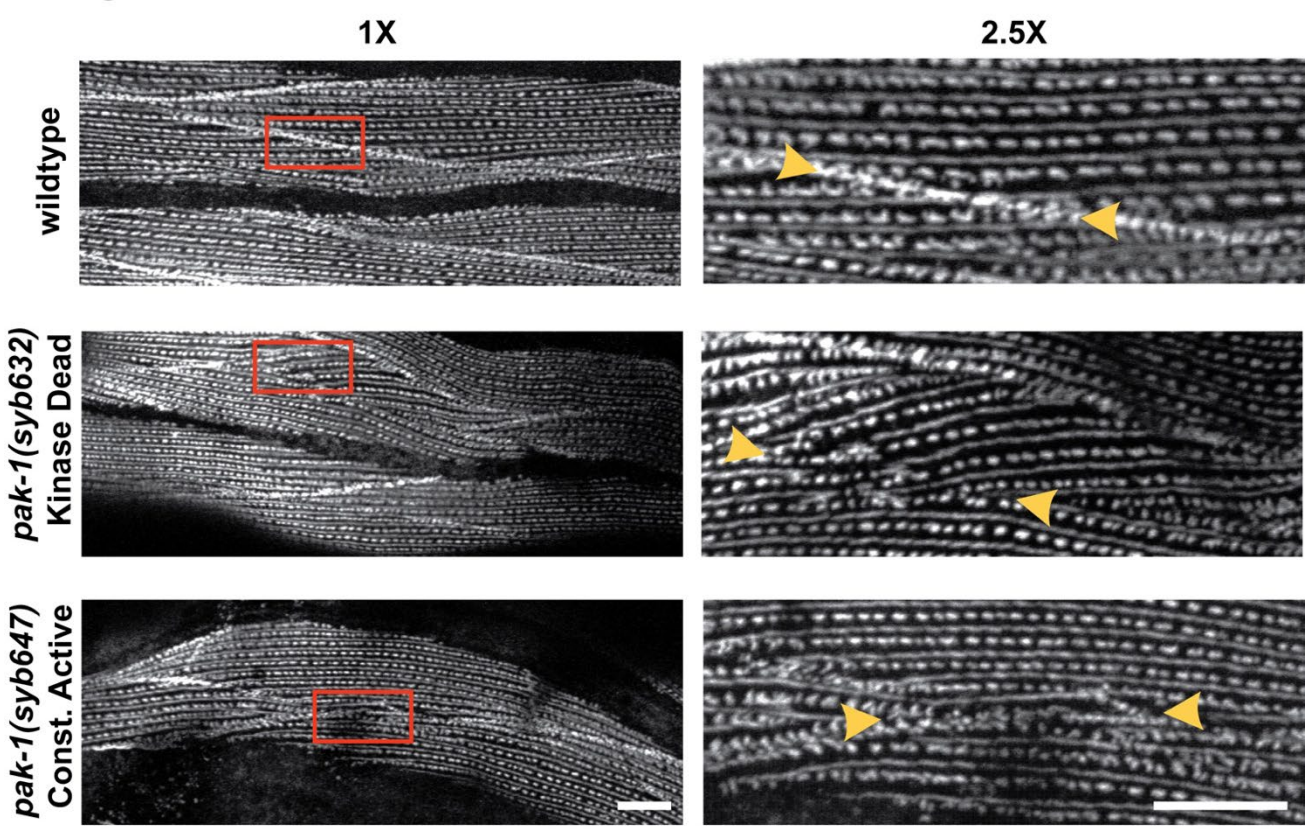

Figure 3.1 Either catalytically dead PAK-1 or constitutively active PAK-1 kinase results in a muscle cell boundary defect. Confocal microcopy imaging of wildtype, *pak-1(syb632)[K324A]* kinase dead, and *pak-1(syb647) [L99F]* constitutively active kinase mutants immunostained with anti-PAT-6 (α-parvin), shown at 1X and 2.5X optical zoom. 2.5X zoom areas are the insets indicated by the red boxes in 1X zoom images. Yellow arrows indicate muscle cell boundaries. In wild type, these structures are well-formed and "tight", but in the *pak-1* mutants they are disrupted or missing. Scale bar, 10 μm.

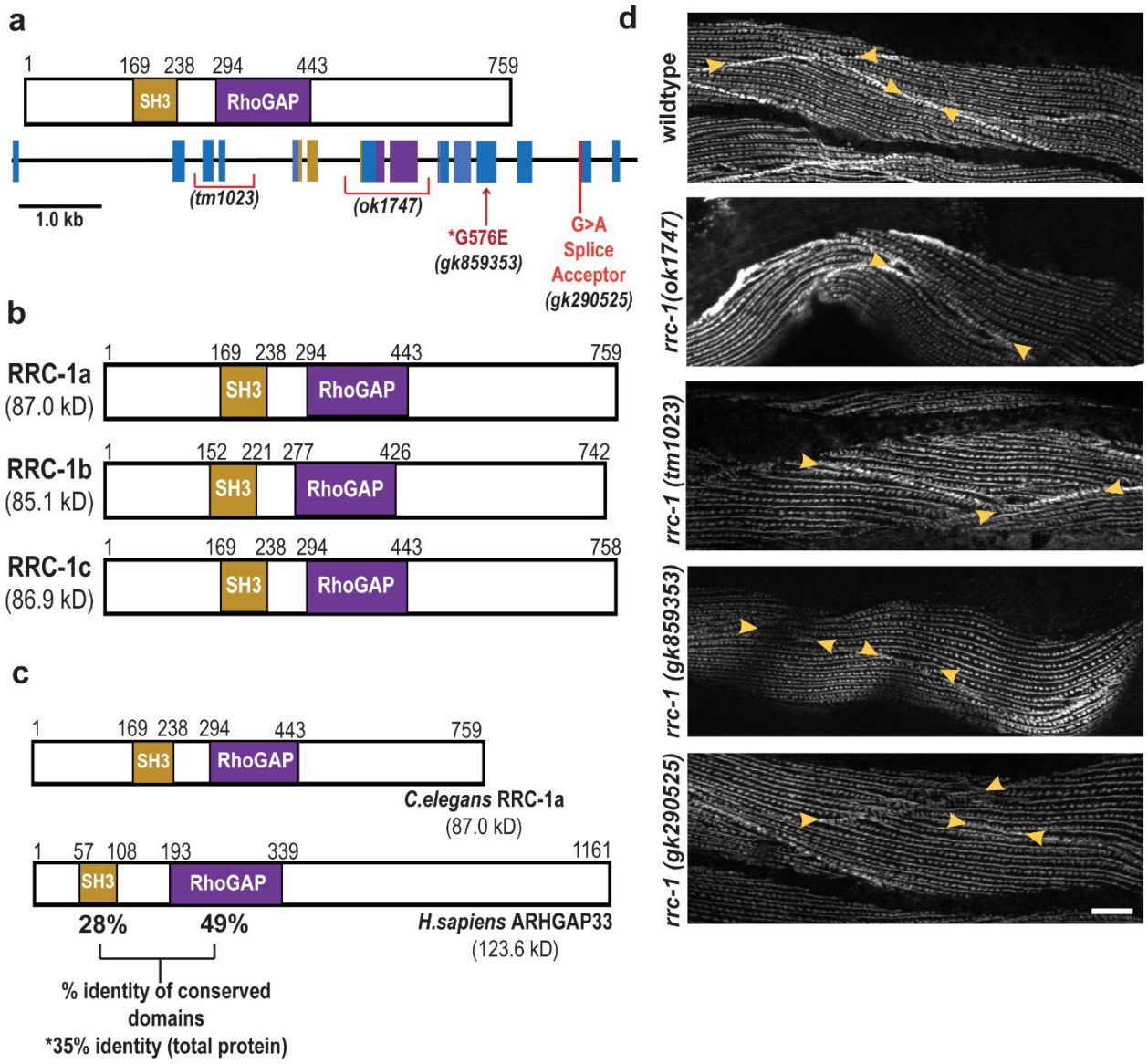

Figure 3.2 Loss of function *rrc-1* mutants show a lack of or disorganization of PAT-6 at muscle cell boundaries. a.) Schematic representation of domains in *C. elegans* RRC-1 isoform A, and the location and nature of the four *rrc-1* mutants within a map of the exon-intron organization of the *rrc-1* gene. **b.)** Schematic showing domain organization of the three predicted RRC-1 isoforms, generated by alternative splicing. **c.)** Schematic showing domain organization of nematode RRC-1a, and the closest ortholog in humans, ARHGAP33, indicating % identities in the overall proteins, and in their SH3 and RhoGAP domains. **d.**) Confocal microscopy imaging of body wall muscle cells immunostained with antibodies to PAT-6 (α-parvin) from wildtype, two RRC-1 out-of-frame deletion allele mutants (*rrc-1(ok1747)* and *rrc-1(tm1023)),* one missense mutation, *rrc-1(gk859353)*, and one splice site mutation, *rrc-1(gk290525),* each outcrossed 5x to wildtype. Arrowheads point to the boundaries between muscle cells. Scale bars, 10µm.

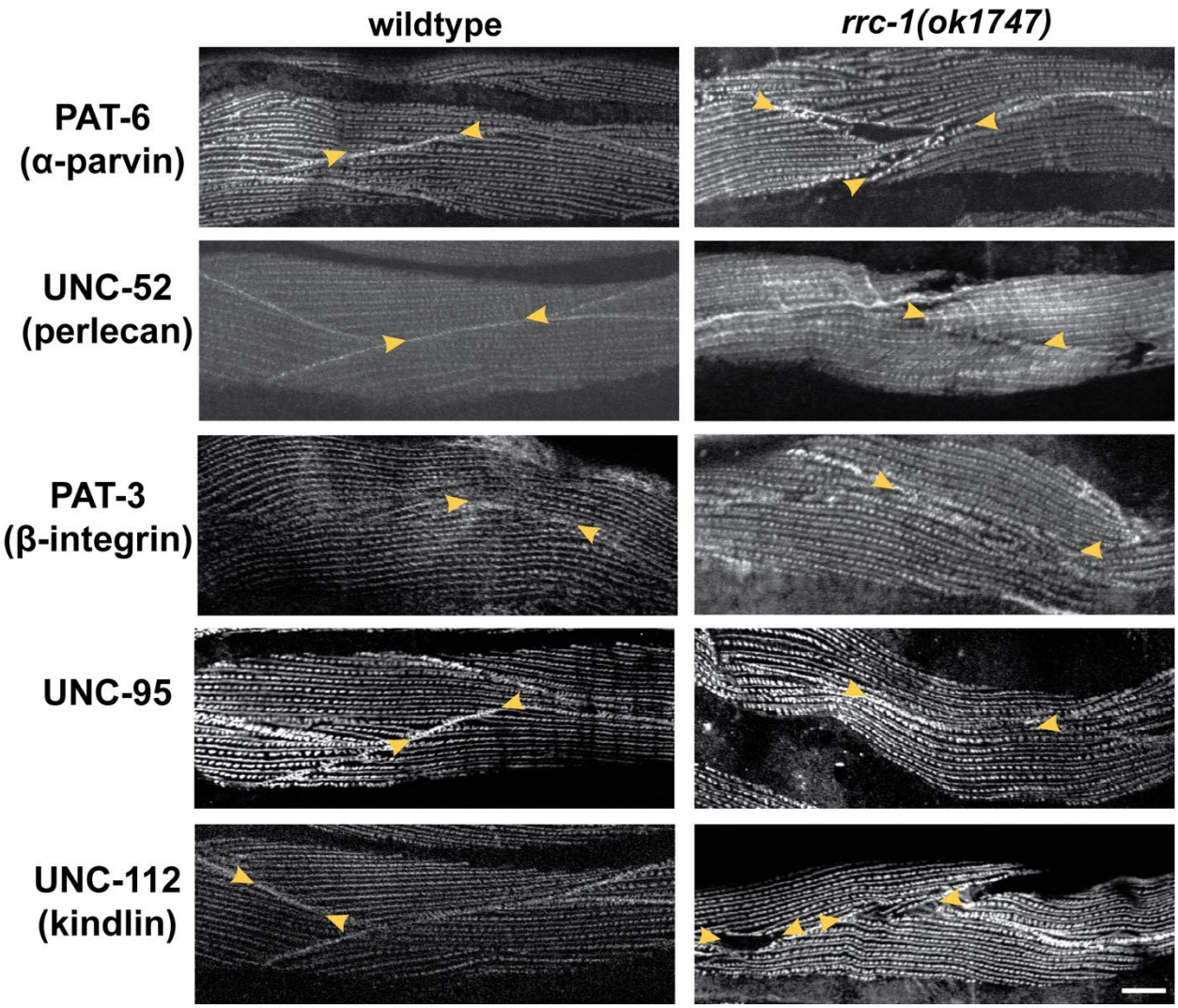

Figure 3.3 Additional IAC components show disruption at the muscle cell boundaries in *rrc-1* mutants. Comparison of wild type vs. *rrc-1(ok1747),* outcrossed 5x to wildtype, immunostained with antibodies to the indicated integrin adhesion complex (IAC) proteins and imaged by confocal microscopy. In parentheses are the names of the mammalian orthologs. Arrowheads denote muscle cell boundaries. Note that all five proteins are present at the muscle cell boundaries in wildtype but are missing or less tightly organized at the muscle cell boundaries in the *rrc-1* deletion mutant. Each image is a representative image obtained from at least 2 fixation and immunostaining experiments, and imaging of at least three different animals. Scale bars, 10µm.

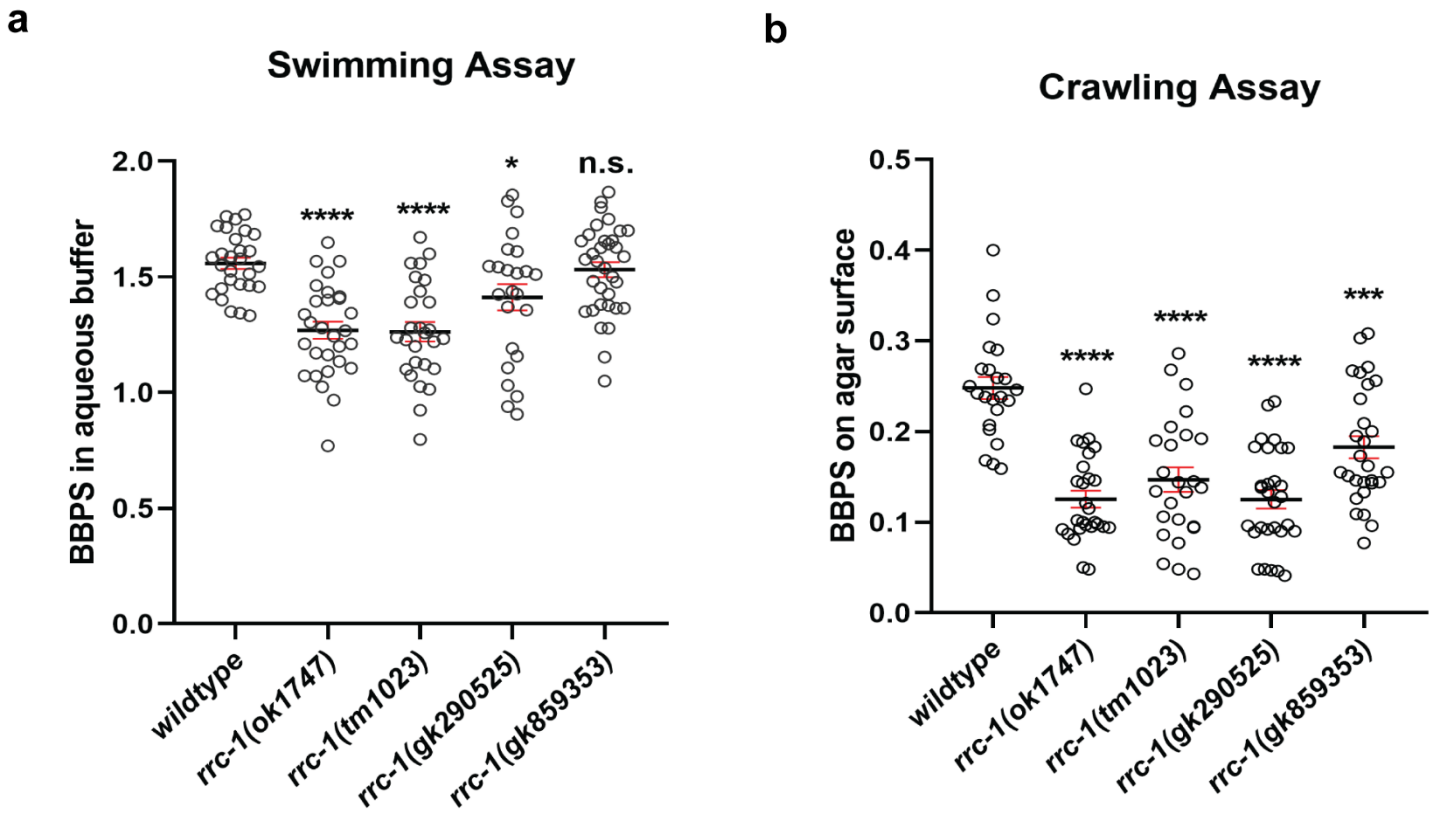

Figure 3.4 Loss of function in rrc-1 mutants show reduced whole animal locomotion. a.) Swimming and **b.)** crawling assays show that RRC-1 deletion mutants *rrc-1(ok1747)* and *rrc-1(tm1023),* a splice acceptor site mutant, *rrc-1(gk290525)*, and a missense mutant, *rrc-1(gk859353),* outcrossed 5x to wildtype result in reduced locomotion as compared to wildtype animals. Body bends per second (BBPS) are quantified for individual animals of each strain. In the graphs, each open circle represents the result from an independently selected animal. The exact n values vary, but n ≥ 23. Welch's t-test was used to test for significance. Error bars indicate SEM, *p≤ .05, ****p≤ .0001.

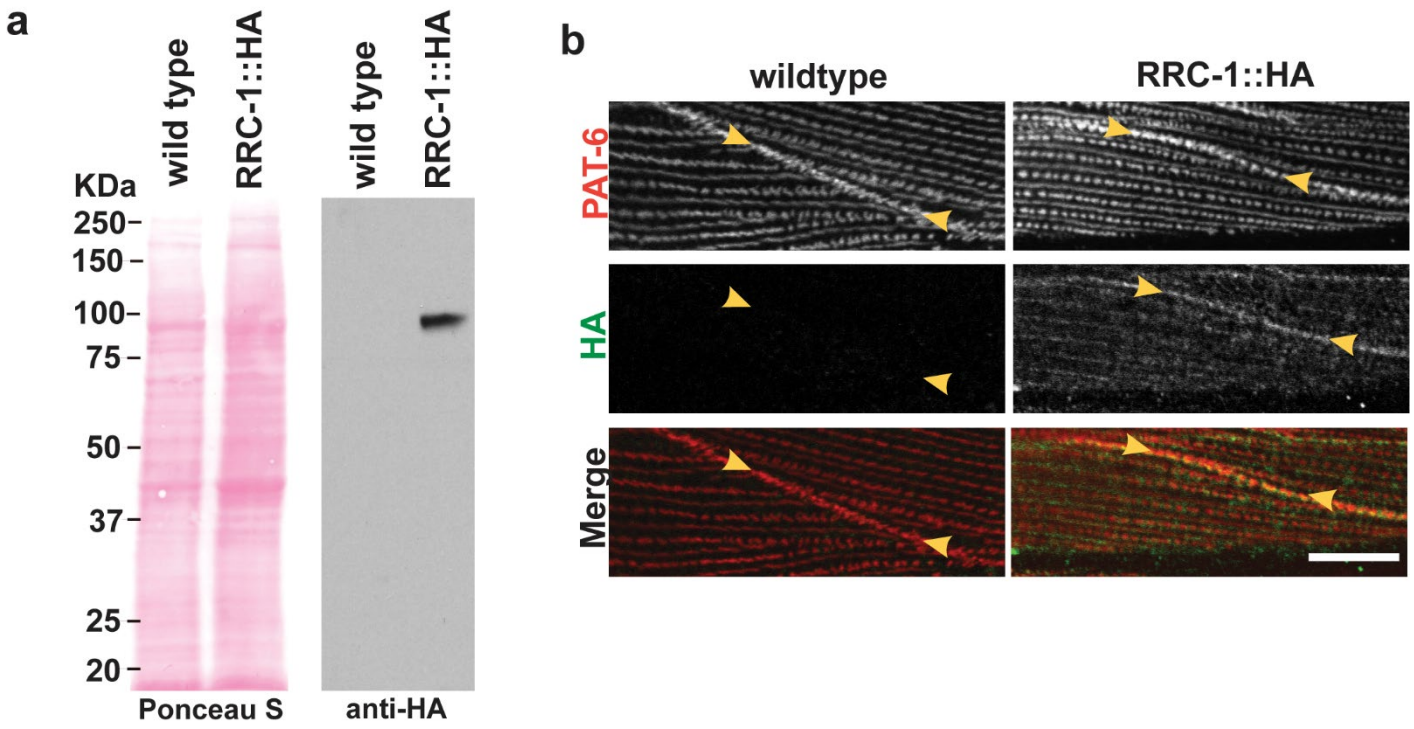

Figure 3.5. HA-tagged RRC-1 localizes to muscle cell boundaries. **a**.) Confirmation that the CRISPR/Cas9-generated strain, *rrc-1(syb4499)* expresses RRC-1::HA. Lysates were prepared from wildtype and *rrc-1(syb4499)*, and portions separated by SDS-PAGE, blotted, and reacted with antibodies to HA. Anti-HA detects a protein of expected size, approximately 90 kDa, from *rrc-1(syb4499)* and not from wild type. **b.)** Confocal microscopy imaging of body wall muscle co-stained with anti-PAT-6 (α-parvin) and anti-HA antibodies in wildtype and the CRISPR generated strain that expresses RRC-1::HA. Note that RRC-1 localizes to the muscle cell boundary, co-localizing with PAT-6. There is weaker localization of RRC-1::HA to the same focal plane as the bases of M-lines and dense bodies, in a striated pattern, but in a diffuse, less-organized manner. Scale bar, 10 μm.

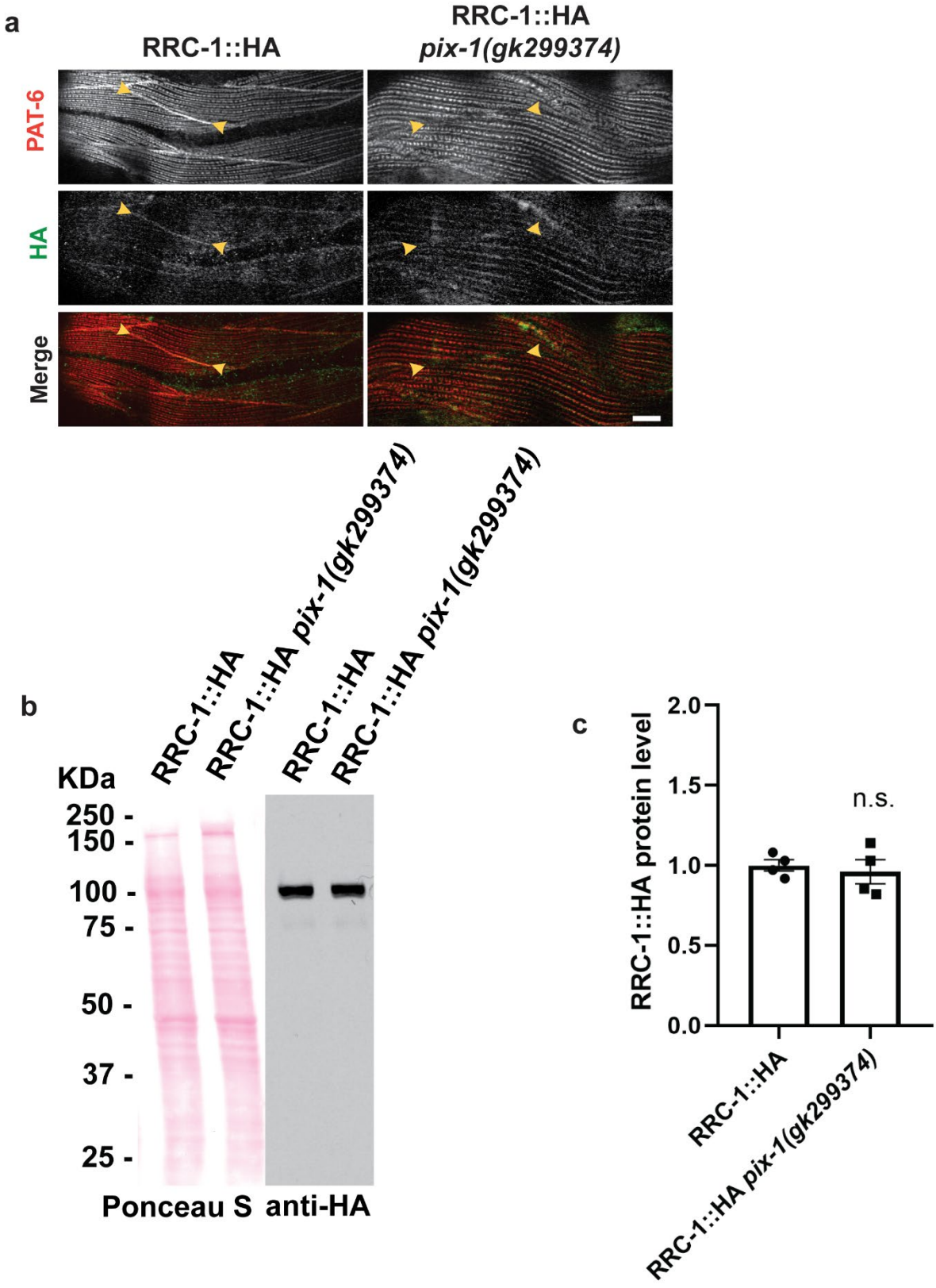
a
RRC-1::HA
RRC-1::HA
pix-1(gk299374)
PAT-6
HA
Merge
b
RRC-1::HA
RRC-1::HA pix-1(gk299374)
RRC-1::HA
RRC-1::HA pix-1(gk299374)
KDa
250 -
150 -
100 -
75 -
50 -
37 -
25 -
Ponceau S
anti-HA
c
RRC-1::HA protein level
2.0
1.5
1.0
0.5
0.0
n.s.
RRC-1::HA
RRC-1::HA pix-1(gk299374)

Figure 3.6. PIX-1 is required for the proper localization of RRC-1 but not the stability of RRC-1. a.) Confocal microscopy imaging of body wall muscle co-stained with anti-PAT-6 (α-parvin) and anti-HA antibodies in the CRISPR generated strain that expresses RRC-1::HA, and in a strain that expresses RRC-1::HA in a *pix-1* null background. Note that when PIX-1 is deficient there is less localization of RRC-1::HA to the muscle cell boundary. Scale bar, 10 μm. **b.)** Western blot showing that the level of RRC-1::HA is the same in wild type vs. the *pix-1* mutant**. c.)** Quantification of HA-tagged protein level in wild type vs *pix-1*mutant show no significant (n.s.) difference using a Welch's t-test for statistical analysis, N=4.

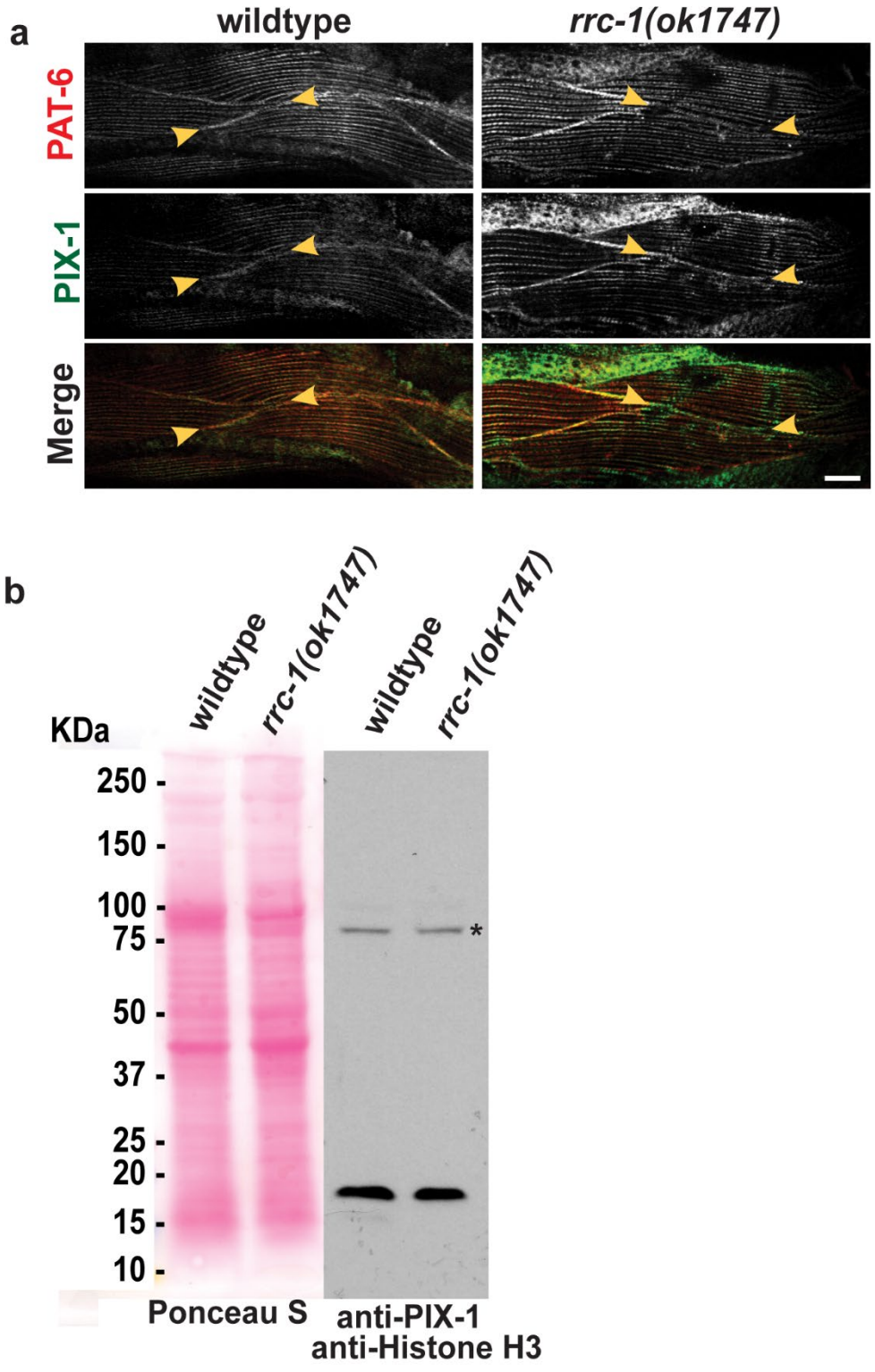
a
wildtype
rrc-1(ok1747)
PAT-6
PIX-1
Merge
b
wildtype
rrc-1(ok1747)
wildtype
rrc-1(ok1747)
KDa
250
150
100
75
50
37
25
20
15
10
*
Ponceau S
anti-PIX-1
anti-Histone H3

Figure 3.7. RRC-1 is not required for the localization or stability of PIX-1. a.) Confocal microscopy imaging of body wall muscle co-stained with anti-PAT-6 (α-parvin) and anti-PIX-1 antibodies in wildtype and in the *rrc-1(ok1747)* mutant. Note there is no change in the localization of PIX-1 at muscle cell boundaries in wildtype vs. *rrc-1(ok1747)*, despite reduced localization of PAT-6 in *rrc-1(ok1747)*. Scale bar, 10 μm. **b.)** Western blot showing that the level of PIX-1 is the same in wild type vs. the *rrc-1* mutant. Histone H3 was used as a loading control.

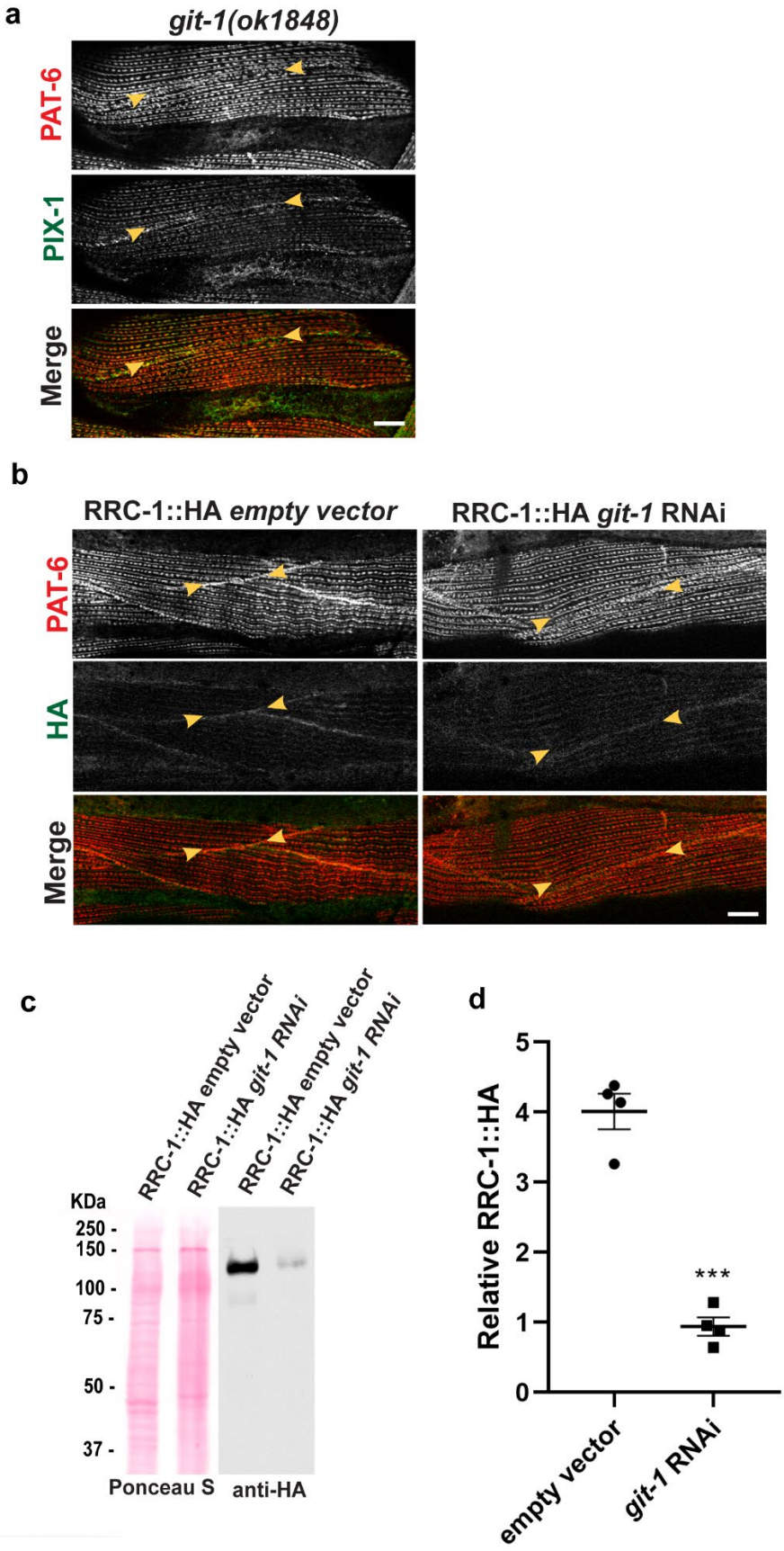
a
git-1(ok1848)
PAT-6
PIX-1
Merge
b
RRC-1::HA empty vector
RRC-1::HA git-1 RNAi
PAT-6
HA
Merge
c
RRC-1::HA empty vector
RRC-1::HA git-1 RNAi
RRC-1::HA empty vector
RRC-1::HA git-1 RNAi
KDa
250 -
150 -
100 -
75 -
50 -
37 -
Ponceau S
anti-HA
d
Relative RRC-1::HA
5
4
3
2
1
0
***
empty vector
git-1 RNAi

Figure 3.8 GIT-1 is not required for the localization of RRC-1, but GIT-1 is required for the stability of RRC-1. a.) Confocal microscopy imaging of body wall muscle co-stained with anti-PAT-6 (α-parvin) and anti-PIX-1 antibodies in wildtype and in the *git-1(ok1848)* deletion mutant. Note that both PAT-6 and PIX-1 show poor localization to the muscle cell boundaries. Scale bar, 10 μm. **b.)** Confocal microscopy imaging of body wall muscle co-stained with anti-PAT-6 (α-parvin) and anti-HA to detect RRC-1::HA in a strain expressing RRC-1::HA with and without feeding bacteria expressing dsRNA for *git-1*. Note that RNAi knockdown of *git-1* does not prevent the localization of RRC-1::HA to the muscle cell boundaries. Scale bar, 10 μm. **c.)** Western blot showing the level of RRC-1::HA in wild type vs. *git-1(RNAi)*. Note that *git-1(RNAi)* results in a reduced level of RRC-1::HA. **d.)** Quantification of HA-tagged RRC-1 protein levels in *git-1 (RNAi)* vs. empty vector control shows that *git-1 (RNAi)* reduces the level of RRC-1::HA to about 23% of the level in wild type. A Welch's t-test for statistical analysis, N=4, was used; Error bars indicate SEM, ***: $p \leq 0.001$.

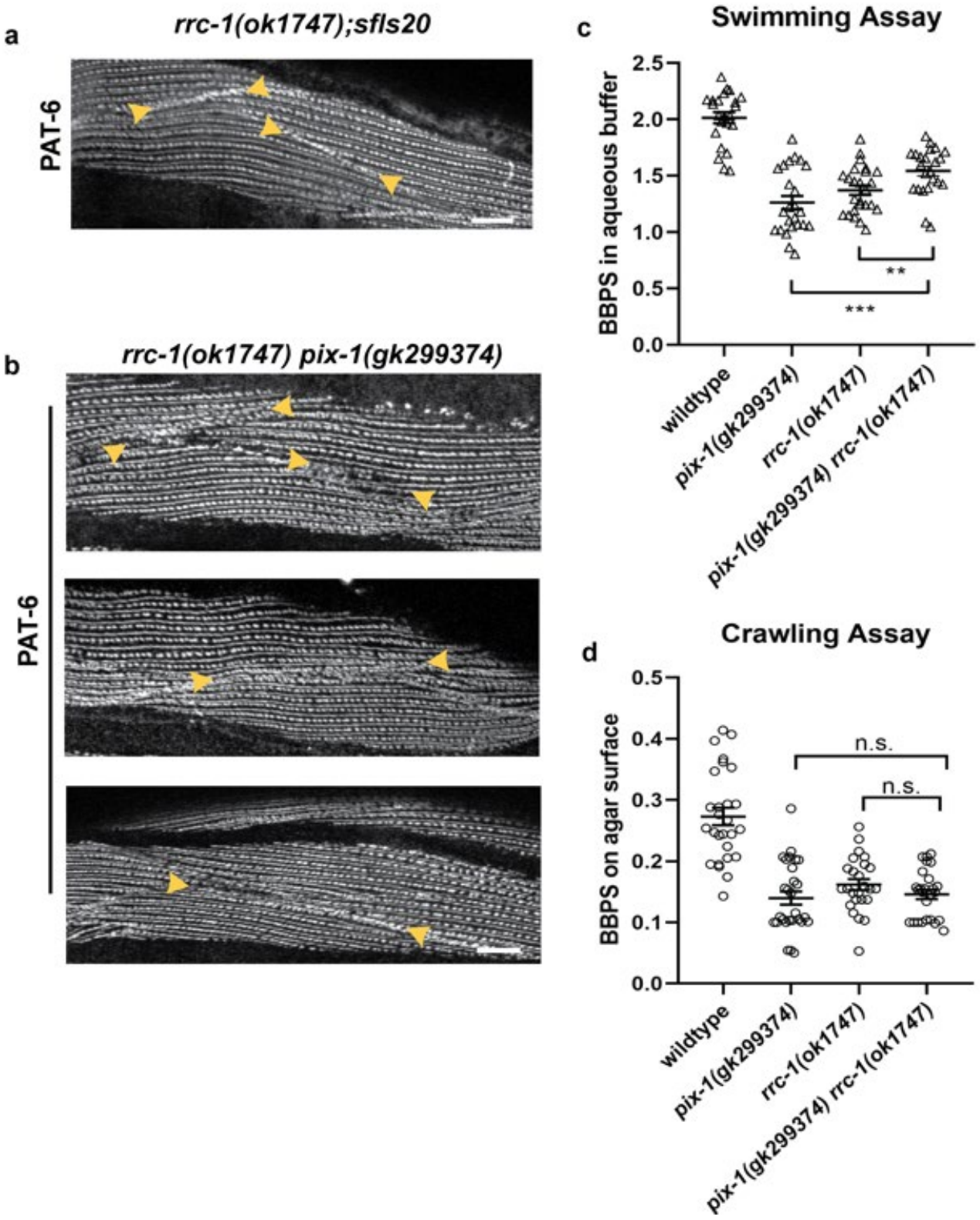
a
rrc-1(ok1747);sfIs20
PAT-6
b
rrc-1(ok1747) pix-1(gk299374)
PAT-6
c
Swimming Assay
BBPS in aqueous buffer
2.5
2.0
1.5
1.0
0.5
0.0
**
***
wildtype
pix-1(gk299374)
rrc-1(ok1747)
pix-1(gk299374) rrc-1(ok1747)
d
Crawling Assay
BBPS on agar surface
0.5
0.4
0.3
0.2
0.1
0.0
n.s.
n.s.
wildtype
pix-1(gk299374)
rrc-1(ok1747)
pix-1(gk299374) rrc-1(ok1747)

Figure 3.9 Double mutant analysis of *rrc-1* and *pix-1* show genetic interaction. a.) Overexpression of PIX-1 in muscle rescues the muscle cell boundary defect of *rrc-1(ok1747)*. Confocal microscopy image of body wall muscle immunostained with anti-PAT-6 antibodies, with arrowheads pointing out the muscle cell boundaries. Note that these boundaries appear nearly like wild type. *sfIs20* is an integrated array in which PIX-1 is overexpressed from the muscle specific promoter of the *myo-3* gene. Scale bar, 10 μm**. b.)** Confocal microscopy images of body wall muscle from three representative individual worms having the genotype *rrc-1(ok1747) pix-1(gk299374)* immunostained with anti-PAT-6 antibodies. The boundaries show variable disruption, with possible partial rescue. Scale bar, 10 μm**. c.)** Swimming and **d.)** crawling assays show that *rrc-1(ok1747), pix-1(gk299374), rrc-1(ok1747) pix-1(gk299374)* show reduced locomotion compared to wildtype. Note that the *rrc-1(ok1747) pix-1(gk299374)* double mutant is significantly faster than both single mutants in swimming but not crawling. Body bends per second (BBPS) are quantified for individual animals of each strain. In the graphs, each open circle represents the result from an independently selected animal. The exact n values vary, but $n \geq 24$. Welch's t-test was used to test for significance. Error bars indicate SEM, *$p \leq .05$, ****$p \leq .0001$.

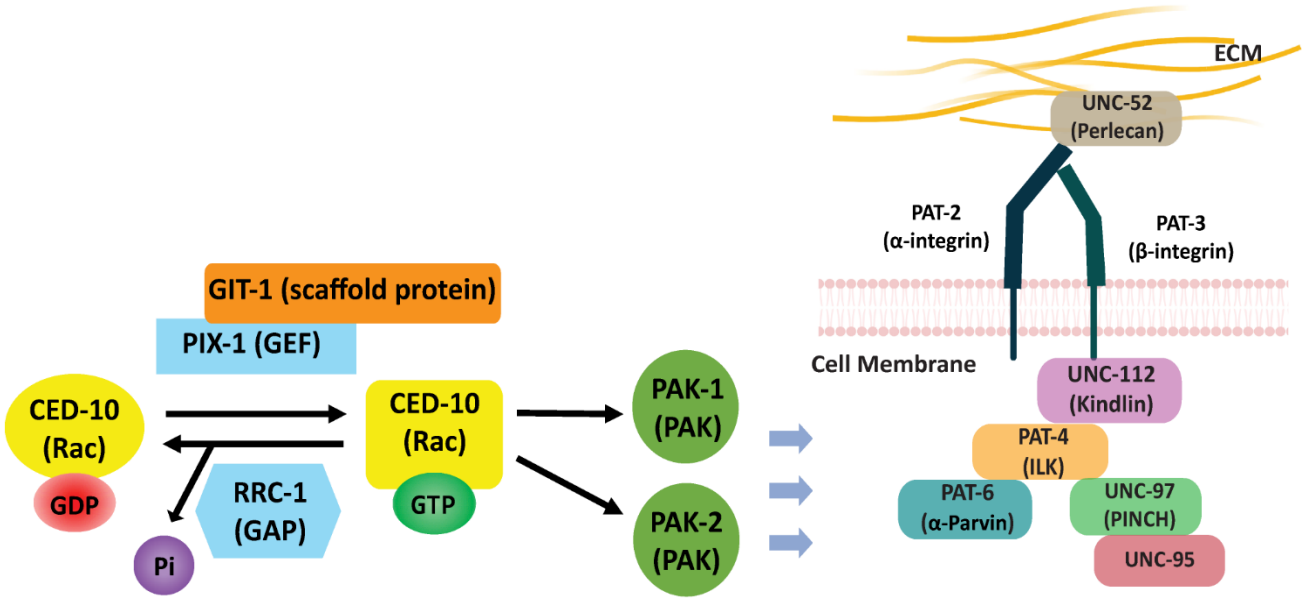

Figure 3.10 RRC-1 is RhoGAP in the PIX-1 pathway. The drawing depicts what we have learned about the PIX-1 pathway in *C. elegans* muscle. In Moody et al. (2020) we demonstrated that for the proper assembly or stability of integrin adhesion sites at the muscle cell boundary, the RacGEF, PIX-1, its scaffold, GIT-1, the Rac, CED-10, and the PAK effectors, PAK-1 and PAK-2 are required. The current results demonstrate that the RhoGAP, RRC-1 is the GAP for the PIX pathway, based on the similarity of *pix-1* and *rrc-1* phenotypes, and genetic interactions of *rrc-1* with *pix-1* and *git-1*. The blue arrows indicate that, by some still unknown mechanisms, this Rac cycling pathway is required for the assembly or stability of integrin adhesion complexes at muscle cell boundaries. Core components of this complex are depicted to the right, with the names of the mammalian proteins shown in parentheses.

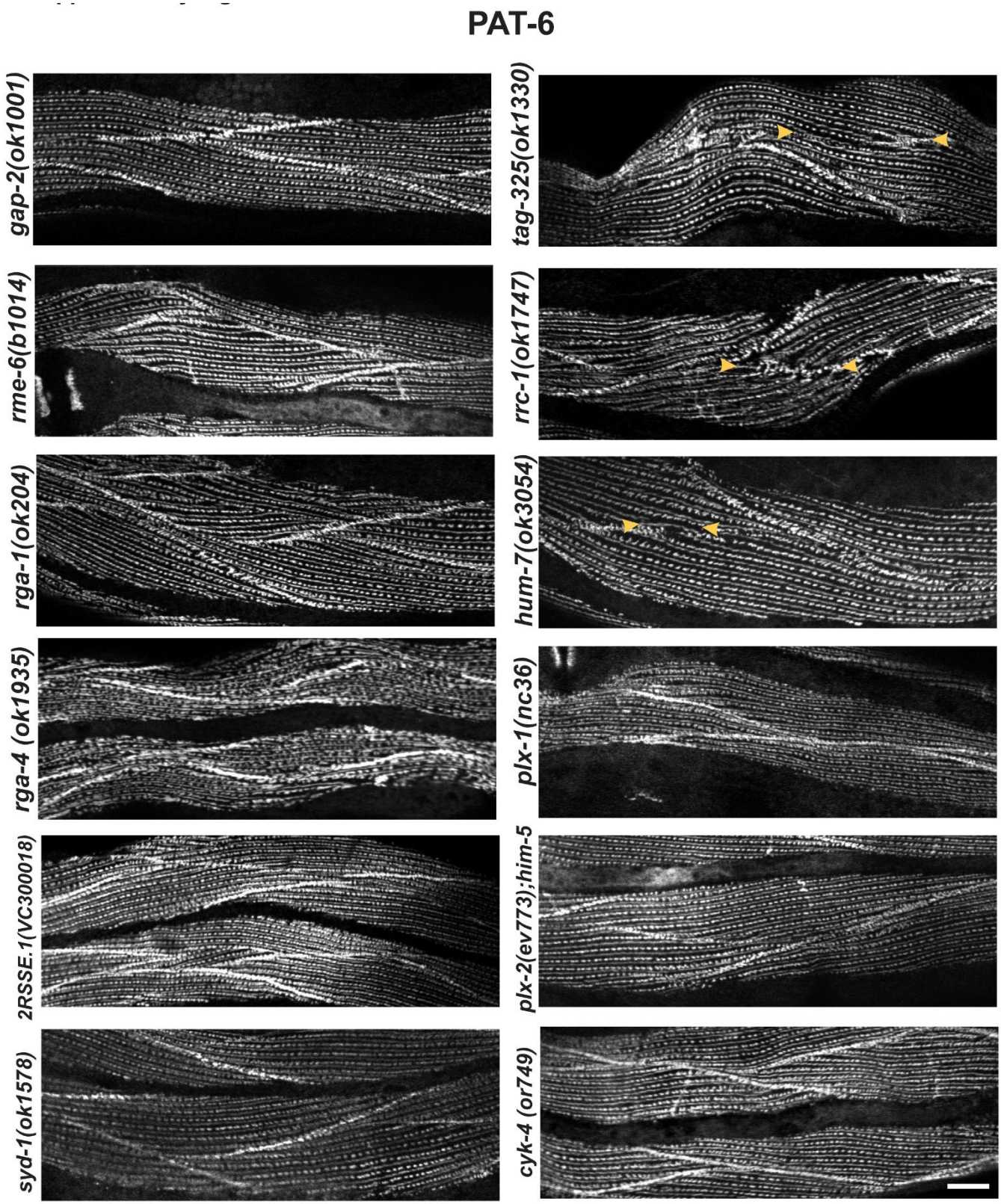
PAT-6
gap-2(ok1001)
tag-325(ok1330)
rme-6(b1014)
rrc-1(ok1747)
rga-1(ok204)
hum-7(ok3054)
rga-4 (ok1935)
plx-1(nc36)
2RSSE.1(VC300018)
plx-2(ev773);him-5
syd-1(ok1578)
cyk-4 (or749)

Supplementary Figure 1 (cont.)

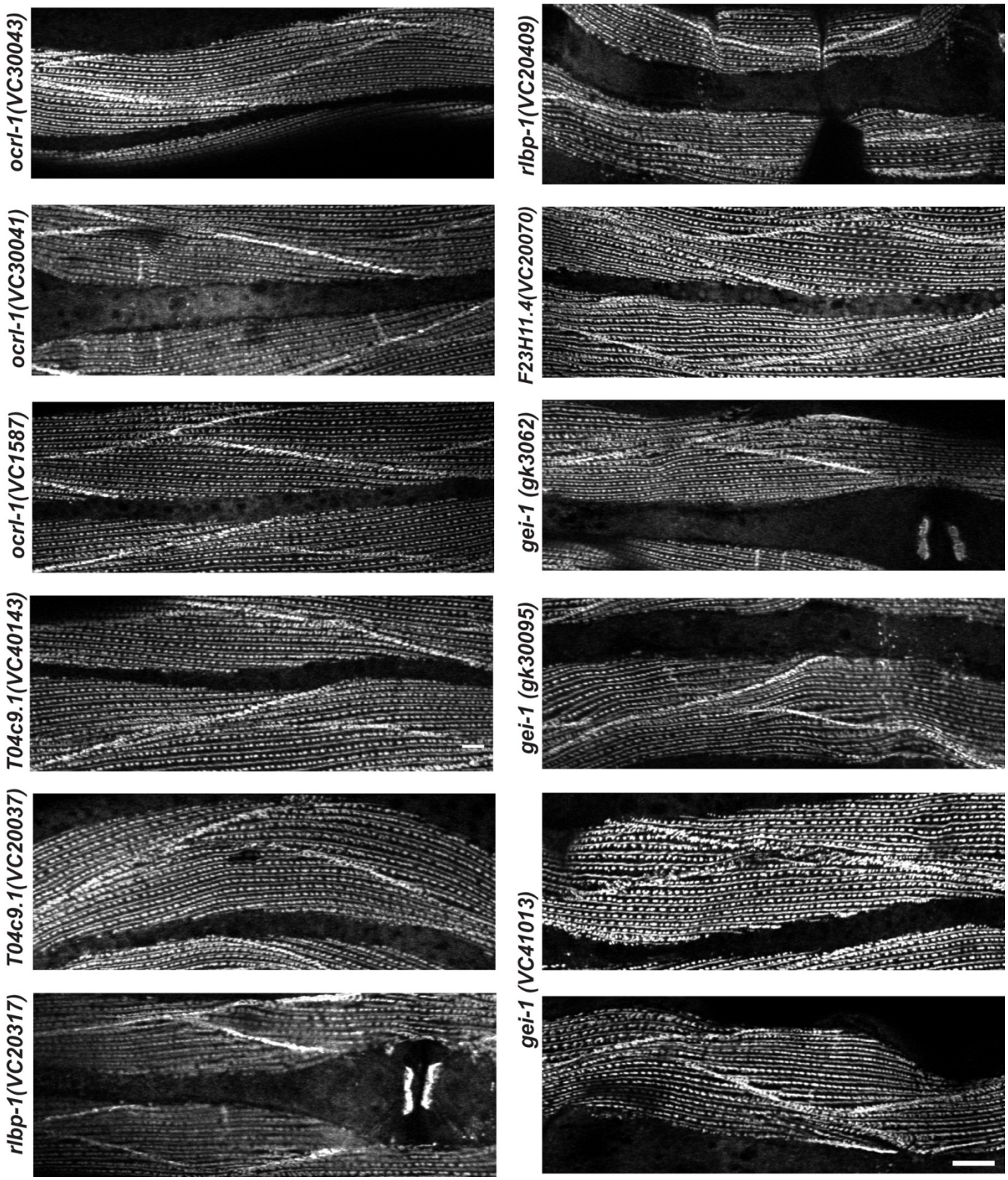

Figure 3.1S RhoGAP Screening Results Confocal microscopy imaging of 18 mutants that harbor RhoGAP domains that are also expressed in muscle immunostained with antibodies to PAT-6 (α-parvin). Scale bar, 10 μm**.**

Genes with RhoGAP domains	Muscle Expression	MCB phenotype
2RSSE.1, isoform a	Yes	No
CHIN-1	No	No
CYK-4	Yes	No
F23H11.4, isoform a	Yes	No
GAP-1	No	No
GAP-2, isoform a	Yes	No
GAP-3, isoform a	No	No
GEI-1, isoform a	Yes	No
HUM-7, isoform a	Yes	Yes
OCRL-1, isoform a	Yes	No
PAC-1, isoform a	No	No
PES-7	No	No
PLX-1, isoform a	Yes	No
PLX-2	Yes	No
RGA-1, isoform a	Yes	No
RGA-2	yes	No
RGA-3	No	No
RGA-4, isoform a	Yes	Yes*
RGA-5, isoform b	No	No
RGA-6, isoform a	No	No
RLBP-1, isoform a	Yes	No
RME-6, isoform a	Yes	No
RRC-1, isoform a	Yes	Yes
SPV-1, isoform a	No	No
SRGP-1, isoform a	No	No
SYD-1, isoform a	Yes	No
T04C9.1, isoform a	Yes	No
TAG-325, isoform a	Yes	No
Y34B4A.8, isoform a	No	No
Y92H12BL.4	No	No

Table 3.1S RhoGAP Screening Results in tabular form.

```
[C.elegans]  --------MEGIEE-SFAPL-------SPKSPFARRNGRSLRIQRLVDCQHFHYSSVELG  44
[H.sapiens]  MVARSTDSLDGPGEGSVQPLPTAGGPSVKGKPGKRLSAPRGPFPRLADCAHFHYENVDFG  60
                    ::*  * *. **          .*  * ..    : **.** ****..*::*

[C.elegans]  PVRVAIIAINADEN----ATERIKMRVESESNSWLVERSREDWAVFDRQLHRCVFERRHS 100
[H.sapiens]  HIQLLLSPDREGPSLSGENELVFGVQVTCQGRSWPVLRSYDDFRSLDAHLHRCIFDRRFS 120
              ::: :   . . .        : ::* .:..** * ** :*:  :* :****:*:**.*

[C.elegans]  RLDELFPLIHLE--TAKFEEVLVKYTERLSELTGSIITCYPVLKFLEIDSRGGHFEPAEE 158
[H.sapiens]  CLPELPPPPEGARAAQMLVPLLLQYLETLSGLVDSNLNCGPVLTWMELDNHGRRLLLSEE 180
              * ** *  .    :  :  :*::* * ** *..* :.* ***.::*:*.:* ::  :**

[C.elegans]  TSINVPAIAAAVVTKDFEPTESSQLRLRVGDIVSITEMSTASPSEQTFWKAKLTISNQKI 218
[H.sapiens]  ASLNIPAVAAAHVIKRYTAQAPDELSFEVGDIVSVIDMPPT--EDRSWWRG--------- 229
             :*:*:**:*** * * :     .:* :.******: :*  :  .::::*:.

[C.elegans]  VDPQNARLGFEIGYFPRDCVMLIDDKRLPNPLNNEQKA----------------STR--- 259
[H.sapiens]  ------KRGFQVGFFPSECVELFTERPGPGLKADADGPPCGIPAPQGISSLTSAVPRPRG 283
                   : **::*:** :** *: ::  *.   : :                    *

[C.elegans]  ----NARRYMT-------TMFRNRRREPIFGLELTDLYMRTGKKVPVIVEKCCASIEDQG 308
[H.sapiens]  KLAGLLRTFMRSRPSRQRLRQRGILRQRVFGCDLGEHLSNSGQDVPQVLRCCSEFIEAHG 343
                   * :*          *.  *: :** :* :   .:*:.** ::. *.  ** :*

[C.elegans]  IVTGIYRQCGIQSNIQRLRAKFDSGAEPDLHEFG-QRDIYSVSSLLKQYFRQLPNPLFTY 367
[H.sapiens]  VVDGIYRLSGVSSNIQRLRHEFDSERIPELSGPAFLQDIHSVSSLCKLYFRELPNPLLTY 403
             :* **** .*:.******* :***   *:*   .  :**:***** * ***:*****:**

[C.elegans]  QAYPKLIEAFEKEDSLSEKVESLRFSLETMPEAHYRTAKFLMEHLTRLCKSKSLTDMTSK 427
[H.sapiens]  QLYGKFSEAMSVPGE-EERLVRVHDVIQQLPPPHYRTLEYLLRHLARMARHSANTSMHAR 462
             * * *: **:.  .. .*::  ::  :: :*  **** ::*:.**:*:.: .: *.* ::

[C.elegans]  NLAIVWSPNLFRPPPTLN--GADTHLLSGLNVHTAICDFFIENSESLFVNDIDEEQ---- 481
[H.sapiens]  NLAIVWAPNLLRSMELESVGMGGAAAFREVRVQSVVVEFLLTHVDVLFSDTFTSAGLDPA 522
             ******:***:*     .   ..:  :  :.*::.: :*:: : : ** : : .

[C.elegans]  SKCTSVEN-S---------FTTISK----------------------------SATMSD 502
[H.sapiens]  GRCLLPRPKSLAGSCPSTRLLTLEEAQARTQGRLGTPTEPTTPKAPASPAERRKGERGEK 582
             .:*   .  *         : *:.:                              .   ..

[C.elegans]  MRSESESKWPRFFRGKSVEGFWKFNRKQQTSTGELCGSPTSEVKWRSRSTRS------HS 556
[H.sapiens]  QRKPGGSSWKTFFAL---------GRGPSVP-------RKKPLPWLGGTRAPPQPSGSRP 626
              *. . *.*  **           .*  ..         .. : * . :        :

[C.elegans]  TDAAFQSSRTDSFIQLMHTGMDQIREGMRIF-------RARARSMRPTSRPPPSPRTRRA 609
[H.sapiens]  DTVTLRSAKSEESLSSQASGAELLGAGGAPASATPTPALSPGRSLRPHLIPLL-LRGAEA 685
               .:::*::::. :.   :* : :  *            : .**:**   *    *  .*


[C.elegans]  RFSNGSSNN-VQKLN------ESDIQHEI---PLATTEPSITPEPKNTVDPHQIMTRTIS 659
[H.sapiens]  PLTDACQQEMCSKLRGAQGPLGPDMESPLPPPPLSLLRPGGAPPP-PPKNPARLMALALA 744
              :::...::  .**.        *::  :   **:  .*. :* *    :* ::*: :::
```

```
[C.elegans]  VND---SDDQSFEENGLREMRERKVMFKAAT-----QEHVATFHE-----RSSPVEEWSS 706
[H.sapiens]  ERAQQVAEQQSQQECGGTPPASQ-SPFHRSLSLEVGGEPLGTSGSGPPPNSLAHPGAWVP 803
                   :::** :* *     .:   *: :       * :.*  .       :    *

[C.elegans]  DSRESLHLEM---SRYDNVSPSGTITRNQREPITNL----------------------- 739
[H.sapiens]  GPPPYLPRQQSDGSLLRSQRPMGTSRRGLRGPAQVSAQLRAGGGGRDAPEAAAQSPCSVP 863
             .    *  :    *   .  * **  *. * *

[C.elegans]  SPAAQMLFFESSRA-----------SHLFSA---------------------------- 759
[H.sapiens]  SQVPTPGFFSPAPRECLPPFLGVPKPGLYPLGPPSFQPSSPAPVWRSSLGPPAPLDRGEN 923
             * .    **. :              *:

[C.elegans]  ------------------------------------------------------------ 759
[H.sapiens]  LYYEIGASEGSPYSGPTRSWSPFRSMPPDRLNASYGMLGQSPPLHRSPDFLLSYPPAPSC 983


[C.elegans] ------------------------------------------------------------ 759
[H.sapiens] FPPDHLGYSAPQHPARRPTPPEPLYVNLALGPRGPSPASSSSSSPPAHPRSRSDPGPPVP 1043


[C.elegans] ------------------------------------------------------------ 759
[H.sapiens] RLPQKQRAPWGPRTPHRVPGPWGPPEPLLLYRAAPPAYGRGGELHRGSLYRNGGQRGEGA 1103


[C.elegans] ----------------- 759
[H.sapiens] GPPPPYPTPSWSLHSEG 1120
```

Figure 3.2S Sequence Alignment of RRC-1 and human ARHGAP33. The protein sequences for C. elegans RRC-1 and human ArhGAP33 are shown here in alignment using CLUSTAL program. The SH3 domain is highlighted in yellow and the RhoGAP is highlighted in purple. * indicate conserved residues between these two sequences, , and ":" and "." indicate residues that are conserved in the two sequences.

Information on the generation of CRISPR/Cas9 strains

* PAM site is marked by square

PHX632:
Sg1: CCGAAGCGGAGGTGGCTATCAAG
Sg2: TATTGAAATTAGTACCGAAGCGG

>Repair template
tacttgtgtattacatgcccttagttttagagtatttttttaagttaaaaacaataaaaacgtgtaccacatttttatttctaggtttaggaaataatctttctaagcctggagaggaaaaatgtatatcacgtttaaattatatggagaaatgaatgaaaatttaattcaatttcaaaatgagggcatgtaatacacaagtaccgaatttttcccaagttctctataacatataagtatattttcagTACACAAAACCGAAAGAGGAGGAAGAAAAAATTCCAGACCTTTCAAAAGGACAATTTGGTGTACAGGCCAGAGGTCAAAAAGCTAAGAAAAAGATGACTGACGCTGAAGTGCTGACTAAGCTCCGTACCATTGTGTCTATCGGAAATCCAGATCGAAAATATAGAAAAGTTGATAAAATCGGCTCAGGTGCATCTGGTTCTGTGTACACCGCTATTGAAATTAGTACGGAAGCGGAGGTGGCTATTGCTCAGATGAACCTGAAGGATCAACCAAAGAAGGAATTGATCATTAATGAGATTTTGGTGATGCGTGAGAATAAGCATGCAAATATTGTAAATTATTTGGATTCGTATTTGGTGTGCGATGAATTATGGGTAGTGATGGAGTATCTTGCCGGTGGATCATTGACTGATGTTGTCACGGAGTGCCAGATGGAGGATGGAATTATTGCAGCTGTTTGCAGAGAAGTTCTTCAAGCGCTTGAATTCCTCCACAGCCGCCACGTCATTCACAGAGATATTAAATCTGACAATATTCTTTTGGGAATGGATGGTTCGGTGAAATTGAgtaagattataatttttaatgcttttgcaaccctacttctgtgaatttcagCCGACTTTGGATTCTGTGCTCAGCTCTCGCCGGAGCAAAGAAAACGCACGACAATGGTCGGAACTCCATACTGGgtgagtgatggaaattgaaaaagcgaataggaaattaatgtttgacaattgcagATGGCGCCGGAAGT

PHX647:
sg1: CCTGAAGCATGGGCACGTCTTCT
sg2: CCTCAGGCAGTGTTGGACGCGCT

>Repair template
ttctgacaccggtcgcaaccgctaatcgtaccagattaacgtgaatgctaatagtaagctaaaaactaaaaactactacttttacttttccctcagtcaaaaaatcattataaacaaatctcaatttataataatattttgcaaccgttaattcagtgcattatcttctaaaaacgtgttattcttgaaaccatggttagtgttaataaagcttgcgtttttgagacgttttaagaaaacaaatccatacgagaaaaatttaagtgaagccaattatcacgaacatgtattcaaccaaagatagtttcttctaaagacctatgaaattgtcccaatttttttagtatgaagaggtctgttttgtcgaatagacttgagaaactactgtagaatcttatttataaacttttctcagaaacttttgctccttatcaacaatataaattttcagGGAATGCCTGAGGCATGGGCACGTTTGTTTACAGACTCACAGATCTCAAAACAAGAGCAGCAACAGAATCCTCAAGCAGTGTTGGACGCGCTCAAATACTACACACAAGGCGAAAGCAGCGGCCAGAAGTGGTTGCAGTACGATATGAgtaagtaacccgtagtcagtcttgctaatggagctcattcttctacagTGTTTATAGATGACGCACCTTCTCGGACGCCATCATACGGACTGAAACCGCAACCATATAGCACATCATCCCTGCCGTATCATGGCAATAAAATTCAGGATCCAAGAAAGATGAATCCAATGACAACCAGTACAAGTAGTGCGGGGTATAACAGCAAGCAAGGAGTTCCTCCGACGACGTTTAGTGTAAATGAGAATAGATCGAGTATGCCACCGgtaagtgggaagaataatcttgaagttcatattgattgcttcagAGTTATGCACCGCCACCGGTCCCCCATGGTGAAACTCCTGCTGATATTGTTCCTCCCGCTATCCCTGATAGGCCGGCAAGGACGTTGAGTATTgtgagtagaatttttgg

PHX4499:
sg1: CCGATAACTAACCTTTCTCCAGC
sg2: CCTTTCTCCAGCTGCACAAATGC
sg3: CCAGTCATTTGTTCTCTGCATAA

>Repair template
aattctgaaatacaggttgtaaaaaaaagataatggcaaccatcttatttttcagAACACGTGGCAACATTCCATGAAAGATCGAGTCCTGTAGAAGAATGGTCAAGTGATTCTAGAGAGAGTCTTCATCTTGAAATGTCCCGTTATGATAACG

TATCTCCAAGTGGTACTATTACAAGAAgtgagtttaaaaaaaaaaatttatgacattaacaaatatgtagaaagcag
tctttcttttattgtatttcaaatgggtaacagcaaaattactttaatacaaagtttcaaagtcaataatccacagc
aaattcaaacatttcttgtggtttttgatctgtacaaaataaatcttagccaaatttggtcaatttccagccacaa
acactataatttcacaataacacaataattcttggcgtttcagATCAACGAGAACCGATAACTAACTTGTCTCCAGC
TGCACAAATGCTCTTTTTCGAATCTTCTCGAGCGAGTCATTTGTTCAGCGCATACCCATACGATGTTCCAGATTAC
GCTGGTGGATCTTACCCATACGATGTTCCAGATTACGCTGGTGGATCTTACCCATACGATGTTCCAGATTACGC
TTAAttgaatttccacctctttcatgatattttgttcattgtattgttgactacttttcaactttatttctttat
cgtcttaaatttttaaagaaccagtgttccatttttcatttcctcatatttttcttctacttctcaattgtcttca
agcaattcctgatcatttttatttgtttcgtgtttttgattataaattatttatatacaaacacacaattttcaaa
caattgtgatgcgtgataacatcgctgaattgtatttttgaaattataaaagaaacgcggaatacaagacctaatta
ctagaatttactgaatttaaataaacacttttagtgatttatttcgttttgaaaattttccgcgatcctgatttga
agaattataacaatttcaatcaattctaatttttattttcaatattttgttcaaagttcaaaacgatattgtggagt
tgtaaaaaaaattaaaatatatattcaaatatgcattacat

Figure 3.3S sgRNAs and repair template information for generation of CRISPR/Cas9 strains.

Discussion

The studies reported here have identified RRC-1 as a Rho family GAP acting in the PIX-1 pathway that is critical for the assembly or stability of one type of IAC in *C. elegans* muscle. Prior to our work, a GAP for a PIX pathway in any organism or cell type was unknown. Our conclusions that RRC-1 functions as a GAP for the PIX pathway are based upon the following: (1) Loss of function for mutations in the GEF, PIX-1, and the GAP, RRC-1, have the same phenotype, i.e. loss of IAC accumulation at the adhesion plaques of the muscle cell boundary (MCB), but not at the M-lines or dense bodies. (2) RRC-1 and PIX-1 each localize to the MCB. (3) GIT-1, a scaffold for assembly of PIX-1 and PAK-1, when knocked down by RNAi results in a reduced level of RRC-1. (4) The genes *rrc-1*, *pix-1* and *git-1* interact genetically in a complex way: wild type *pix-1* is required for the proper localization of RRC-1 but not its stability; *rrc-1* is not required for the localization or stability of PIX-1; *git-1* is not required for the localization of RRC-1 but is required for its stability; overexpression of PIX-1 can suppress the phenotype of *rrc-1*; whereas single mutants in *rrc-1* or *pix-1* result in reduced whole animal locomotion, a *pix-1 rrc-1* double mutant shows some improvement in locomotion. (5) Both PIX-1 and RRC-1 affect the activity of Rac: we have reported that a *pix-1* null mutant has reduced levels of activated GTP-bound CED-10 (Rac) in nematode muscle (Moody et al., 2020). By expressing nematode RRC-1 in mammalian tissue culture cells, Delawary et al. (2007) have reported that RRC-1 has GAP activity towards mammalian Rac1 and Cdc42 but not RhoA. Figure 10 summarizes what we now know about the *pix-1* pathway in *C. elegans* body wall muscle. Of course, we still do not know the substrates for PAK-1 and PAK-2 protein kinases in muscle and

how their phosphorylation results in the assembly or maintenance of IACs at the muscle cell boundary.

The PIX pathway has been shown to be functionally important in multiple organisms and tissues, ranging from mammalian nervous (Ramakers et al., 2012) and immune (Missy et al, 2008) systems, to nematode germline (Lucanic and Cheng, 2008), migration of neuroblasts (Dyer et al., 2010), tension-dependent morphogenesis of epidermal cells (Zhang et al., 2011), early embryonic elongation (Martin et al., 2014), and muscle (Moody et al. 2020). Given that we have identified a possible human ortholog for RRC-1, ARHGAP33 (Figure 2c), we propose that this protein is the GAP for the PIX pathway in human muscle or other tissues.

In addition to *rrc-1*, our screening of mutants in 18 Rho GAP proteins expressed in muscle revealed two other genes that when mutated result in MCB defects, *hum-7* and *rga-4* (Supplementary Figure 1). *hum-7* encodes a 213 kDa protein with Rho GAP domain near its C-terminus and a myosin class IX motor domain in its N-terminal half. Inspection of two independently-generated mutants have the same MCB-specific defect as *rrc-1* and *pix-1*. *rga-4* has an even more interesting phenotype—it shows disorganization of all three IAC sites—MCBs, M-lines and dense bodies. However, we only examined a single mutant allele, the intragenic deletion *rga-4(ok1935)*, and it had not been outcrossed to wild type. *rga-4* encodes a 1126 aa protein with the only recognizable domain being the Rho GAP domain. RGA-4 has been reported to act redundantly with another Rho GAP protein, RGA-3, in the germ line and early embryo, and to inactivate RHO-1 (RhoA) of *C. elegans* (Schmutz et al., 2007). Interestingly, we have previously reported that RNAi knockdown of RHO-1 (RhoA) results in disorganization of

the A-bands in the body wall muscle of adult nematodes (Qadota et al., 2008). I leave the investigation of *hum-7* and *rga-4* in muscle for future studies.

That loss of function of a GEF, PIX-1, a positive regulator of Rac, and loss of function of a GAP, RRC-1, a negative regulator of Rac, have the same defect, suggests that the maintenance of integrin adhesion complexes at the MCB is a dynamic process. Consistent with these results, if we increase or eliminate the protein kinase activity of a known effector of the PIX-1 pathway, PAK-1, we also observe defects in the MCB (Figure 1). This dynamic property of the IACs at the MCB might explain why the genetic interaction of the two genes is complicated. If the IACs at MBCs were not dynamic we would expect that *rrc-1* mutants would have a phenotype opposite from the phenotype of *pix-1* mutants, and that an *rrc-1 pix-1* double mutant would have a wild type phenotype. However, the phenotypes of *rrc-1* and *pix-1* are the same, and the double mutant shows some partial suppression only in swimming and not crawling locomotion assays (Figure 9c and d). And interestingly, overexpression of PIX-1 results in suppression of the MCB defect in an *rrc-1* mutant (Figure 9a). These data are difficult to interpret. One possible explanation, however, is that the GAP, RRC-1, might be another effector of the PIX pathway, not just the expected PAK-1 and PAK-2. Thus, PIX-1 overexpression results in more molecules of active Rac, and then these active Racs bind to the GAP, RRC-1, and this produces an additional downstream signal. There is precedence for a protein being both a GAP and an effector: For the GTPase EF-Tu, GTP bound EF-Tu binds to the ribosome, so the ribosome is the "effector" and this results in addition of one amino acid to a growing polypeptide, but the ribosome also functions as a GAP to promote GTP hydrolysis, resulting in dissociation of EF-Tu•GDP from the ribosome (Krab and Parmeggiani, 2002). That is, for the GTPase EF-Tu, the

ribosome is both an effector and a GAP. Another example was provided from studies in S. cerevisiae on the ARF GTPase Arf1-3p. All four genes recovered from a high-copy suppressor screen of a loss of function mutant of *arf1-3* encode ARF GAPs (Zhang et al., 1998). However, at this time we cannot distinguish between our results on RRC-1 revealing an alternative effector output, or that this is simply a neomorphic phenotype resulting from overexpression of PIX-1.

Materials and Methods

C. elegans strains

All nematode strains were grown on NGM pates using standard methods and maintained at 20° (Brenner, 1974). Most strains were obtained from the Caenorhabditis Genetics Center. The wild type strain was N2 (Bristol). Strains containing mutations in 18 genes encoding proteins with RhoGAP domains and also expressed in muscle, are listed in Supplementary Table 1 and in Supplementary Figure 1. The following strains were generated during this study:

GB340: *pak-1(syb647)*, which contains a L99F mutation in PAK-1, was generated by CRISPR/Cas9 by SunyBiotech (described below) as PHX647, and then outcrossed 4X to wild type.

GB341: *pak-1(syb632)*, which contains a K324A mutation in PAK-1, was generated by CRISPR/Cas9 by SunyBiotech (described below) as PHX632, and then outcrossed 1X to wild type.

GB342: *rrc-1(syb4499)*, which expresses RRC-1 with an HA tag fused to its C-terminus (RRC-1::HA), was generated by CRISPR/Cas9 by SunyBiotech (described below) as PHX4499.

GB343: *rrc-1(ok1747)* was outcrossed 5X to wild type.

GB344: *rrc-1(tm1023)* was outcrossed 5X to wild type.

GB345: *rrc-1(gk290525)* was outcrossed 5X to wild type

GB346: *rrc-1(gk859353)* was outcrossed 5X to wild type

GB347: *rrc-1(ok1747) pix-1(gk299374)* was generated by recombination starting with GB343, and GB291 [*pix-1(gk299374)* outcrossed 5X to wild type; Moody et al. 2020].

GB348: *rrc-1(syb4499) pix-1(gk299374)* was generated by recombination starting with GB342 and GB291.

GB349: *rrc-1(ok1747); sfIs20* by crossing GB343 into *sfIs20* which is an integrated array which overexpresses PIX-1 from a muscle specific promoter (Moody et al. 2020).

CRISPR/Cas9 generation of nematode strains expressing kinase dead and kinase constitutively-active PAK-1, and HA-tagged RRC-1. The CRISPR/Cas9 procedures were carried out by SunyBiotech (http://www.sunybiotech.com). Details about the sgRNAs and repair templates used are given in Supplementary Figure 3. The resulting strains are:

PHX647, *pak-1(syb647)* which has an L99F mutation predicted to make the PAK-1 protein kinase constitutively activePHX632, *pak-1(syb632)* which has a K324A mutation predicted to make the PAK-1 protein kinase catalytically dead PHX4499, *rrc-1(syb4499)* which expresses RRC-1 with a C-terminal HA tag.

Immunostaining and confocal microscopy of body wall muscle. Adult worms were fixed and immunostained using the method described by (Nonet et al. 1997). Antibodies were used at 1:200 dilution except as noted: anti-PAT-6 (rat polyclonal)(Warner et al., 2013), anti-UNC-52 (mouse monoclonal MH2)(Mullen et al., 1999), anti-PAT-3 (1:100 dilution; mouse monoclonal MH25 purified from ascites culture)(Francis and Waterston, 1985; Gettner et al., 1995), anti-UNC-95 (rabbit polyclonal Benian-13)(Qadota et al., 2007), anti-UNC-112 (1:100 dilution)(Hikita et al., 2005),

anti-MHC A (mouse monoclonal 5–6) (Miller et al., 1983), anti-UNC-89(rabbit polyclonal EU30)(Benian et al., 1996),
anti-ATN-1 (mouse monoclonal MH35) (Francis and Waterston, 1991), anti-HA (mouse monoclonal; H3663;
Sigma-Aldrich), and anti-GFP (rabbit polyclonal; Thermo Fisher, A11122). Secondary antibodies, used at 1:200 dilution, included anti-rabbit Alexa 488, anti-rat
Alexa 594, and anti-mouse Alexa 594, all purchased from Invitrogen. Images were captured at room temperature with a Zeiss confocal system (LSM510) equipped
with an Axiovert 100M microscope and an Apochromat x63/1.4 numerical
aperture oil immersion objective, in 1× and 2.5× zoom mode. For all the confocal images the color balances were adjusted by using Adobe Photoshop (Adobe, San Jose, CA).

Swimming and crawling assays. For swimming assays day two asynchronous adults were harvested from one 6 cm NGM OP50 seeded plate with M9 buffer. Animals were subsequently washed free from bacteria using M9 buffer and then pelleted at ratio of 1:1 (worm: buffer). 2 ml of M9 buffer followed by five microliters of worm suspension were added to the center area of one unseeded 6 cm NGM plate. Each strain was allowed to adapt for five minutes before recording swimming movement. The recordings were done using a dissecting stereoscopic microscope fitted with a CMOS camera (Thorlabs). For all strains a total of fifteen, 10-sec. videos were recorded from various sections of the plate with each video tracking an average of 8 individual animals. Video data was analyzed by Image J WrmTracker software plug-in to obtain body bends per second (BBPS) for individual animals. Worms that moved out of frame and

outliers were removed during data analysis and an average of 20 animals were analyzed for each strain. The resulting BBPS values for each mutant strain was compared to wildtype and further tested for statistically significant differences using Welch's T-test.

For crawling assays day two adults were harvested as described above, except for the use of 0.2g/L gelatin in M9 buffer. Five microliters of worm suspension was added to the center of a 6 cm unseeded NGM plate and then the excess liquid was removed using a twisted KimWipe. After a five-minute adaptation time, worm crawling movement was recorded as mentioned above. BBPS values for individual animals were extracted from each video. The resulting values for each strain were compared to wild type for statistical analysis using Welch's T-test for significance.

Protein sequence analysis. Nematode RRC-1a, b, and c were obtained from Wormbase. A BLAST homology search identified human orthologs of the nematode protein using the NCBI PubMed database. The domain organization for RRC-1 and the orthologs were analyzed by the online PFAM database. PubMed pBLAST database was used to align human ARHGAP33 amino acid sequence with nematode RRC-1 to determine the percent identities for each domain and total protein.

Knockdown of GIT-1 via RNAi feeding. RNAi by feeding was performed as described previously (Timmons et al., 2001; Miller et al. 2009). GIT-1 cDNA was generated via PCR amplification of the 5'-most 1,077 nucleotides of the GIT-1 cDNA sequence using the RB2

cDNA library as a template with the following primers--GIT-1 FWD: 5'GCGGGATCCATGTACACAGCAGAGGCGCTT 3'which includes a BamHI restriction enzyme (RE) site and GIT-1 REV: 5'CGCCTCGAGTGCTGGATTGTCTCCAGTGAT 3', which includes an XhoI RE site. The ~1kb amplicon was digested and ligated into the BamHI and XhoI sites of the pPD129.36 vector and used to transform competent XL1 Blue E. Coli cells on LB + ampicillin plates overnight at 37 °C. Individual colonies from the GIT-1 cDNA pPD129.36 clones were grown overnight in liquid culture, plasmids prepared, and confirmed by restriction digestion. A resulting GIT-1 pPD129.36 clone and empty vector pPD129.36 plasmids were used to transform competent HT115 (DE3) RNAi feeding bacteria, and a resulting colony from each was grown as an overnight liquid culture. The resulting bacteria were used to seed 6cm and 10 cm NGM plates. To conduct RNAi feeding experiments, 15-20 L4 stage worms were added to 25 NGM *git-1* RNAi and 25 empty vector in HT115 (DE3) bacteria 6cm plates and left overnight. Then following day, ten worms were transferred from the 6cm plates to the 10cm plates under the same conditions and allowed to lay eggs for approximately 8 hrs before being picked. The eggs on the plate were allowed to hatch for ~48 hrs before being harvested for conducting fixation for immunostaining or making lysates for SDS PAGE, followed by Western blotting analysis. (Miller et. al 2009)

Western blot analysis. The method of Hannak et al. (2002) was used to prepare total protein lysates from wild-type, rrc-1(ok1747) 5X O.C., RRC-1::HA, RRC-1::HA *pix-1(gk299374)*, RRC-1::HA; RNAi empty vector, and RRC-1::HA; *git-1 (RNAi)* mixed-stage animals. Equal amounts of total protein were separated on 10% polyacrylamide-SDS- Laemmli gels, transferred

to nitrocellulose membranes, reacted with affinity purified, E. coli-OP50-absorbed anti-PIX-1a (Moody et al., 2020), anti-HA (rabbit monoclonal cat. no. C29F4 from Cell Signaling Technology) at 1:1,000 dilution, and anti-histone H3 (rabbit polyclonal ab1791, Abcam, Inc.; 1:40,000 dilution), then reacted with goat anti-rabbit immunoglobulin G conjugated to HRP (GE Healthcare) at 1:10,000 dilution, and visualized by ECL. Protein bands were quantitated by comparing to total Ponceau S staining or to histone H3.

Chapter 4

Discussion and Conclusions

A large amount of information is available on the composition of IACs, and how the key molecule integrin is activated. However, there are several important gaps in our understanding of IACs: (1) Although IACs are built around an activated integrin and a set of core proteins, IACs can vary in composition, and how this variation is regulated is unknown. For example, in C. elegans muscle IAC sites include dense bodies, M-lines, and adhesion complexes at MCBs that have common core proteins, however, there are also proteins specific to each location. (2) It is not known what determines where an IAC forms and when it forms. The "when" question is perhaps best considered in a motile cell in which IACs form at the leading edge of the moving cell, and IACs disassemble at the trailing edge, but the molecular signaling involved is still a major gap in the field. The "where" question is best exemplified in striated muscle, in which the IACs of costameres have specific patterning and spatial organization. Although the spacing of costameres follows the spacing of adjacent Z-disks in the peripheral myofibrils, it is also known that myofibril assembly occurs from "the outside in", in which signals from the ECM dictate the assembly of nascent myofibrils. My discovery that the PIX signaling pathway determines whether IACs form at the MCB is thus a major insight into the question of what molecular mechanisms dictate where IACs will form.

Previous work in *S. cerevisiae* and *C. elegans* has provided evidence to support the idea that the cycling requirement of GTPases yields the same loss function phenotype for a GEF or GAP of the same pathway as highlighted in Chapters 2 and 3. This hypothesis was the foundation for screening for loss of function in genes encoding a GAP protein, after I had established the loss of function phenotype for the GEF pix-1. I screened available mutants in GAP proteins expressed in

muscle for the same loss of IAC components at the MCB as found in *pix-1* mutants. From this screen, I identified two such genes in which loss of function results in the boundary defect, *rrc-1* and *hum-7*, but decided to focus my efforts on rrc-1. I leave hum-7 to be studied by a future member of the Benian lab. In addition, I have elucidated a PIX pathway in *C. elegans* body wall muscle by examining mutants in various known components of this pathway in both *C. elegans* and mammals. Thus, I have discovered that the scaffold protein GIT-1 is involved, and that CED-10, and not MIG-2 or RAC-2, is the relevant RAC, and that the relevant effectors are PAK-1 and PAK-2, but not MAX-2. My findings highlight a useful genetic analysis approach for elucidating the members of a GTPase signaling pathway that relies on the cycling requirement of most G-proteins.

The regulation of the PIX pathway seems to be rather dynamic in nature based on the results described in Chapters 2 & 3. Interestingly, this could suggest the presence of a GTPase dissociation inhibitor (GDI) that has yet to be well characterized. Currently, there is only one established GDI protein in the *C. elegans* proteome which is characterized as a Rab GTPase dissociation inhibitor, according to Wormbase. Gdi-1 is a 50kD protein comprised mostly of a large GDP dissociation inhibitor, which sequesters inactive GTPase proteins in the cytosol and prevents activation via GEFs. Mammals possess three GDI proteins, which suggest that these GDIs have evolved into three distinct proteins throughout evolution. While it is unlikely that this dissociation inhibitor will have any Rho GTPase activity, the notion that these proteins are not well characterized does provide some potential for the GDI to possess additional unknown GTPase capabilities. An interesting example was shown in Lohmer et al., 2016, which shows that the Rho GTPase, CDC-42 coordinates with GDI-1 by linking to unidentified pathways to promote invadopodium formation in *C. elegans*, as knockout of both genes causes an enhanced phenotype. Lee et al., 2010

also show data suggesting that gdi-1 and dys-1 interact; RNAi knockdown of gdi-1 results in a reduction of muscle degeneration in a *dys-1* mutant background than in the control empty vector. Therefore, an additional approach is to obtain *gdi-1* mutants or conduct RNAi experiments like those described in Chapter 3 of this thesis. Subsequently, the mutant animals would be compared to the appropriate controls to assess the muscle cell boundary structures, as well as the localization of gdi-1 in muscle.

Our lab collaborated with Jennifer Kwong's laboratory (Emory, Dept. of Pediatrics) to generate a heart-specific knockout of the mouse PIX-1 ortholog called β-PIX. These β-PIX heart KO mice develop a dilated cardiomyopathy (DCM) at 8 months of age. Thus, I can hypothesize that one new human cardiomyopathy gene encodes β-PIX (ARHGEF7). As I have shown the same muscle phenotype for deficiency of the nematode ortholog of ARHGEF7 (PIX-1) as for deficiency of other known members of the PIX pathway (RRC-1, GIT-1, PAK-1, and Rac), possible new cardiomyopathy genes in humans might be expanded by five additional genes. Our *C. elegans* work also shows that the worm ortholog, PIX-1, is required for the assembly or stability of costamere-like structures. This is consistent with previous studies in humans and mice showing that deficiency of costamere proteins results in cardiomyopathy (Benian and Epstein, 2011). Current and future work on the β-PIX heart KO mice, will include characterizing the heart muscle IACs, the costameres, to determine if they show similar abnormalities to what I have observed in our nematode mutants. Moreover, once the lab publishes a paper on the β-PIX heart KO mice, we can probably convince a clinical genetic lab to add the human β-PIX gene to their panel of known suspected genes involved in cardiomyopathy, currently about 25-50 genes (Pugh et al., 2014). As

noted in the Introduction, there is a need to identify new cardiomyopathy genes as when screening is performed, mutations can only be identified in about half of patients.

Mutant phenotypes in model organisms such as *C. elegans* are often exploited to identify other members of a pathway by genetic modifier screens. However, the phenotype that I observe for members of the *pix-1* pathway, is not well suited for screening for enhancers or modifiers. As the phenotype is subtle—requiring immunostaining to reveal the boundary defect and motility assays to observe the locomotion defect. Therefore, we wondered if the phenotype of loss of function for the *Drosophila* ortholog of PIX-1, called dPix, might be stronger. Thus, the lab initiated a collaboration with the expert fly geneticist, Dr. Krishna Bhat, at the University of South Florida, and his lab found that heart-specific RNAi knockdown of dPix also results in a dilated cardiomyopathy phenotype. Interestingly, *Drosophila* has a single chamber heart called the dorsal tube and is becoming a model to study the heart and genes that cause cardiomyopathies in humans. Heart-specific knockdown resulted in a dorsal tube with an enlarged diameter and slow and irregular “heartbeat”. Most importantly, the adult flies with this knockdown are very slow and uncoordinated in their walking, which provides an easily scorable phenotype for genetic modifiers. When these modifier genes can be identified, their orthologs can also be studied in *C. elegans* and in the mouse, taking advantage of the various attributes of those systems.

The major unanswered question from my work is HOW does the PIX pathway promote the assembly or stability of IACs? (Figure 4.1) Of course, one next step would be to identify the substrates of PAK-1 and/or PAK-2 kinases. One way to approach this is to compare the total phospho-proteome of wild type to the *pak-1* kinase-dead and *pak-1* constitutively active mutant worms. This approach sounds good in principle, however, proteomic techniques have yielded large

sets of data that are difficult to assess for significance. Another challenge is the ubiquitous expression of PAK kinases in several cell types in addition to the lack of technical methods to easily isolate large amounts of muscle cells. Therefore, it is likely that this approach would lead to the identification of substrates that are not relevant to muscle. Another way to look for direct or indirect substrates (perhaps from a PAK kinase cascade) would be to take a candidate approach. For example, we could conduct immunoprecipitations of various core components of the IAC (e.g., UNC-112, PAT-4) and examine phosphorylation status in wild type vs. a mutant in the PIX-1 pathway. Again, we hope that genetic modifiers identified from the *Drosophila* screens will help us identify PAK substrates.

Another unresolved issue is why do mutants in the PIX pathway only result in defective adhesions plaques and not defective M-lines and dense bodies, as all three are examples of IACs. One hypothesis is that there are additional RacGEF proteins that are localized to M-lines and dense bodies. I already have evidence for the requirement for a RhoGAP protein at M-lines and dense bodies; in my screen of mutants in 18 genes encoding RhoGAP proteins expressed in muscle, I found one, *rga-4(ok1935)* that has disorganized M-lines and dense bodies but normal MCBs (Fig 3.1S). There are 17 proteins in *C. elegans* that contain RhoGEF (DH) domains and are expressed in muscle and all have human orthologs (Table 2.1S) (Moody et al, 2020). These 17 proteins include PIX-1, UIG-1, and UNC-89, which have been studied previously (Gieseler et al. 2017; Hikita et al. 2005). UNC-89 is localized to M-lines, and the DH domain of UNC-89 activates RHO-1 (RhoA)(Qadota et al., 2008), and thus likely not relevant. UIG-1 supports our hypothesis as UIG-1 is localized to dense bodies and is a GEF for Cdc42 (Hikita et al., 2005). Of the other 14 proteins, one of them, TIAM-1 has been shown to activate CED-10 (Rac) and shown to promote

posterior neurite extension (Zheng et al., 2016). In addition, UNC-73 has two RhoGEF domains, one that activates Rac and one that activates RhoA (Steven et al., 1998). The muscle intracellular locations of TIAM-1 and UNC-73 are unknown. The muscle intracellular localization and GEF specificity of the other 12 proteins are also unknown. As shown in Appendix, I have already begun to explore *unc-73* mutants and have preliminary evidence for disruption of the muscle cell boundaries. However, it would still be interesting to localize UNC-73 in muscle.

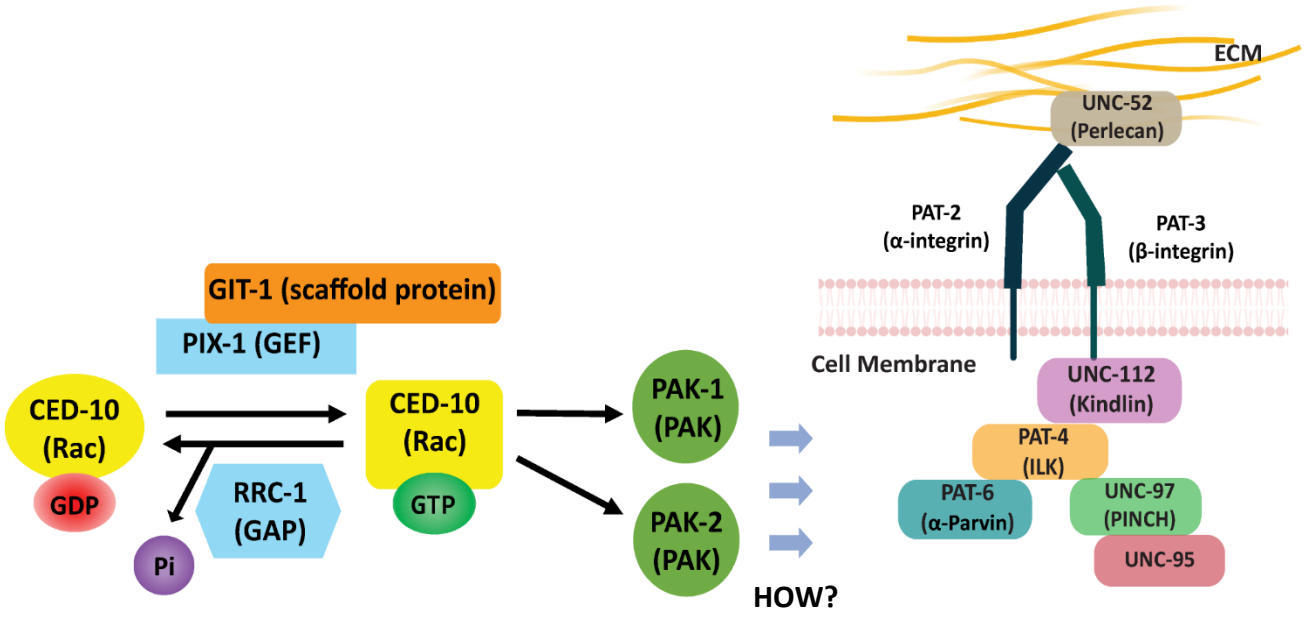

Figure 4.1 PIX-1 pathway has a role in muscle. The drawing depicts what we have learned about the PIX-1 pathway in *C. elegans* muscle. In Moody et al. (2020) we demonstrated that for the proper assembly or stability of integrin adhesion sites at the muscle cell boundary, the RacGEF, PIX-1, its scaffold, GIT-1, the Rac, CED-10, and the PAK effectors, PAK-1 and PAK-2 are required. The current results demonstrate that the RhoGAP, RRC-1 is the GAP for the PIX pathway, based on the similarity of *pix-1* and *rrc-1* phenotypes, and genetic interactions of *rrc-1* with *pix-1* and *git-1*. The blue arrows indicate that, by some still unknown mechanisms, this Rac cycling pathway is required for the assembly or stability of integrin adhesion complexes at muscle cell boundaries. Core components of this complex are depicted to the right, with the names of the mammalian proteins shown in parentheses.

Chapter 5

Appendix/Miscellaneous Data

The contents of this chapter have not been published as of March 2022.

Before my work a RhoGAP for the PIX pathway had yet to be identified. I screened the *C. elegans* proteome for proteins harboring RhoGAP domains that were also expressed in body wall muscle, resulting in 18 proteins total. Subsequently, deletion alleles for all 18 of these genes were obtained from the CGC and further screened using immunostaining with antibodies to PAT-6. This screen resulted in two candidate genes, *rrc-1* and *hum-7*, that may encode GAP proteins for the PIX pathway. While my efforts were focused on the characterization of RRC-1, I did confirm that the phenotype originally observed in *hum-7(ok3054*) was due to *hum-7* loss of function. The evaluation of the *hum-7(tm8236)*, an additional deletion allele also revealed disruption of PAT-6 localization only at the muscle cell boundaries. As shown in Fig.5.1, HUM-7 has a RA domain (Ras associating), followed by a class IX myosin head domain, followed by IQ domains that bind to calmodulin, and finally a RhoGAP domain.

To begin further characterization of HUM-7, I began searching for available mutants with missense mutations that will likely affect function. The Million Mutation Project database (Thompson et al., 2013) provided a total of 17 missense mutations located only in the myosin head region. Narrowing down the list involved a series of sequence analyses, the first step was to conduct multi-sequence alignment for residue conservation amongst *H. sapiens*, *M. musculus*, *D. rerio,* and *C. elegans.* The comparison of myosin proteins and corresponding disease mutations was recommended by our communications with Dr. Sandford Bernstein at the San Diego State University. I performed a pBLAST sequence alignment of HUM-7 with four human myosin heavy chain isoforms, including MYH2,3,6 and 7 (adult fast myosin 2a, embryonic myosin, α-cardiac myosin, and β-cardiac myosin, respectively). Finally, the list of missense mutations was compared to a list of mutations in residues that are known to cause human disease in any four of the myosin

genes based on the sequence data reviewed in Parker and Peckham, 2020. This subsequent analysis elucidated a total of 5 mutants with amino acid substitutions residing in conserved resides of muscle myosin genes analyzed. Interestingly, three of the five are known to be mutated and cause hypertrophic cardiomyopathy (HCM) or Epstein's Anomaly (EA), characterized by malformation of the tricuspid valve and altered right ventricle and interventricular septum. The chart in Table 5.1 are the results of the analysis conducted to choose the missense mutant alleles that will likely affect myosin head function. In the future, the lab can obtain these 3 mutants from the CGC and examine their muscle for possible defects in their muscle cell boundaries. If a muscle cell boundary defect is detected, it would suggest that the function of HUM-7 at the boundaries is primarily through the myosin head, rather than the GAP domain. If no defects are found, we can take a similar approach to analyze missense mutations in the RhoGAP and RA domains.

I discovered that the RacGEF PIX-1 is localized at M-lines, dense bodies, and MCBs, yet it is only required at the MCBs as shown in Chapter 2. Therefore, I hypothesize that PIX-1 is only required at MCBs because there are additional Rac/Cdc42 GEF proteins at M-lines and dense bodies. There are 17 proteins in the *C. elegans* genome that contain RhoGEF (DH) domains that are also expressed in muscle (Moody et al., 2020). UNC-73 is known to be a GEF for Rac and RhoA and has two RhoGEF domains, yet its localization in muscle has yet to be determined. Altogether these factors make it an interesting candidate gene to help elucidate the site-specific assembly of IACs at the MCBs and potentially the other two IAC sites. To investigate the possible role of UNC-73 in muscle, I obtained three independent *unc-73* deletion alleles, *unc-73(rh40)* outcrossed to wildtype 4X, *unc-73(ev802)*, and *unc-73(ce362),* and screened for a loss of PAT-6 localization at muscle IAC sites. Interestingly, each of these mutants exhibits disruption of PAT-

6 localization at the MCB with varying severity, as shown in Figure 5.2. In addition, one of the alleles, *ev802*, also shows disruption in the organization of M-lines and dense bodies. Before concluding that *unc-73* is important for the IACs, we need to outcross *ev802* and *ce362* to wild type approximately 5X, and then repeat the analysis. To localize UNC-73, the lab has already expressed a region of UNC-73 to produce antibodies.

Previous studies have shown β-PIX is an essential gene, as a complete loss of function results in early embryonic lethality in the mouse. To circumvent this limitation in our ability to study the role of β-PIX in muscle function, we developed a cardiomyocyte-specific knockout mouse line in collaboration with Dr. Jennifer Kwong from Emory's Dept. of Pediatrics. Jen directed the creation of a mouse line with loxP sites targeting the sixth exon of β-PIX and then crossed these mice with a transgenic animal expressing Cre recombinase under the control of a cardiomyocyte-specific promoter. The results of this mutation are not distinguishable until the animals reach 8 months old. Preliminary data from the observed phenotypes include cardiac hypertrophy, reduced cardiac function, and pulmonary edema, suggesting that the cardiomyocyte-specific deletion of β-PIX in mice results in dilated cardiomyopathy. As a follow-up, I assessed the structure of individual cardiomyocytes in the mutant mice compared to controls using standard histology. Figure 5.3 contains representative images and quantification of cardiomyocyte cross-sectional areas from β-PIX conditional knockout and control mice. These results indicate that β-PIX deficiency yields a significant increase in cardiomyocyte cross-sectional area, which further supports the idea that cardiomyocyte-specific deletion of β-PIX results in dilated cardiomyopathy in our mouse model.

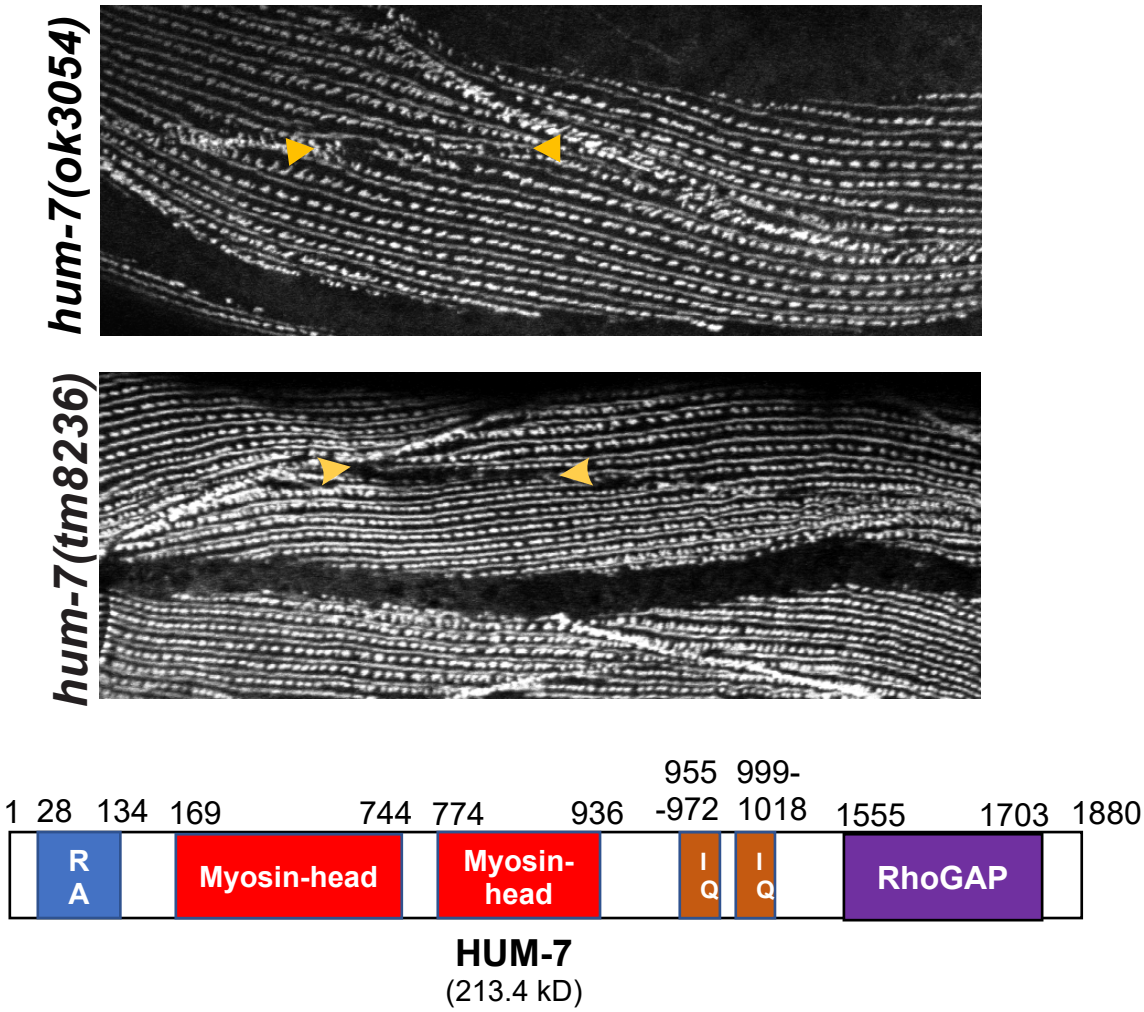

Figure 5.1. HUM-7 loss of function causes disruption of PAT-6 localization only at the attachment plaques between muscle cells. a. Representative images of two independent *hum-7* deletion alleles, *hum-7(ok3054)* and *hum-7(tm8236)* immunostained with antibodies to PAT-6 (α-parvin) showing disruption only at muscle cell boundaries. Yellow arrows indicate areas of muscle cell boundary disruption. **b.** Schematic diagram of HUM-7 protein domain structure predicted by PFAM. From N-to C-terminus these domains are: an RA (Ras associating) domain, a myosin head domain most similar to class IX myosins (there is actually only one myosin head domain; the gap is an artifact of the PFAM program), two IQ domains that are likely to bind to calmodulin, and a RhoGAP domain.

Variation	Allele #	Nucleotide Δ	Substitution	MYH2,3,6,7 alignment residues (respectively)	Human mutation point	Disease
VC40927, plot	gk885757	C->T	C256Y*	S	None	N/A
VC30213, plot	gk438787	C->T	G288S*	K,A,G,S	MYH7 (S205)	(HCM)
VC40396, plot	gk617639	C->T	S317N	S#	MYH7 (S241)	EA
VC40666, plot	gk753500	A->T	F319I	F#	MYH7 (F244)	HCM
VC20024, plot	gk311927	G->A	H409Y*	S,S,S N	None	N/A
VC40940, plot	gk891475	A->G	Y452H*	E	MYH3 (E374) MYH7 (E373)	Arthrogryposis HCM
VC40409, plot	gk622784	C->T	A476T*	A,A,G,G	MHY7 (G398)	HCM
VC40175, plot	gk498411	A->C	Y510D*	Y	None	N/A
VC40327, plot	gk575959	C->T	A524T*	Q,Q,T,T	None	N/A
VC20741, plot	gk388552	C->T	E583K*	E#	MYH6 (E501) MYH7 (E500)	Other defects HCM
VC41014, plot	gk928055	C->T	E652K*	E	None	N/A
VC40544, plot	gk686048	C->T	G670D*	G	None	N/A
VC20752, plot	gk391871	G->A	H707Y*	Does not align	N/A	N/A
VC20341, plot	gk101289	T->G	I878L	I	None	N/A
VC20216, plot	gk101288	G->A	A881V	K	None	N/A
VC40752, plot	gk793962	A->T	V893D*	K,K,R,R	MYH7 (R719) MYH6 (R721)	HCM Other defects
VC40983, plot	gk912120	T->C	N923S	H	None	N/A

HUM-7 MMP Allele List (order based on position) **Analysis Based on MYH2,3, 6 & 7**

Table 5.1 Sequence Analysis of MMP *hum-7* mutant alleles. List of the 17 *hum-7* mutant alleles available from the MMP database that reside in the myosin head domain, indicated by the columns underlined with red. Each row provides the details of the allele, columns (left to right) indicate the variation number, the allele number, the nucleotide change, and the resulting amino acid change. *C. elegans* HUM-7 was aligned with human MYO9B, mouse unconventional myosin IX and zebrafish unconventional myosin IX orthologs using the CLUSTAL multi-sequence alignment database. The highlighted strains indicate mutations in residues conserved across nematode, zebrafish, mouse, and human orthologs. The asterisks (*) indicate non-conservative amino acid changes resulting from mutation. The second part of the analysis, indicated by the columns underlined in green, was conducted using pBLAST to align HUM-7 with each of the four human muscle myosin isoforms (MYH2: adult fast myosin 2a, MYH3: embryonic myosin, MYH6:α-cardiac myosin, and MYH7: β-cardiac myosin). The fifth column indicates whether the residue conserved amongst class IX myosins is also conserved in class II (muscle) myosins. The 5 residues that are conserved are highlighted in light blue. Amongst these 5, three, indicated by "#", are known to be mutated and cause hypertrophic cardiomyopathy (HCM) or Epstein's Anomaly (EA) which is a malformation of the tricuspid valve and altered right ventricle and interventricular septum (Parker and Peckham, 2020).

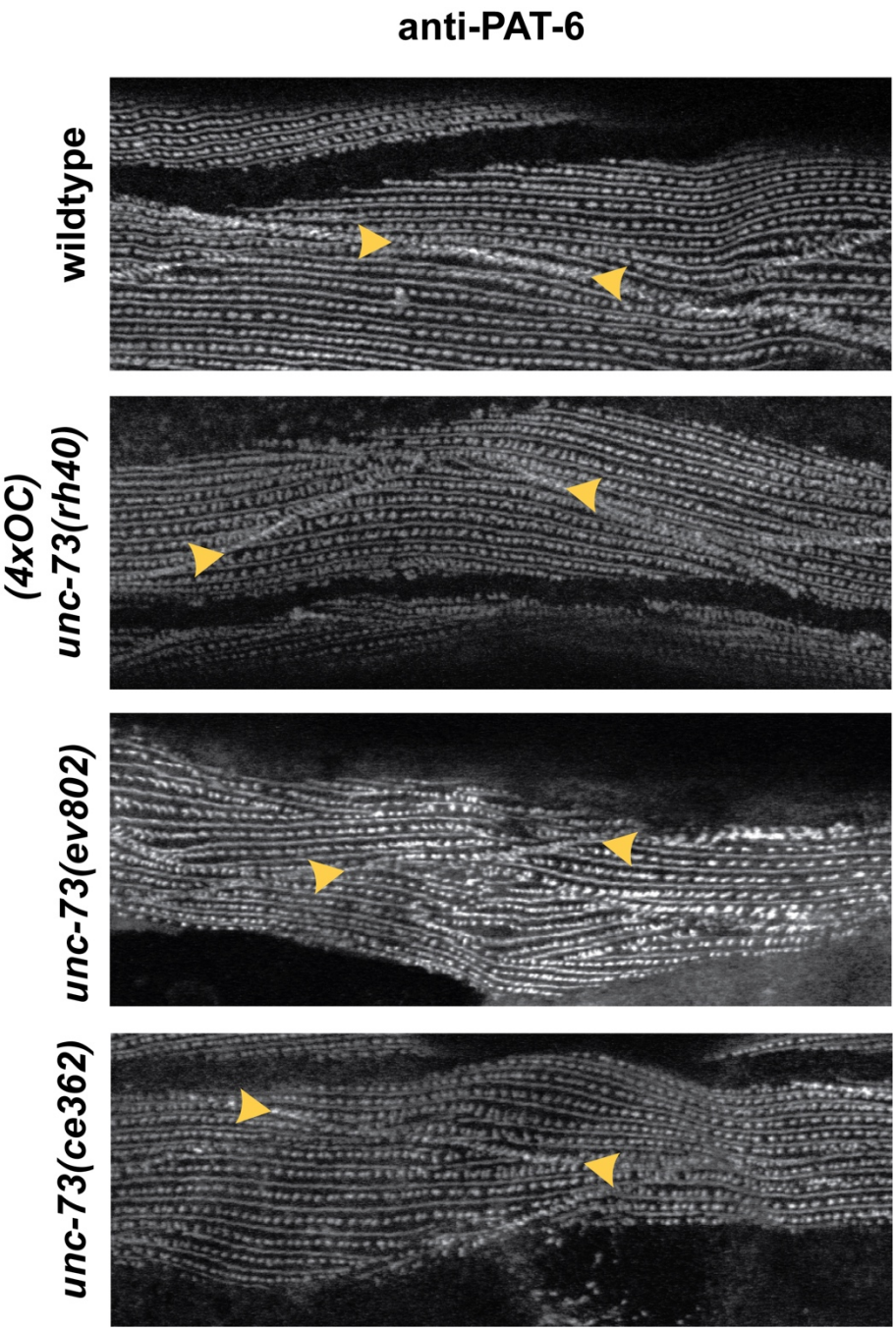

Figure 5.2. *unc-73* loss of function alleles exhibits either disruption or loss of PAT-6 at muscle cell boundaries. Confocal microscopy imaging of body wall muscle cells in young adult animals immunostained with antibodies to PAT-6 (α-Parvin) in wildtype, showing normal zipper-like structures and three independent *unc-73* deletion alleles, *unc-73(rh40)* outcrossed to wildtype 4X, *unc-73(ev802)*, and *unc-73(ce362)*. Yellow arrows indicate muscle cell boundary structures that show a loss or lack of PAT-6 accumulation comparable to wildtype. An asterisk (*) indicates additional defects in the organization of M-lines and dense bodies in the *ev802* allele.

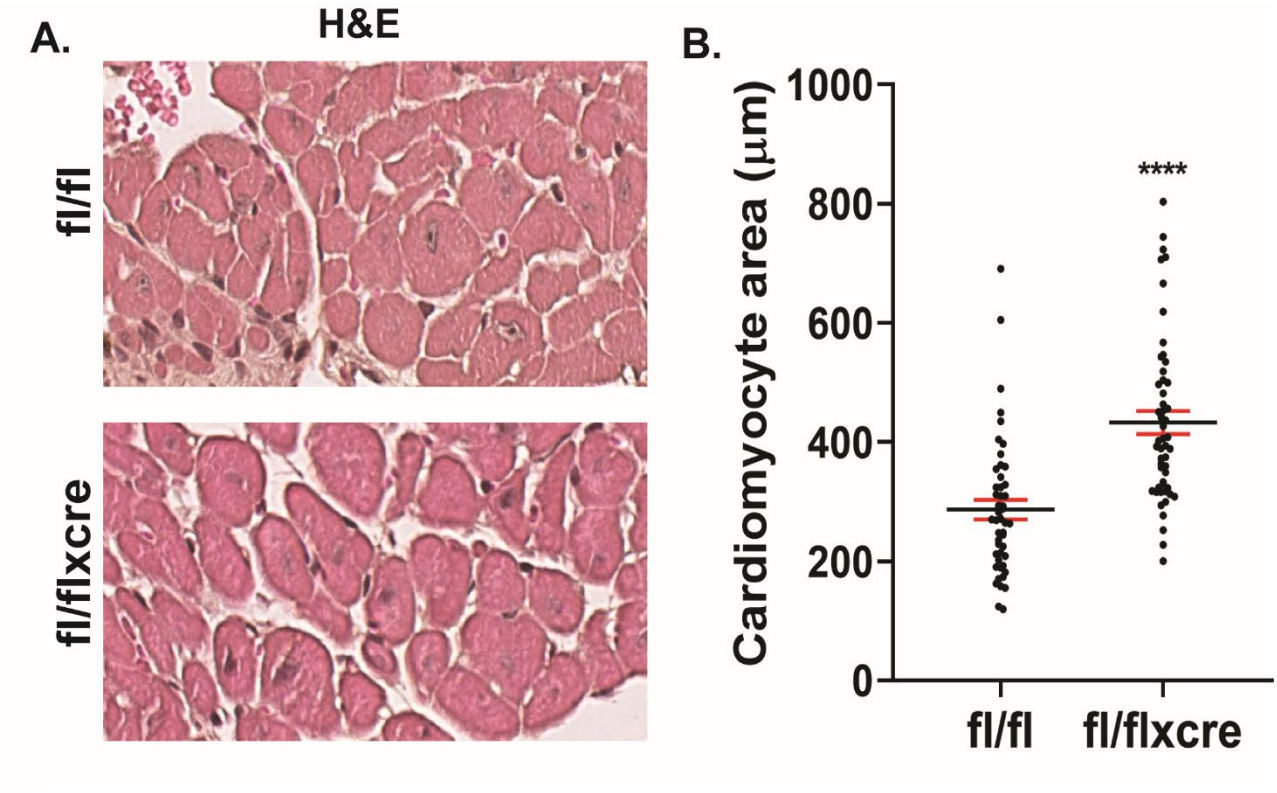

Figure 5.3 Cardiomyocyte cross-sectional areas are significantly increased in *β-PIX* conditional knockout A. Representative images of hematoxylin and eosin staining of heart sections from 8-month-old control (fl/fl) and β-PIX knockout (fl/flxcre) mice. Images shown at 40X magnification. **B.** Quantification of individual cross-sectional areas. 25 measurements were taken from each animal from control (n=2) and β-PIX knockout (n=2). Solid black line represents the average cross-sectional area, error bars in red indicate SEM, (****p-values ≤0.0001).

Works Cited

Adamson, P., Marshall, C. J., Hall, A. & Tilbrook, P. A. (1992). Post-translational modifications of p21rho proteins. *J. Biol. Chem*. 267, 20033–20038

Aghazadeh, B., Zhu, K., Kubiseski, T. J., Liu, G. A., Pawson, T., Zheng, Y., & Rosen, M. K. (1998). Structure and mutagenesis of the Dbl homology domain. *Nature structural biology*, *5*(12), 1098–1107.

Amin, E., Jaiswal, M., Derewenda, U., Reis, K., Nouri, K., Koessmeier, K. T., Aspenström, P., Somlyo, A. V., Dvorsky, R., & Ahmadian, M. R. (2016). Deciphering the Molecular and Functional Basis of RHOGAP Family Proteins: a systematic approach toward selective inactivation of Rho family proteins. *J. Biol. Chem*., 291(39), 20353–20371.

Ananthakrishnan, R., & Ehrlicher, A. (2007). The forces behind cell movement. *International journal of biological sciences*, *3*(5), 303–317.

Anthis, N.J., Campbell, I.D. (2011). The tail of integrin activation. *Trends Biochem*. Sci. 36, 191-198.

Bachir, A.I., Zareno, J., Moissoglu, K., Plow, E.F., Gratton, E., Horwitz, A.R. (2014). Integrin-associated complexes form hierarchically with variable stoichiometry in nascent adhesions. *Curr. Biol*. 24, 1845-1853.

Benian GM, Epstein HF. (2011). Caenorhabditis elegans muscle: a genetic and molecular model for protein interactions in the heart. *Circ. Res*. 109, 1082-1095.

Benian, G.M., Tinley, T,L., Tang, X. & Borodovsky, M. (1996). The *Caenorhabditis elegans* gene *unc-89*, required for muscle M-line assembly, encodes a giant modular protein composed of Ig and signal transduction domains. *J. Cell Biol.* 132, 835-848.

Bernards, A. and Settleman, J. (2004). GAP control: regulating the regulators of small GTPases. *Trends Cell Biol*. 14, 377-385.

Berndt, N., Hamilton, A. D., & Sebti, S. M. (2011). Geranylgeranyltransferase-1 inhibitors. *Protein Prenylation Part B*, *30* , 129–163.

Boudhraa Z, Carmona E, Provencher D and Mes-Masson A-M (2020) Ran GTPase: A Key Player in Tumor Progression and Metastasis. *Front. Cell Dev. Biol.* 8:345.

Brenner, S. (1974). The genetics of Caenorhabditis elegans. *Genetics* 77, 71-94.

Brown JL, Stowers L, Baer M, Trejo JA, Coughlin S, Chant J. (1996). Human Ste20 homologue hPAK1 links GTPases to the JNK MAP kinase pathway. *Curr Biol.* 6, 598-605.

Canman JC, Lewellyn L, Laband K, Smerdon SJ, Desai A, Bowerman B, Oegema K. (2008). Inhibition of Rac by the GAP activity of centralspindlin is essential for cytokinesis. *Science*. 322, 1543-1546.

Case, D.A. et al. (2018). AMBER 2018. University of California, San Francisco.

Castillo-Lluva, S., Tatham, M. H., Jones, R. C., Jaffray, E. G., Edmondson, R. D., Hay, R. T., & Malliri, A. (2010). SUMOylation of the GTPase Rac1 is required for optimal cell migration. *Nat. Cell Biol.*, *12*(11), 1078–1085.

Chang, F., Lemmon, C., Lietha, D., Eck, M. & Romer, L. (2011). Tyrosine phosphorylation of Rac1: a role in regulation of cell spreading. *PLoS ONE* 6, e28587.

Chikumi, H., Barac, A., Behbahani, B. Gao, Y., Teramoto,H, Zheng, Y., and Gutkind, S. (2004). Homo- and hetero-oligomerization of PDZ-RhoGEF, LARG and p115RhoGEF by their C-terminal region regulates their *in vivo* Rho GEF activity and transforming potential. *Oncogene* 23, 233–240.

Corrado, D., Link, M.S., Calkins, H. (2017). Arrhythmogenic right ventricular cardiomyopathy. N. *Engl. J. Med*. 376, 61-71.

Delawary M, Nakazawa T, Teuka T, Sawa M, Iino Y, Takenawa T, Yamamoto T. (2007). Molecular characterization of a novel RhoGAP, RRC-1 of the nematode C. elegans. *Biochem and Biophys Res Comm.* 357, 377-382.

Deng, S. & Huang, C. (2014). E3 ubiquitin ligases in regulating stress fiber, lamellipodium, and focal adhesion dynamics. *Cell Adh. Migr*. 8, 49–54.

Dumont, N. A., Wang, Y. X., & Rudnicki, M. A. (2015). Intrinsic and extrinsic mechanisms regulating satellite cell function. *Development* (Cambridge, England), 142(9), 1572–1581.

Dyer, J. O., Demarco, R. S. & Lundquist, E. A. (2010) Distinct roles of Rac GTPases and the UNC-73/Trio and PIX-1 Rac GTP exchange factors in neuroblast protrusion and migration in C. elegans. *Small GTPases* 1, 44–61.

Ervasti, J. M. & Sonnemann, K. J. (2008). Biology of the striated muscle dystrophin-glycoprotein complex. *Int. Rev. Cytol.* 265, 191–225.

Ervasti, J.M. (2003). Costameres: the Achilles' heel of Herculean muscle. *J. Biol. Chem*. 278, 13591-13594.

Frame, M. C., Fincham, V. J., Carragher, N. O., & Wyke, J. A. (2002). v-Src's hold over actin and cell adhesions. *Nature reviews. Molecular cell biology*, *3*(4), 233–245.

Francis, R. & Waterston, R.H. (1985). Muscle organization in C. elegans: localization of proteins implicated in thin filament attachment and I-band organization. *J. Cell Biol.* 101, 1532-1549.

Francis, R. & Waterston, R.H. (1991). Muscle cell attachment in *Caenorhabditis elegans*. *J. Cell Biol.* 114, 465-479.

Frontera, W.R., Ochala, J. Skeletal Muscle: A Brief Review of Structure and Function. *Calcif Tissue Int* **96,** 183–195 (2015).

Gettner, S.N., Kenyon, C. & Reichardt, L.F. (1995). Characterization of beta pat-3 heterodimers, a family of essential integrin receptors in C. elegans. *J. Cell Biol*. 129, 1127-1141.

Gieseler K, Qadota H, Benian GM. Development, structure, and maintenance of C. elegans body wall muscle. 2017. WormBook, ed. The C. elegans Research Community, WormBook, doi/10.1895/wormbook.1.173.1, http://www.wormbook.org

Hafen, B. B., & Burns, B. (2021). Physiology, Smooth Muscle. In *StatPearls*. StatPearls Publishing.

Hancock, J. (2003).Ras proteins: different signals from different locations. *Nat Rev Mol Cell Biol* 4, 373–385.

Hannak, E., Oegema, K., Kirkham, M., Gonczy, P., Habermann, B. & Hyman AA. (2002). The kinetically dominant assembly pathway for centrosomal asters in *Caenorhabditis elegans* is gamma-tubulin dependent. J. Cell Biol. 157, 591-602.

Hao, Y.E., He, D.F., Yin, R.H., Chen, H., Wang, J., Wang, S.X., Zhan, Y. Q., Ge, C.H., Li, C.Y., Yu, M., & Yang, X.M. (2015). GIT2 deficiency attenuates concanavalin A-induced hepatitis in mice. *FEBS open bio*, *5*, 688–704.

Hayashi, Y. K., Chou, F. L., Engvall, E., Ogawa, M., Matsuda, C., Hirabayashi, S., Yokochi, K., Ziober, B. L., Kramer, R. H., Kaufman, S. J., Ozawa, E., Goto, Y., Nonaka, I., Tsukahara, T., Wang, J. Z., Hoffman, E. P., & Arahata, K. (1998). Mutations in the integrin alpha7 gene cause congenital myopathy. *Nature genetics*, *19*(1), 94–97.

Henderson, C.A., Gomez, C.G., Novak, S.M., Mi-Mi, L., Gregorio, C.C. (2017). Overview of the muscle cytoskeleton. *Compr. Physiol.* 7, 891-944.

Hikita, T., Qadota, H., Tsuboi, D., Taya, S., Moerman, D.G., & Kaibuchi, K. (2005). Identification of a novel Cdc42 GEF that is localized to the PAT-3-mediated adhesive structure. *Biochem. Biophys. Res. Commun.* 335, 139-145.

Hodge, R. G., & Ridley, A. J. (2016). Regulating Rho GTPases and their regulators. *Nature reviews. Molecular cell biology*, *17*(8), 496–510.

Horton ER, Byron A, Askari JA, Ng DH, Millon-Frémillon A, Robertson J, Koper EJ, Paul NR, Warwood S, Knight D, Humphries JD, Humphries MJ. (2015). Definition of a consensus integrin adhesome and its dynamics during adhesion complex assembly and disassembly. *Nature Cell Biol.* 17, 1577-1587.

Huang W, Zhou Z, Asrar S, Henkelman M, Xie W, Jia Z. (2011). p21-Activated kinases 1 and 3 control brain size through coordinating neuronal complexity and synaptic properties. *Mol Cell Biol.* 31, 388-403.

Humphries, J. D., Chastney, M. R., Askari, J. A., & Humphries, M. J. (2019). Signal transduction via integrin adhesion complexes. *Current opinion in cell biology*, *56*, 14–21.

Hwang, H., Krajniak, J., Matsunaga, Y., Benian, G. M. & Lu, H. (2014). On-demand optical immobilization of C. elegans for high-resolution imaging and microinjection. *Lab Chip* 14, 3498–3501.

Iden, S., & Collard, J. G. (2008). Crosstalk between small GTPases and polarity proteins in cell polarization. *Nature reviews. Mol. Cell Biol.*, *9*(11), 846–859.

Iyer GH, Garrod S, Woods VL Jr, Taylor SS. (2005). Catalytic independent functions of a protein kinase as revealed by a kinase-dead mutant: study of the Lys72His mutant of cAMP-dependent kinase. *J. Mol. Biol*. 351, 1110-1122.

Jantsch-Plunger V, Gönczy P, Romano A, Schnabel H, Hamill D, Schnabel R, Hyman AA, Glotzer M. (2000). CYK-4: A Rho family gtpase activating protein (GAP) required for central spindle formation and cytokinesis. *J. Cell Biol*. 149, 1391-1404.

Kahn, R. A., Volpicelli-Daley, L., Bowzard, B., Shrivastava-Ranjan, P., Li, Y., Zhou, C., & Cunningham, L. (2005). Arf family GTPases: roles in membrane traffic and microtubule dynamics. *Biochemical Society transactions*, *33*(Pt 6), 1269–1272.

Katayama, M., Kawata, M., Yoshida, Y., Horiuchi, H.Yamamoto, T.Matsuura, Y., Takai, Y. (1991). The posttranslationally modified C-terminal structure of bovine aortic smooth muscle RhoA p21. *J. Biol. Chem*. 266, 12639–12645.

Krab IM, Parmeggiani A. (2002). Mechanisms of EF-Tu, a pioneer GTPase. *Progr. Nucl. Acids Res. and Mol. Biol.* 71, 513-551.

Kwon, T., Kwon, D. Y., Chun, J., Kim, J. H., & Kang, S. S. (2000). Akt protein kinase inhibits Rac1-GTP binding through phosphorylation at serine 71 of Rac1. *J. Biol Chem.*, *275*(1), 423–428.

Lang, P., Gesbert, F., Delespine-Carmagnat, M., Stancou, R., Pouchelet, M., & Bertoglio, J. (1996). Protein kinase A phosphorylation of RhoA mediates the morphological and functional effects of cyclic AMP in cytotoxic lymphocytes. *The EMBO journal*, *15*(3), 510–519.

Lee AY, Perreault R, Harel S, Boulier EL, Suderman M, Hallett M, et al. (2010) Searching for Signaling Balance through the Identification of Genetic Interactors of the Rab Guanine-Nucleotide Dissociation Inhibitor *gdi-1*. *PLoS ON*E 5(5): e10624.

Li L, Bainbridge MN, Tan Y, Willerson JT, Marian AJ. (2017). A potential oligogenic etiology of hypertrophic cardiomyopathy: a classic single-gene disorder. *Circ. Res.* 120, 1084-1090.

Liang X, Sun Y, Ye M, Scimia MC, Cheng H, Martin J, Wang G, Rearden A, Wu C, Peterson KL, Powell HC, Evans SM, Chen J. (2009). Targeted ablation of PINCH1 and PINCH2 from murine myocardium results in dilated cardiomyopathy and early postnatal lethality. *Circ.* 120, 568-576.

Lohmer LL, Clay MR, Naegeli KM, Chi Q, Ziel JW, Hagedorn EJ, et al. (2016) A Sensitized Screen for Genes Promoting Invadopodia Function In Vivo: CDC-42 and Rab GDI-1 Direct Distinct Aspects of Invadopodia Formation. *PLoS Genet.* 12(1): e1005786.

Lucanic M, Cheng HJ. (2008). A RAC/CDC-42-independent GIT/PIX/PAK signaling pathway mediates cell migration in C. elegans. *PLoS Genet*. 4, e1000269.

Manser, E., Loo, T.H., Koh, C.G., Zhao, Z.S., Chen, X.Q., Tan, L., Tan, I., Leung, T., & Lim, L. (1998). PAK kinases are directly coupled to the PIX family of nucleotide exchange factors. *Molecular cell*, *1*(2), 183–192.

Marei, H., Carpy, A., Woroniuk, A., Vennin, C., White, G., Timpson, P., ,Macek, B., and Malliri, A. (2016). Differential Rac1 signalling by guanine nucleotide exchange factors implicates FLII in regulating Rac1-driven cell migration. *Nat Commun* 7, 10664.

Martin E, Harel S, Nkengfac B, Hamiche K, Neault M, et al. (2014) *pix-1* Controls Early Elongation in Parallel with *mel-11* and *let-502* in *Caenorhabditis elegans. PLOS ONE* 9(4): e94684.

Meissner, B., Warner, A., Wong, K., Dube, N., Lorch, A., McKay, S.J., Khattra, J., Rogalski, T., Somasiri, A., Chaudhry, I., Fox, R.M., Miller, D.M., Baillie, D.L., Holt, R.A., Jones, S.J.M., Marra, M.A., Moerman, D.G. (2009). An integrated strategy to study muscle development and myofilament structure in C. elegans. *PLoS Genetics* 5, e1000537.

Mercer, K. B., Miller, R. K., Tinley, T. L., Sheth, S., Qadota, H., & Benian, G. M. (2006). Caenorhabditis elegans UNC-96 is a new component of M-lines that interacts with UNC-98 and paramyosin and is required in adult muscle for assembly and/or maintenance of thick filaments. *Molecular biology of the cell*, *17*(9), 3832–3847.

Mercer, K. B., Flaherty, D. B., Miller, R. K., Qadota, H., Tinley, T. L., Moerman, D. G., & Benian, G. M. (2003). Caenorhabditis elegans UNC-98, a C2H2 Zn finger protein, is a novel partner of UNC-97/PINCH in muscle adhesion complexes. *Molecular biology of the cell*, *14*(6), 2492–2507.

Michelitch M, Chant J. (1996). A mechanism of Bud1p GTPase action suggested by mutational analysis and immunolocalization. *Curr. Biol.* 6, 446-454.

Miller, D.M., Ortiz, I., Berliner, G.C. & Epstein, H.F. (1983). Differential localization of two myosins within nematode thick filaments. *Cell* 34, 477-490.

Miller, R.K., Qadota, H., Stark, T.J., Mercer, K.B., Wortham, T.S., Anyanful, A., Benian, G.M. (2009). CSN-5, a component of the COP9 signalosome complex, regulates the levels of UNC-96 and UNC-98, two components of M-lines in C. elegans muscle. *Mol. Biol. Cell* 20, 3608-3616.

Missy K, Hu B, Schilling K, Harenberg A, Sakk V, Kuchenbecker K, Kutsche K, Fischer KD. (2008). AlphaPIX Rho GTPase guanine nucleotide exchange factor regulates lymphocyte functions and antigen receptor signaling. *Mol Cell Biol*. 28, 3776-3789.

Mitani, S. (1995). Genetic regulation of mec-3 gene expression implicated in the specification of the mechanosensory neuron cell types in Caenorhabditis elegans. *Dev. Growth Diff*. 37, 551–557.

Miyamoto, Y., Torii, T., Yamamori, N., Ogata, T., Tanoue, A., & Yamauchi, J. (2013). Akt and PP2A reciprocally regulate the guanine nucleotide exchange factor Dock6 to control axon growth of sensory neurons. *Science signaling*, *6*(265), ra15.

Moody, J.C., Qadota, H., Reedy, A.R., Okafor, C.D., Shanmugan, N., Matsunaga, Y., Christian, C.J., Ortlund, E.A., Benian, G.M. (2020). The Rho-GEF PIX-1 directs assembly or stability of lateral attachment structures between muscle cells. *Nature Commun*. 2020 Oct 6;11(1):5010.

Morita, K., Hirono, K., Han, M. (2005). The Caenorhabditis elegans ect-2 RhoGEF gene regulates cytokinesis and migration of epidermal P cells. *EMBO Rep. 6*, 1163-1168.

Mukund, K., & Subramaniam, S. (2020). Skeletal muscle: A review of molecular structure and function, in health and disease. *Wiley interdisciplinary reviews. Systems biology and medicine*, *12*(1), e1462.

Mullen, G.P., Rogalski, T.M., Bush, J.A., Gorji, P.R. & Moerman, D.G. (1999). Complex patterns of alternative splicing mediate the spatial and temporal distribution of perlecan/UNC-52 in Caenorhabditis elegans. *Mol. Biol. Cell* 10, 3205-3221.

Nahabedian, J. F., Qadota, H., Stirman, J. N., Lu, H. & Benian, G. M. (2012) Bending amplitude—a new quantitative assay of C. elegans locomotion: identification of phenotypes for mutants in genes encoding muscle focal adhesion components. *Methods* 56, 95–102.

Navarro-Lérida, I., Sánchez-Perales, S., Calvo, M., Rentero, C., Zheng, Y., Enrich, C., & Del Pozo, M. A. (2012). A palmitoylation switch mechanism regulates Rac1 function and membrane organization. *The EMBO journal*, *31*(3), 534–551.

Navarro-Lérida, I., Sánchez-Álvarez, M., & Del Pozo, M. Á. (2021). Post-Translational Modification and Subcellular Compartmentalization: Emerging Concepts on the Regulation and Physiopathological Relevance of RhoGTPases. *Cells*, *10*(8), 1990.

Nigon VM, Félix MA. History of research on C. elegans and other free-living nematodes as model organisms. In: WormBook: The Online Review of *C. elegans* Biology [Internet]. Pasadena (CA): WormBook; 2005-2018.

Nonet, M.L., Grundahl, K., Meyer, B.J. & Rand, J.B. (1993). Synaptic function is impaired but not eliminated in *C. elegans* mutants lacking synaptotagmin. *Cell* 73, 1291-1305.

Nussbaum-Krammer, C.I., Neto, M.F., Brielmann, R.M., Pedersen, J.S. & Morimoto, R.I. (2015). Investigating the spreading of toxicity of prion-like proteins using the metazoan model organism C. elegans. *J. Vis. Exp*. 95, 52321.

Olson M. F. (2018). Rho GTPases, their post-translational modifications, disease-associated mutations and pharmacological inhibitors. *Small GTPases*, *9*(3), 203–215.

Park, H. O., Chant, J., & Herskowitz, I. (1993). BUD2 encodes a GTPase-activating protein for Bud1/Rsr1 necessary for proper bud-site selection in yeast. *Nature*, *365*(6443), 269–274.

Pérez, A., Marchán, I., Svozil, D., Sponer, J., Cheatham, T. E., 3rd, Laughton, C. A., & Orozco, M. (2007). Refinement of the AMBER force field for nucleic acids: improving the description of alpha/gamma conformers. *Biophysical journal*, *92*(11), 3817–3829.

Peter, A. K., Cheng, H., Ross, R. S., Knowlton, K. U., & Chen, J. (2011). The costamere bridges sarcomeres to the sarcolemma in striated muscle. *Progress in pediatric cardiology*, *31*(2), 83–88.

Pugh, T.J., Kelly, M.A., Gowrisankar, S., Hynes, E., Seidman, M.A., Baxter, S.M., Bowser, M., Harrison, B., Aaron, D., Mahanta, L.M., Lakdawala, N.K., McDermott, G., White, E.T., Rehm, H.L., Lebo, M., Funke, B.H. (2014). The landscape of genetic variation in dilated cardiomyopathy as surveyed by clinical DNA sequencing. *Genetics in Med* 16, 601-608.

Qadota H, Matsunaga Y, Nguyen KCQ, Mattheyses A, Hall DH, Benian GM. (2017). High resolution imaging of muscle attachment structures in C. elegans. *Cytoskeleton* 74, 426-442.

Qadota, H., Moody, J. C., Lesanpezeshki, L., Moncrief, T., Kitzler, D., Bhat, P. D., Vanapalli, S. A., Oberhauser, A. F., & Benian, G. M. (2020). A Region of UNC-89 (Obscurin) Lying between Two Protein Kinase Domains Is a Highly Elastic Spring Required for Proper Sarcomere Organization. *Journal of molecular biology*, *432*(17), 4799–4814.

Qadota, H., Blangy, A., Xiong, G., & Benian, G.M. (2008). The DH-PH region of the giant protein UNC-89 activates RHO-1 GTPase in C. elegans body wall muscle. *J. Mol. Biol*. 383, 747-752.

Qadota, H., Mercer, K.B., Miller, R.K., Kaibuchi, K. & Benian GM. (2007). Two LIM domain proteins and UNC-96 link UNC-97/pinch to myosin thick filaments in *Caenorhabditis elegans* muscle. *Mol. Biol. Cell* 18, 4317-4326.

Ramakers, G.J., Wolfer, D., Rosenberger, G., Kuchenbecker, K., Kreienkamp, H.J., Prange-Kiel, J., Rune, G., Richter, K., Langnaese, K., Masneuf, S., Bösl, M.R., Fischer, K.D., Krugers, H.J., Lipp, H.P., van Galen, E., Kutsche, K. (2012). Dysregulation of Rho GTPases in the αPix/Arhgef6 mouse model of X-linked intellectual disability is paralleled by impaired structural and synaptic plasticity and cognitive deficits. *Hum Mol Genet* 21, 268-286.

Razidlo, G. L., Wang, Y., Chen, J., Krueger, E. W., Billadeau, D. D., & McNiven, M. A. (2013). Dynamin 2 potentiates invasive migration of pancreatic tumor cells through stabilization of the Rac1 GEF Vav1. *Dev. cell*, *24*(6), 573–585.

Reiner, D.J., & Lundquist, E.A. (2018). Small GTPases. *WormBook : the online review of C. elegans biology*, *2018*, 1–65.

Reza, N., Musunuru, K., Owens, A.T. (2019). From hypertrophy to heart failure: what is new in genetic cardiomyopathies. *Curr. Heart Fail.* Rep. 16, 157-167.

Riedl, J., Crevenna, A. H., Kessenbrock, K., Yu, J. H., Neukirchen, D., Bista, M., Bradke, F., Jenne, D., Holak, T. A., Werb, Z., Sixt, M., & Wedlich-Soldner, R. (2008). Lifeact: a versatile marker to visualize F-actin. *Nature methods*, *5*(7), 605–607.

Roe, D. R. & Cheatham, T. E. III (2013). PTRAJ and CPPTRAJ: software for processing and analysis of molecular dynamics trajectory data. *J. Chem. Theory and Computation* 2013 *9* (7), 3084-3095

Rossman, K. L., Der, C. J., & Sondek, J. (2005). GEF means go: turning on RHO GTPases with guanine nucleotide-exchange factors. *Nature reviews. Molecular cell biology*, *6*(2), 167–180.

Ryckaert, J.P., Ciccotti, G. & Berendsen, H. J. Numerical integration of the cartesian equations of motion of a system with constraints: molecular dynamics of n-alkanes. J. Comput. Phys. 23, 327–341 (1977).

Schaefer, A., Reinhard, N. R., & Hordijk, P. L. (2014). Toward understanding RhoGTPase specificity: structure, function and local activation. *Small GTPases*, *5*(2), 6.

Schlenker, O. & Rittinger, K. (2009). Structures of dimeric GIT1 and trimeric beta-PIX and implications for GIT-PIX complex assembly. *J. Mol. Biol.* 386, 280–289.

Schmalzigaug R, Rodriguiz RM, Bonner PE, Davidson CE, Wetsel WC, Premont RT. (2009). Impaired fear response in mice lacking GIT1. *Neurosci Lett.* 458, 79-83.

Schmidt, A., & Hall, A. (2002). Guanine nucleotide exchange factors for Rho GTPases: turning on the switch. *Genes & development*, *16*(13), 1587–1609.

Schmutz, C., Stevens, J., Spang, A. (2007). Functions of the novel RhoGAP proteins RGA-3 and RGA-4 in the germ line and in the early embryo of C. elegans. *Development* 134, 3495-3505.

Schonegg S, Constantinescu AT, Hoege C, Hyman AA. (2007). The Rho GTPase-activating proteins RGA-3 and RGA-4 are required to set the initial size of PAR domains in Caenorhabditis elegans one-cell embryos. *Proc Natl Acad Sci U S A*. 104, 14976-14981.

Small, T. M., Gernert, K. M., Flaherty, D. B., Mercer, K. B., Borodovsky, M., & Benian, G. M. (2004). Three new isoforms of Caenorhabditis elegans UNC-89 containing MLCK-like protein kinase domains. *Journal of molecular biology*, *342*(1), 91–108.

Song, E.H., Oh, W., Ulu, A., Carr, H.S., Zuo, Y., & Frost, J.A. (2015). Acetylation of the RhoA GEF Net1A controls its subcellular localization and activity. *Journal of cell science*, *128*(5), 913–922.

Stenmark H. (2009). Rab GTPases as coordinators of vesicle traffic. *Nature reviews. Molecular cell biology*, *10*(8), 513–525.

Steven, R., Kubiseski, T. J., Zheng, H., Kulkarni, S., Mancillas, J., Ruiz Morales, A., Hogue, C. W., Pawson, T., & Culotti, J. (1998). UNC-73 activates the Rac GTPase and is required for cell and growth cone migrations in C. elegans. *Cell*, *92*(6), 785–795.

Sun, Z., Lambacher, A., Fassler, R. (2014). Nascent adhesions: from fluctuations to a hierarchical organization. *Curr. Biol.* 24, R801-R803.

Sweeney, H. L., & Hammers, D. W. (2018). Muscle Contraction. *Cold Spring Harbor perspectives in biology*, *10*(2), a023200.

Tadokoro, S., Shattil, S.J., Eto, K., Tai, V., Liddington, R.C., de Pereda, J.M., Ginsberg, M.H., Calderwood, D.A. (2003). Talin binding to integrin beta tails: a final common step in integrin activation. *Science* 302, 103-106.

Takada, Y., Ye, X. & Simon, S. (2007). The integrins. *Genome Biol.* 8, 215.

Taylor, J., Turner, E.H., Hillier, L.W., Moerman, D.G., Waterston, R.H. (2013). The million mutation project: a new approach to genetics in Caenorhabditis elegans. *Genome Res.* 23, 1749-1762.

Thompson O, Edgley M, Strasbourger P, Flibotte S, Ewing B, Adair R, Au V, Chaudhry I, Fernando L, Hutter H, Kieffer A, Lau J, Lee N, Miller A, Raymant G, Shen B, Shendure J.(2013). The million mutation project: a new approach to genetics in Caenorhabditis elegans. *Genome Res*. 23, 1749–1762.

Timmons, L., Court, D.L., Fire, A. (2001). Ingestion of bacterially expressed dsRNAs can produce specific and potent genetic interference in C. elegans. *Gene* 263, 103-112.

Tong, J., Li, L., Ballermann, B., & Wang, Z. (2013). Phosphorylation of Rac1 T108 by extracellular signal-regulated kinase in response to epidermal growth factor: a novel mechanism to regulate Rac1 function. *Mol. Cell. Biol.*, *33*(22), 4538–4551.

Uygur, A., & Lee, R. T. (2016). Mechanisms of Cardiac Regeneration. *Developmental cell*, *36*(4), 362–374.

Volinsky N, Gantman A, Yablonski D. (2006). A Pak- and Pix-dependent branch of the SDF-1alpha signalling pathway mediates T cell chemotaxis across restrictive barriers. *Biochem* J. 397, 213-222.

Wan, J., Roth, A. F., Bailey, A. O., & Davis, N. G. (2007). Palmitoylated proteins: purification and identification. *Nature protocols*, *2*(7), 1573–1584.

Wang, H. R., Zhang, Y., Ozdamar, B., Ogunjimi, A. A., Alexandrova, E., Thomsen, G. H., & Wrana, J. L. (2003). Regulation of cell polarity and protrusion formation by targeting RhoA for degradation. *Science (New York, N.Y.)*, *302*(5651), 1775–1779.

Wang, J., Wang, W., Kollman, P.A. & Case, D.A. (2006). Automatic atom type and bond type perception in molecular mechanical calculations. *J. Mol. Graph. Model*. 25, 247260.

Warner, A., Xiong, G., Qadota, H., Rogalski, T., Vogl, A.W., Moerman, D.G. & Benian, G.M. (2013). CPNA-1, a copine domain protein, is located at integrin adhesion sites, and is required for myofilament stability in *C. elegans*. *Mol. Biol. Cell* 24, 601-616.

Waterston, R. H., Hirsh, D. & Lane, T. R. (1984). Dominant mutations affecting muscle structure in C. elegans that map near the actin gene cluster. *J. Mol. Biol.* 180, 473–496.

Wennerberg, K., Rossman, K. L., & Der, C. J. (2005). The Ras superfamily at a glance. *J. of Cell Sci.*, *118*(Pt 5), 843–846.

White DE, Coutu P, Shi Y-F, Tardif J-C, Nattel S, Arnaud RS, Dedhar S, Muller WJ. (2006). Targeted ablation of ILK from the murine heart results in dilated cardiomyopathy and spontaneous heart failure. *Genes & Dev*. 20, 2355-2360.

Wilson, K. J., Qadota, H. & Benian, G. M. (2012) Immunofluorescent localization of proteins in Caenorhabditis elegans muscle. *Methods Mol. Biol.* 798, 171–181 (2012).

Won, H., Mah, W., Kim, E., Kim, J.W., Hahm, E.K., Kim, M.H., Cho, S., Kim, J., Jang, H., Cho, S.C., Kim, B.N., Shin, M.S., Seo, J., Jeong, J., Choi, S.Y., Kim, D., Kang, C., & Kim, E. (2011). GIT1 is associated with ADHD in humans and ADHD-like behaviors in mice. *Nature medicine*, *17*(5), 566–572.

Wood, W. B., & Waterston, R. H. (1988). Muscle. In *The nematode caenorhabditis elegans* (pp. 281–335). Chapter, Cold Spring Harbor Laboratory.

Worthylake, D. K., Rossman, K. L., & Sondek, J. (2000). Crystal structure of Rac1 in complex with the guanine nucleotide exchange region of Tiam1. *Nature*, *408*(6813), 682–688.

Ye F, Petrich BG, Anekal P, Lefort CT, Kasirer-Friede A, Shattil SJ, Ruppert R, Moser M, Fassler R, Ginsberg MH. (2013). The mechanism of kindlin-mediated activation of integrin a11bb3. *Curr. Biol.* 23, 2288-2295.

Zenke, F.T., King, C.C., Bohl, B.P., Bokoch, G.M. (1999). Identification of a central phosphorylation site in p21-activated kinase regulating autoinhibition and kinase activity. *J Biol Chem*. 274, 32565-32573.

Zhang H, Landmann F, Zahreddine H, Rodriguez D, Koch M, Labouesse M. (2011). A tension-induced mechanotransduction pathway promotes epithelial morphogenesis. *Nature* 471, 99-103.

Zhang Z, Um Y, Veevers J, Peter AK, Manso AM, Bradford WH, Nancy DD, Peterson KL, Knowlton KU, Ross RS, Zhou X, Chen J. (2016). Postnatal loss of kindlin-2 leads to progressive heart failure. *Circ. Heart Fail*. 9:e003129.